

POLITECNICO DI TORINO

Master's degree in Mechatronic Engineering



Master's Degree Thesis

Design of an avalanche rescue robot: state of the art of avalanche research technologies with focus on ground penetrating radar

Supervisor

Prof. Stefano **MAURO**

Co-supervisors

Ing. Matteo **GAIDANO**

Ing. Matteo **MELCHIORRE**

Candidate

Matthieu **REVIL**

16th April 2021

Summary

The avalanche phenomena affects the mountain environments, especially during winter seasons. This kind of event can be naturally caused or can be generated by humans. The number of skiers who practice freeride activities in the ski areas or away from the ski resorts is in rapid increase. This factor causes an increase of avalanche accidents. For this purpose, it is important to develop technologies able to quickly detect people buried under an avalanche, in order to improve the survival probability in case of accident. The goal of this thesis is to study and analyze the state of the art of avalanche research technologies, and to propose a possible implementation solution able to improve the current technologies.

The paper is divided in four chapters. In the first chapter are reported some catastrophic accidents caused by avalanches. In the second part of the introductory chapter are analyzed the survival curve, the avalanches causes and the avalanches characteristics. The second chapter describes the state of the art of the technologies used for avalanche research purposes. In this section are analyzed the following technologies: ARTVA, RECCO, smartphone apps, 4G technology, GPS detection systems, breath and skin detection sensors, radar detection, and ground penetrating radar. At the end of this chapter are discussed all the positive and negative factors of all the analyzed technologies. In the third chapter is analyzed an experiment conducted using the ground penetrating radar technology transported by a drone. The experience has been performed in Gressoney la Trinité, a place inside the Monterosa ski resort. The results of this study have been discussed during the section. Finally, in the last chapter it is proposed a possible combination of different technologies in order to improve the searching time and the precision during avalanche research rescues.

Acknowledgements

First of all, I want to thank the professors Stefano Mauro and Alberto Godio, the engineers Matteo Melchiorre, Matteo Gaidano, Diego Franco, Andrea Vergnano, Alessandro Ainardi and the Monterosa ski spa who helped me during the development of the thesis. Then I want to thank my family and all my friends who supported me during the last years.

Table of contents

SUMMARY	3
ACKNOWLEDGEMENTS	4
LIST OF TABLES	9
LIST OF FIGURES	10
ACRONYMS.....	15
INTRODUCTION	17
CHAPTER 1: STUDY OF AVALANCHE PHENOMENA	18
1.1 CATASTROPHIC HISTORICAL EVENTS.....	18
Plurs, Switzerland, 4 th September 1618	18
Wellington, Washington, 1 st March 1910.....	18
Tyrolean Alps, 13 th December 1916.....	19
Swiss-Austrian-Italian Alps, 1950-1951.....	19
Blons, Austria, 12 th January 1954	19
Yungay, Peru, 31 st May 1970	20
Lahaul Valley, India, early March 1979	20
North Ossetia, Russia, 21 st September 2002	21
Siachen Glacier region, 7 th April 2012	21
Rigopiano, Italy, 18 th January 2017.....	21
1.2 SURVIVAL CURVE	22
Survival Phase (0 minutes-15 minutes).....	22
Asphyxiation phase (15 minutes-45 minutes)	23
Waiting phase (45 minutes-90 minutes).....	23
Hypothermia phase (90 minutes-180 minutes).....	23
1.3 AVALANCHES CAUSES	23
Weather	23
Snowpack	24
Cornices.....	25

Terrain.....	25
Human.....	26
1.4 AVALANCHES CHARACTERISTICS	26
Characteristics of avalanches in Himalayan region	26
Characteristics of avalanches in Italy	30
CHAPTER 2: STATE OF THE ART OF AVALANCHE RESEARCH	
TECHNOLOGIES	33
TECHNOLOGIES CURRENTLY IN USE.....	36
2.1 ARTVA.....	36
2.2 RECCO	38
RLC resonant circuit	39
2.3 SMARTPHONE APPS TECHNOLOGY.....	40
TECHNOLOGIES IN DEVELOPMENT	43
2.4 4G TECHNOLOGY.....	43
2.5 GPS DETECTION TECHNOLOGY	45
Banff test	46
Fernie test.....	50
Discussion of the results	54
2.6 BREATH AND SKIN DETECTION SENSORS	55
2.7 RADAR DETECTION TECHNOLOGY	57
Radio frequency device detection	57
Detection of heartbeat and breathing using microwave transceiver	60
Life signal detection using an on-chip solid state microwave sensor	61
Distance detection using microwave transceiver	64
2.8 GROUND PENETRATING RADAR (GPR)	65
GPR system sliding on the ground surface.....	67
GPR system mounted on a helicopter	69
Airborne ground penetrating radar	75

Localization algorithm	80
COMPARISON OF TECHNOLOGIES	87
CHAPTER 3: PRACTICAL TEST WITH GPR TECHNOLOGY TRANSPORTED BY A DRONE	90
Test configuration	90
Instrumentation	93
Collection and analysis of GPR data	95
Analysis of the results	99
CHAPTER 4: CONCLUSIONS	101
BIBLIOGRAPHY.....	102

List of Tables

Table 1: Rescue method for buried avalanche victims, 2003/04-2012/13.....	33
Table 2: Summary of search technologies used by avalanche search apps	41
Table 3: Propagation through snow of 4G signal, Copper Mountain test	44
Table 4: GPS satellite tracking, Banff	47
Table 5: GPS signal attenuation, Banff	47
Table 6: GPS position error, Banff	48
Table 7: Position accuracy of least-squares solutions, Banff	49
Table 8: GPS satellite tracking, Fernie	51
Table 9: GPS signal attenuation, Fernie	51
Table 10: GPS position error, Fernie	52
Table 11: Position accuracy of least-squares solutions, Fernie	53
Table 12: Frequency bands of RF front-ends found in modern RF devices	58
Table 13: Advantages and disadvantages of avalanche research technologies.....	88
Table 14: Weather conditions in Sant’Anna test	93
Table 15: Acquisition parameters, Sant’Anna test	95

List of figures

Fig 1.1-a: Plurs, 4 th September 1618	18
Fig 1.1-b: Wellington, 1 st March 1910.....	18
Fig 1.1-c: Tyrolean Alps, December 1916	19
Fig 1.1-d: Swiss-Austrian-Italian Alps, 1950-1951.....	19
Fig 1.1-e: Blons, 12 th January 1954	20
Fig 1.1-f: Yungay, 31 st May 1970.....	20
Fig 1.1-g: Lahaul Valley, March 1979	20
Fig 1.1-h: Pakistan, 7 th April 2012.....	21
Fig 1.1-i: Rigopiano, 18 th January 2017	21
Fig 1.2-a: Survival curve.....	22
Fig 1.3-a: Point release avalanche.....	24
Fig 1.3-b: Slab avalanche	24
Fig 1.3-c: Cornice example.....	25
Fig 1.4-a: Distribution of avalanche accidents on slope angle	27
Fig 1.4-b: Distribution of avalanche accidents on slope exposure.....	27
Fig 1.4-c: Percent of accidents while on move and in static mode.....	28
Fig 1.4-d: Monthly distribution of avalanche accidents in Himalaya.....	28
Fig 1.4-e: Weather during avalanche accidents.....	29
Fig 1.4-f: Weather situation during accident within 24 h of the cessation of storm	29
Fig 1.4-g: Timing of avalanches in Himalayan region.....	29
Fig 1.4-h: Avalanche accidents during warning or otherwise	29
Fig 1.4-i: Avalanche victims in Italy	30
Fig 1.4-j: Avalanche victims distribution following activity categories	31
Fig 1.4-k: People who are present at the avalanche time	31

Fig 1.4-l: Avalanche accidents during 1985-1994 and 2000-2009 periods.....	32
Fig 2-a: Avalanche rescue phases	34
Fig 2-b: Avalanche rescue phases without transceiver search and in absence of phone coverage	35
Fig 2-c: Avalanche rescue phases without shovel	35
Fig 2.1-a: ARTVA devices.....	36
Fig 2.1-b: ARTVA research with one rescuer.....	37
Fig 2.1-c: ARTVA research with more rescuers.....	37
Fig 2.2-a: Example of RECCO technology research	38
Fig 2.2-b: RLC series resonance circuit.....	39
Fig 2.2-c: Resonant frequency point	40
Fig 2.5-a: GNAT circuit board	45
Fig 2.5-b: Banff test site GPS receivers placement at Banff.....	46
Fig 2.5-c: GPS receivers placement at Banff	46
Fig 2.5-d: GNAT2 horizontal position error at various snow depths, Banff.....	48
Fig 2.5-e: GNAT2 position error under 1.5 m of snow, Banff	49
Fig 2.5-f: Fernie test site	50
Fig 2.5-g: GPS receivers placement at Fernie	50
Fig 2.4-h: GNAT3 horizontal position error at various snow depths, Fernie.....	52
Fig 2.5-i: GNAT3 position error under 2 m of snow, Fernie.....	54
Fig 2.6-a: a) Volunteer entrapped in the chamber. b) Sensor array. c) Image of a single sensor. d) Nanoparticles form a porous sensing network as shown by (e) scanning electron microscopy.	56
Fig 2.6-b: Sensor array measurements	56
Fig 2.7-a: Schematic setup for the detection of defect mobile phones	58
Fig 2.7-b: Time characteristics of a transmitted received signal of a RF filter	59
Fig 2.7-c: Frequency characteristics of received signals from two different defect devices	59
Fig 2.7-d: Block scheme of the microwave transceiver	60

Fig 2.7-e:Breathing detection	61
Fig 2.7-f: Heartbeat detection.....	61
Fig 2.7-g: Experimental setup of igloo	61
Fig 2.7-h: Measurement scheme using on-chip solid state microwave sensor	62
Fig 2.3-i: Breathing and heartbeat detection using solid state microwave sensor. a)phase measurements for breathing; b)FFT result for breathing; c)phase measurements for heartbeat; d)FFT result for heartbeat.	63
Fig 2.7-j: Breathing signals and corresponding FFT results for different powers..	64
Fig 2.7-k: Block diagram of a FMCW radar.....	65
Fig. 2.8-a: Example of GPR utilization.....	66
Fig. 2.8-b: Technical principle of ground penetrating radar	66
Fig 2.8-c: Setup of the radar system in the designed sledge.....	67
Fig 2.8-d: Results from radar detection objects in the snowpack at 900 MHz.....	68
Fig 2.8-e: Left image: radar antenna emission with target reflection. Right image: temporal shape of the emitted electromagnetic pulse.	70
Fig 2.8-f: Left image: a-scan signal recorded within the time window. Right image: image of a radargram.....	71
Fig 2.8-g: First column: velocity profiles (depth versus x). Second column: corresponding radargrams (τ versus x).....	71
Fig 2.8-h: Left image: radargram after removing clutter and noise. Right image: result of minimizing the BV (bounded variation) functional for each column of the radargram.	72
Fig 2.8-i: Results of the matched filter.....	73
Fig 2.8-j: Results of algorithm applied to real life data	74
Fig 2.8-k: Artificial avalanche accumulation	76
Fig. 2.8-l: Results of the aerial tramway experiment.....	77
Fig 2.8-m: Results of the chairlift experiment	79
Fig 2.8-n: Left side: raw radar data u_0 . Right side: data u_1 after pre-processing step	81
Fig 2.8-o: Potential p_x composition.....	82

Fig 2.8-p: Snowpack boundaries in the radargram	83
Fig 2.8-q: Extracted snowpack representation	84
Fig 2.8-r: Result of the matched filter applied to us without preparation of the snowpack.....	84
Fig 2.8-s: Scaling function	85
Fig 2.8-t: Prepared snowpack representation	85
Fig 2.8-u: Result of the data processing algorithm	86
Fig 3-a: First snow mound configuration.....	90
Fig 3-b: ARTVA buried under snow	91
Fig 3-c: Second snow mound configuration.....	91
Fig 3-d: Buried skis	92
Fig 3-e: Scheme of the test field.....	92
Fig 3-f: Field test environment in Sant'Anna	93
Fig 3-g: VENTURE VFF_H01 drone	94
Fig 3-h: Instrumentation setup scheme	94
Fig 3-i: Flight paths of the drone	96
Fig 3-j: Radargram of line L1	97
Fig 3-k: Radargram and signal envelope processing of line L2	97
Fig 3-l: Radargram of line L3	98
Fig 3-m: Drone flight during the test	98
Fig 3-n: Radargram of the fourth flight of the drone.....	99
Fig 3-o: Relationship between wavelength and frequency	100

Acronyms

AINEVA: Associazione Interregionale Neve e Valanghe, Avalanche Services

ARTVA: Search device of people overwhelmed in avalanches

BV: Bounded Variation

CW: Continuous Wave

DSP: Digital Signal Processing

EM: Electromagnetic

FET: Field-Effect Transistor

FFT: Fast Fourier Transform

FMCW: Frequency Modulation Continuous Wave

GNAT: Global Navigation Asset Tracker

GPR: Ground Penetrating Radar

HSGPS: High Sensitivity Global Positioning System

LTE: Long Term Evolution

NLOS: No Line Of Sight

PC: Personal Computer

RF: Radio Frequency

RSRP: Reference Signal Receive Power

RSSI: Received Signal Strength Indicator

SAR: Search And Rescue

SNR: Signal to Noise Ratio

TOF: Time of Flight

UAV: Unmanned Aerial Vehicle

UWB: Ultra Wide Band

Introduction

The initial goal of this thesis was to project a drone able to accomplish avalanche rescue operations. The basic idea was to realize an aerial vehicle with an incorporated search technology, that was capable to quickly detect a victim with a wide search range in all kinds of situations, also when people don't wear avalanche beacon transceivers. Then, the starting project consisted also in a ground robot connected with the drone, that was able to perform a more accurate search. Once the position of the buried subject has been identified, the drone must place the robot on the surface of the snowpack, and this second device have to identify and clear the airways of the buried person (in order to increase the survival time of the victim). With the aim of carrying this idea forward, during the thesis was studied and discussed the state of the art of avalanche research technologies, in order to understand which technology is most suitable for an aerial research, and which technique is more accurate and can be utilized during the ground research with the robot. For this purpose, it is very important to analyze the search speed, the search time, the search range and the search precision of each research technology. Within the paper, technologies currently in use and technologies under development were discussed.

Chapter 1: Study of avalanche phenomena

1.1 Catastrophic historical events

Historically, avalanches caused a large number of victims. In this section are reported some big events recorded over the years [1].

Plurs, Switzerland, 4th September 1618

On 4th September 1618 the town of Plurs in Switzerland was destroyed by a massive avalanche (fig 1.1-a). Only four people who were not in the village at the time survived. The other 2427 people died.



Fig 1.1-a: Plurs, 4th September 1618 [1]

Wellington, Washington, 1st March 1910

At the end of February 1910, a violent blizzard hit the little town of Wellington, 340 cm of snow fell down. Just after 1 a.m. on March 1st, a slab of snow broke away from the side of Windy Mountain. A big mass of snow (half a mile long and a quarter of a mile wide) fell against the town and the railroad (fig 1.1-b). Ninety-six people were killed, of which 35 passengers, 58 Great Northern employees on the trains, and three railroad employees in the depot.



Fig 1.1-b: Wellington, 1st March 1910 [1]

Tyrolean Alps, 13th December 1916

During World War one, a large number of Italian and Austrian soldiers died in a series of avalanches caused by a mixture of massive snowfall and man-made explosives. An entire barracks was destroyed, burying 250 officers. All avalanche events caused nearly 10000 deaths. The following image shows a representation of the soldiers during that time period (fig 1.1-c).



Fig 1.1-c: Tyrolean Alps, December 1916 [1]

Swiss-Austrian-Italian Alps, 1950-1951

During the winter season 1950-1951 (known as winter of terror), large amount of snows fell down in the European Alps. A series of over 600 avalanches caused more than 100 deaths in Austria, and 92 victims in Switzerland. Also Italy was hit by several avalanches. In total 265 people died. The figure below shows one of these events (fig 1.1-d).



Fig 1.1-d: Swiss-Austrian-Italian Alps, 1950-1951 [1]

Blons, Austria, 12th January 1954

This is considered the worst avalanche in Austria's history. The village of Blons was destroyed by a dry-snow avalanche called the Falv. Nine hours later, another avalanche hit the village, burying 115 people (included a team of rescuers). Totally more than 200 people lost their lives. In the image are represented people during research operations (fig 1.1-e).



Fig 1.1-e: Blons, 12th January 1954 [1]

Yungay, Peru, 31st May 1970

On 31st May 1970, an earthquake off the coast of Peru caused an avalanche on Mount Huascaran (fig 1.1-f). The avalanche moved down at a speed of 100 MPH with a big mass of ice, muds and rocks. It ran nearly 11 miles, burying the towns of Yungay and Ranrahirca. Estimates said that the earthquake killed over 20000 people, including the deaths caused by the avalanche.



Fig 1.1-f: Yungay, 31st May 1970 [1]

Lahaul Valley, India, early March 1979

Over a five day period, a series of snowstorms caused several avalanches that fell down the hills of the Himalayas in Himachal Pradesh state (fig 1.1-g), dumping up to 20 feet of snow on the inhabited valley and causing about 200 deaths.



Fig 1.1-g: Lahaul Valley, March 1979 [1]

North Ossetia, Russia, 21st September 2002

A glacial collapse on Mount Kazbek caused an avalanche that hit Karmadon Gorge, burying several villages and causing 150 victims. Between the casualties there was the Russian actor/director Sergei Bodrov Jr. with his production crew.

Siachen Glacier region, 7th April 2012

On 7th April 2012, an avalanche hit a military base in Pakistan near the Siachen Glacier region, trapping 140 soldiers and civilians under meters of snow. On 29 May 2012, Pakistan declared that the 129 soldiers and 11 civilians were all dead. The image illustrates the rescuers in action (fig 1.1-h).



Fig 1.1-h: Pakistan, 7th April 2012 [1]

Rigopiano, Italy, 18th January 2017

Another catastrophic event, happened on 18th January 2017 in Italy, when a big avalanche buried an entire hotel (fig 1.1-i). The disaster was the deadliest avalanche of the last years in Italy [2]. The avalanche was caused by a combination of heavy snowfall and seismic activity in the Abruzzo region. The snow hit the Hotel Rigopiano with a speed of around 100 km/h. The hotel collapsed almost entirely. Since the road was blocked, rescuers reached the site on skis, on foot and by helicopter. Hundreds of people worked hard until all survivors and bodies had been recovered. During the researches, the rescuers use technology and drones, which helped to identify spots where people might be trapped, and to track body heat, phone signals and other data. After two days of rescue efforts in very critical conditions, rescuers made contact with a group of 11 survivors in an air pocket. Totally, 29 people died in the accident.



Fig 1.1-i: Rigopiano, 18th January 2017 [2]

1.2 Survival curve

When an avalanche occurs, in order to save victims it is important to know the survival time of the people buried under the snow. This factor is very important for the study of a technology able to help the rescuers in the avalanche research. The survival curve (fig 1.2-a) represents the relationship between the minutes along which the people remain buried and the survival chances.

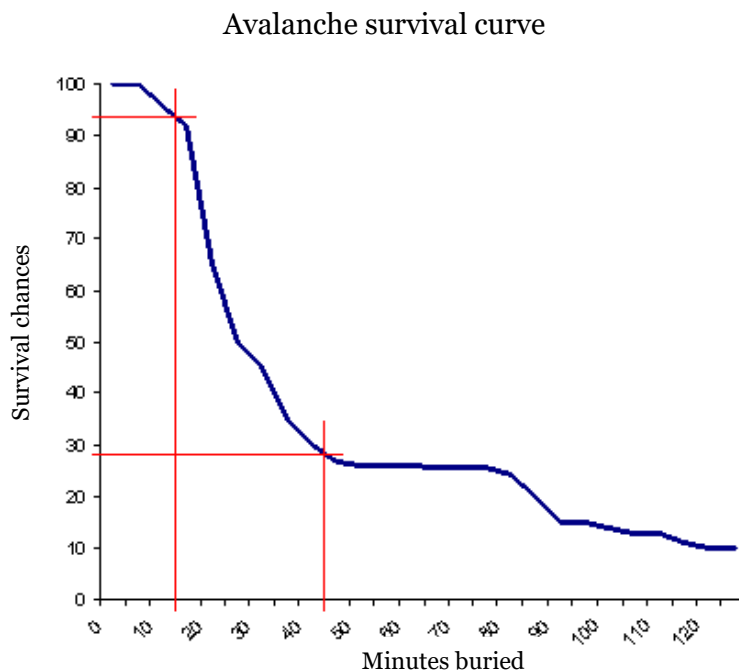


Fig 1.2-a: Survival curve [3]

The data reported in the figure above were collected by the Swiss Avalanche Research Center at Davos for accidents between 1981 and 1991 [3]. The graph shows that of 123 skiers extracted from an avalanche in the first 15 minutes of burial, only 8 were dead and 6 were injured. More specifically, the curve can be divided in four phases:

- Survival phase;
- Asphyxiation phase;
- Waiting phase;
- Rescue phase.

Survival Phase (0 minutes-15 minutes)

In the first 15 minutes the 93% of the buried people are still alive. The most of the deaths occur when the victims hit rocks or trees. During spring, the wet snow avalanches increase the probability to suffocate or crush skiers, but in this period avalanche phenomena is less common.

Asphyxiation phase (15 minutes-45 minutes)

In this interval of time, two thirds of people die from asphyxiation. Excluding the wet snow avalanches, the snow contains a great amount of oxygen and is permeable. If buried people can clear airways and the snow doesn't compress their thorax, they can usually breathe. During this phase, the air either becomes exhausted or the victims' respiration condenses and freezes causing the impermeability of the surrounding snow.

Waiting phase (45 minutes-90 minutes)

In the time interval between 45 minutes and the hypothermia phase, if the victim has found an air pocket is in a phase of relative security, the buried person is able to survive for a considerable period. In this phase, the two causes of death are the slow asphyxia and the hypothermia.

Hypothermia phase (90 minutes-180 minutes)

For the victims of an avalanche, the risk of hypothermia is high, especially when people remain buried for a long period of time. Hypothermia occurs when the body temperature is below 35 °C (the body temperature in normal conditions is around 37 °C). When the body temperature decreases under 29 °C the probability of survival is very low. When the body is cooled, the blood is diverted from the extremities to the vital organs. Afterward, when the body is warmed there is the risk of causing death by thermal shock.

In conclusion, it is possible to say that to survive an avalanche is important to be rescued in the first 15 minutes. After this interval of time, the probability of remaining alive decreases substantially.

1.3 Avalanches causes

In order to prevent avalanche accidents, it's important to know all the factors that can cause this phenomenon. The principal causes are reported below [4].

Weather

The meteorological factors that are the main causes of avalanches are the following:

- Snowfall (principal cause), that weighs down the snow surface and weakens the stability of the snowpack;
- Wind speed and direction, which can create cornices and snow accumulations;

- Temperature, that can change the consistency of the snowpack.

Snowpack

The consistency of the snowpack is an important factor that can be very useful to evaluate the avalanche risk. A report of 93 fatal avalanche accidents in Canada between 1972 and 1991 indicates that the major part of them were caused by dry snow slabs [5]. This is due to the reason that in the last years the number of recreationists (freeriders, ski mountaineers, etc.) is significantly increased, and these skiers search dry snow conditions.

The type of avalanche release depends on the cohesion of the unstable snow. There are substantially two kinds of detachment:

- Point release avalanche: begins in relatively cohesionless snow when a small volume of snow, typically the size of a snowball, slips and drags additional snow in motion forming an inverted “V” below the initial point (fig 1.3-a).
- Slab avalanche: in this case there is a good cohesion in the snowpack, and the release begins as a shear failure in a weak snow layer below the relative cohesive layer of the slab (fig 1.3-b).

The majority of fatal accidents are a consequence of slab avalanches because they are often larger than point releases and are frequently triggered from a point below the top of the avalanche. It is more difficult to evaluate the snowpack stability when the weak layers capable of releasing slab avalanches are deeply buried and underlie layers of old snow. Typically, new snow layers are not as deeply buried as old snow layers, as a consequence slab avalanches involving only layers of new snow are smaller and less devastating than those including layers of old snow.



Fig 1.3-a: Point release avalanche [6]



Fig 1.3-b: Slab avalanche [4]

Cornices

Many avalanches are cornice-triggered [4]. In general, this factor causes avalanches in the following conditions:

- During snowstorm or heavy drifting;
- 24-48 hours after snowstorms or heavy drifting;
- During sudden temperature rise.

The cornices are very dangerous specially for the climbers and the ski mountaineers, because they can pass over it and generate a detachment (fig 1.3-c).



Fig 1.3-c: Cornice example [4]

Terrain

The morphology of the terrain is another factor that must be taken into account during the avalanche risk evaluation. There are many features that characterize an avalanche terrain [4]:

- Slope angle: the major part of avalanches run on slopes between 25 and 45 degrees.
- Ground surface: smooth ground it's more subject to avalanches than rough ground. Nevertheless, when the rough ground is covered by snow the surface becomes smooth and subject to avalanches in presence of new snowfall. The avalanche phenomena is very rare in wooded areas.
- Slope profile: convex slopes are more dangerous than uniform or concave slopes. The point of maximum convexity is a site of tension fracture in the snowpack, which causes slab avalanches. The ridges are usually protected from avalanches.
- Lee slopes: lee slopes are very risky after storm or heavy drifting. In these zones there is a great accumulation of snow that overloads the underlying snowpack increasing the avalanche risk.
- Slope exposure: north, south east and south west exposed slopes are the most dangerous for avalanche detachments. The southern side of the mountain is the sunniest and is very unstable after a snowfall.

Human

All the causes described before are the main factors that generate an avalanche event. However, the major part of these accidents are due to a dangerous environment coupled with a human error.

1.4 Avalanches Characteristics

In order to better understand the avalanche phenomena, it's important to analyze the characteristics of past avalanche accidents. In this paragraph are explored the characteristics of avalanche events happened in the Himalayan region and in Italy. The Alps (data from Italian mountains are very similar to those of the other alpine regions) and the Himalaya are among the most important mountain ranges in the world and a lot of information about avalanche phenomena are available. The data of Italy includes also the events that took place in the Apennines.

Characteristics of avalanches in Himalayan region

In the Himalayan region of India, an average of 30-40 people lost their life every year. In addition to this, there are also considerable material damages. The data reported below are the result of an analysis of the avalanche events in this region between the winter seasons 1970/71 and 2000/01 [7]. The necessity of movement (skiing, winter sports, etc.) and the poor knowledge about the nature of the snowpack on mountains makes the travelers vulnerable to avalanche risk. During the last years, the trend of avalanche accidents is increasing due to a continuous growth of activities related to winter tourism. The reasons of these accidents can be resumed as follow:

- Interaction between man and nature;
- While the past avalanche accidents were the result of a lack of knowledge, the present accidents are due to a high risk that people are ready to take.

Generally the Himalayan slopes are quite steep and without vegetation except in a few areas, which have forest line maximum up to 3000 m. The major part of avalanches that killed people take place in slopes between 30 and 45 degrees. Of these, the slopes of 31-35° are the most dangerous (33% of deaths). The avalanches of small and medium size from slopes between 46-50° cause the 9% of victims. Small proportions of accidents (4%) happen in slope among 25-30°, that often consist in wet snow avalanches. The following graph shows the results of this study (fig 1.4-a).

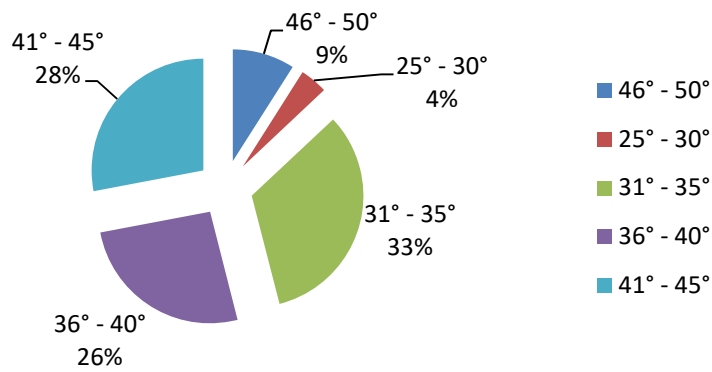


Fig 1.4-a: Distribution of avalanche accidents on slope angle [7]

The slopes exposed to north, south east and south west constitute about 50% of the total avalanche accidents. The southerly slopes are those that receive the maximum sunshine and immediately after the snowfall, when an high number of people are in movement, release avalanches. On the other hand, the northerly slopes remain in unstable state for longer period and they cause the 13% of accidents. The figure below illustrates the distribution of avalanches considering the slope exposure (fig 1.4-b).

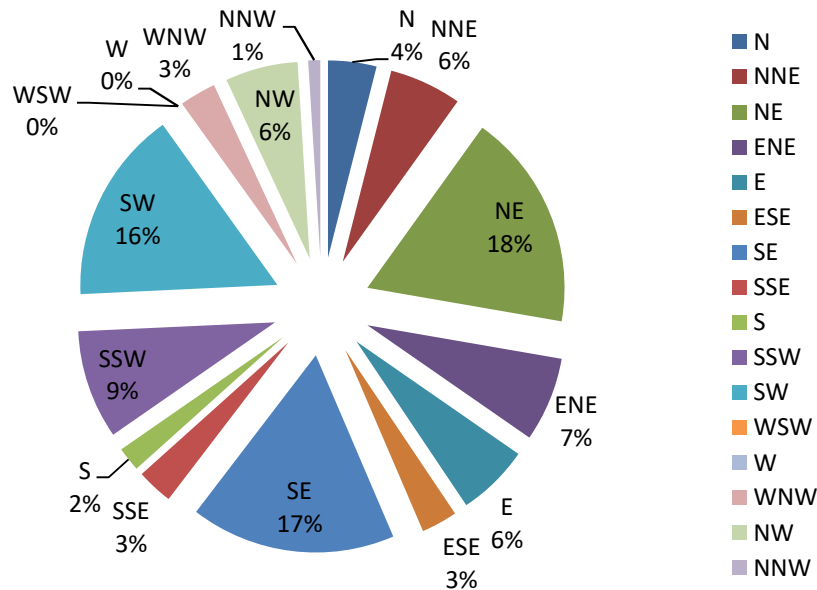


Fig 1.4-b: Distribution of avalanche accidents on slope exposure [7]

During the last years, in India the static accidents (related to avalanches affecting homes) are on decrease and the accidents while people moving is going to increase. The following image (fig 1.4-c) shows the percentage of accidents in Himalayan region when people are on movement, and when they are inside a structure. The data are collected starting from 1970/71 until 2000/01. It is possible to see that the major part of the avalanches hits people during movements.

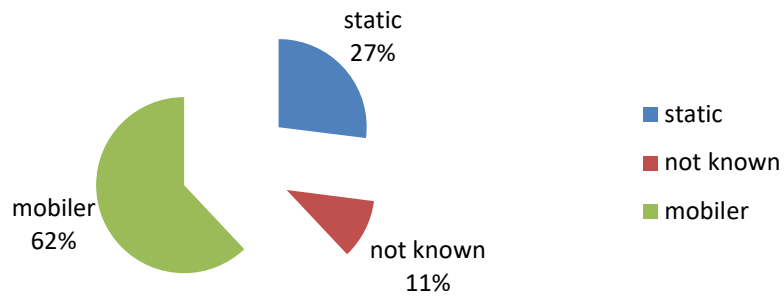


Fig 1.4-c: Percent of accidents while on move and in static mode [7]

The majority of avalanche accidents in Western Himalayan region start from November and almost culminate in May. In Himalaya the three months between January and March constitute the 71% of avalanche events. The 36% of them happen in March. The histogram (fig 1.4-d) illustrates the distribution of the events during the months of the year.

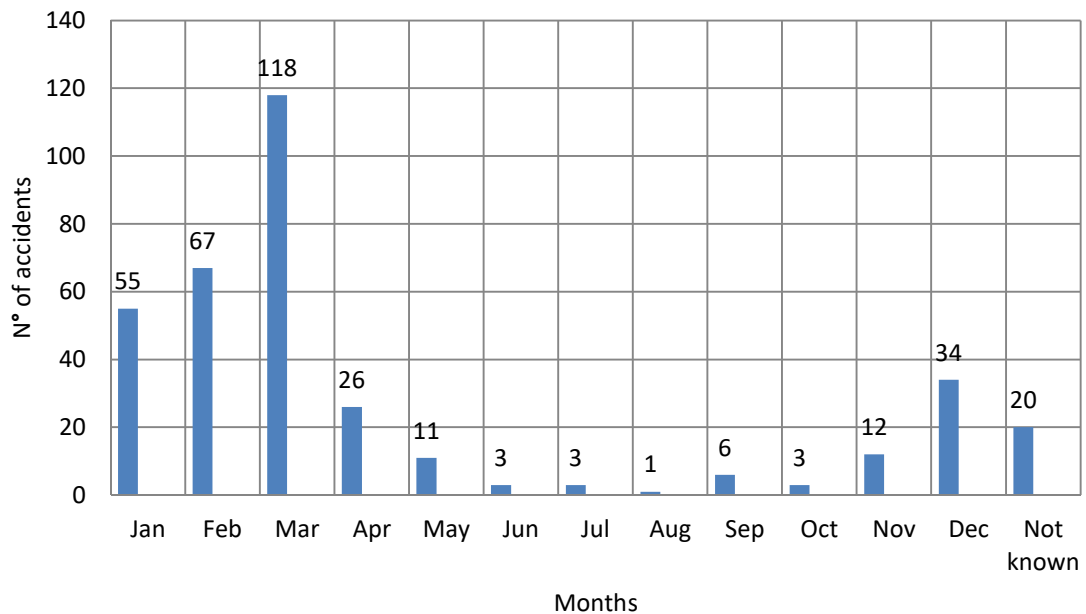


Fig 1.4-d: Monthly distribution of avalanche accidents in Himalaya [7]

The snowfall periods constitute the dominant weather situation when avalanche accidents happen. Among the total accidents, 46% took place during snowfall, 23% during cloudy conditions and 21% during clear weather conditions. Immediately after the end of the storm, the clear weather situation constitute the 64% of the total accidents. During cloudy conditions after the snowfall, take place the 24% of accidents. The next two graphs (fig 1.4-e and fig 1.4-f) show the percentage distribution of the two situations described before inside the Himalayan region.

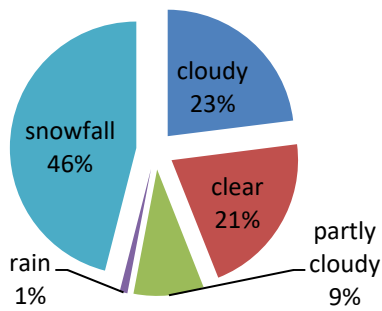


Fig 1.4-e: Weather during avalanche accidents [7]

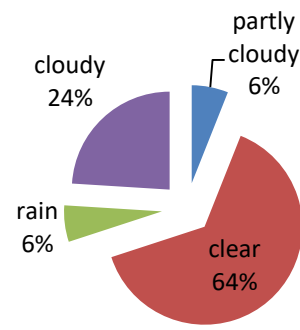


Fig 1.4-f: Weather situation during accident within 24 h of the cessation of storm [7]

The major part of avalanche accidents happen during daytime. Between them, 41% take place in the time interval from 10:00 h to 15:00 h. The other time slot in which there are a lot of mishaps is between 06:00 h and 10:00 h (31%). These two periods represent the time when people are on movement. The results of the study are reported below (fig 1.4-g).

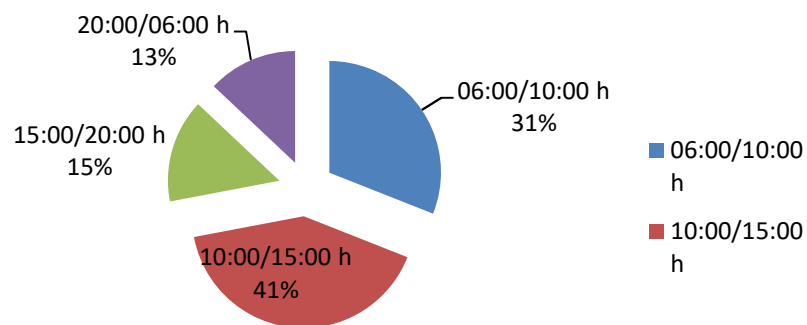


Fig 1.4-g: Timing of avalanches in Himalayan region [7]

The 45% of recorded accidents are caused by warning period. During this period the consistency of the snowpack change and the avalanche risk increase. The figure below (fig 1.4-h) represents the status of registered accidents during warning, non-warning and advisory period.

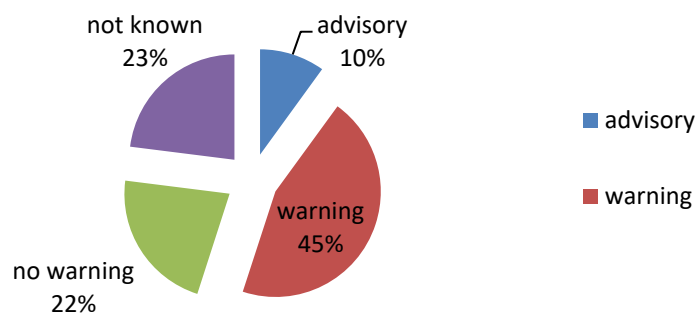


Fig 1.4-h: Avalanche accidents during warning or otherwise [7]

Characteristics of avalanches in Italy

In order to better understand the avalanche phenomena is important to analyze the past events. In this section are reported the results of an investigation conducted by AINEVA. 950 avalanche accidents have been analyzed between 1985 and 2009. Seracs collapses are taken into account only if events caused an avalanche.

During the period 1967-2009, 827 people died in avalanche accidents in Italy [8]. This means that 19 people lost their lives every year. During the last 35 years, 3308 people were caught in avalanche events in Italy. Between them, 691 died (almost 21%) and 2617 survived (about 79%). These data are collected by AINEVA [9]. The histogram (fig 1.4-i) represents the distribution of avalanche deaths from 1985 to 2020 in Italy.

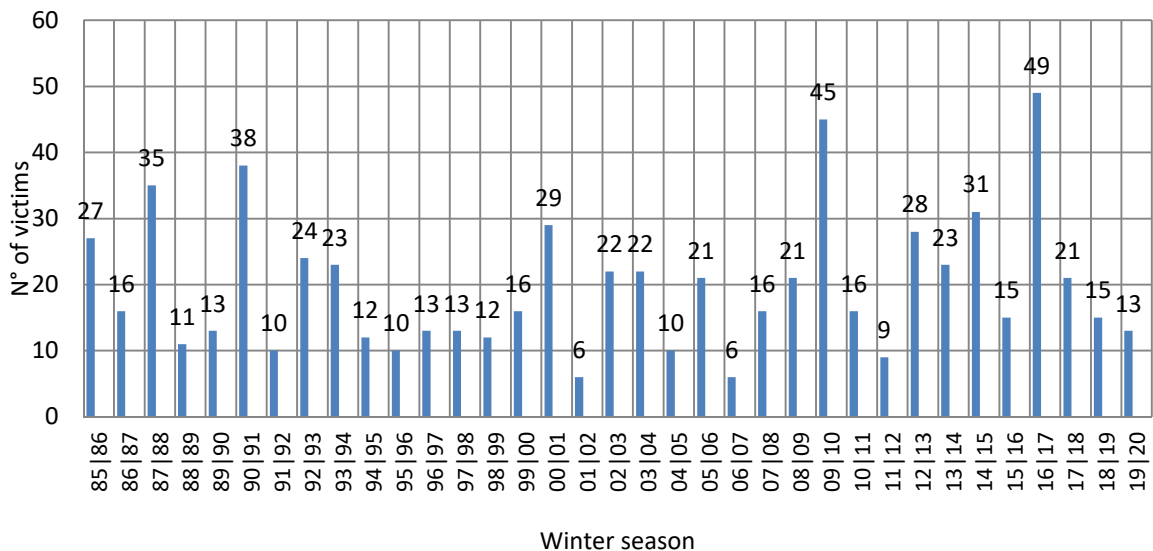


Fig 1.4-i: Avalanche victims in Italy

The avalanche accidents include two main activity categories:

- Recreational activities that include freeride (skier and snowboarder), skiing on the track and mountaineering (ice-fall climbing included);
- Non-recreational activities (including accidents along roads or inside buildings).

In Italy, backcountry touring is the activity with the highest number of fatal accidents (49%), with an average of 9 victims per year. Mountaineering activities constitute the second source of fatalities (19%), as in the last ten years the accidents related to ice climbing and summer ascension are growing. Avalanche mishaps during freeride activities are the third source of accidents in Italy (17%), with a medium of 4 deaths every year. The graph below (fig 1.4-

j) shows the classification of avalanche victims following activity categories.

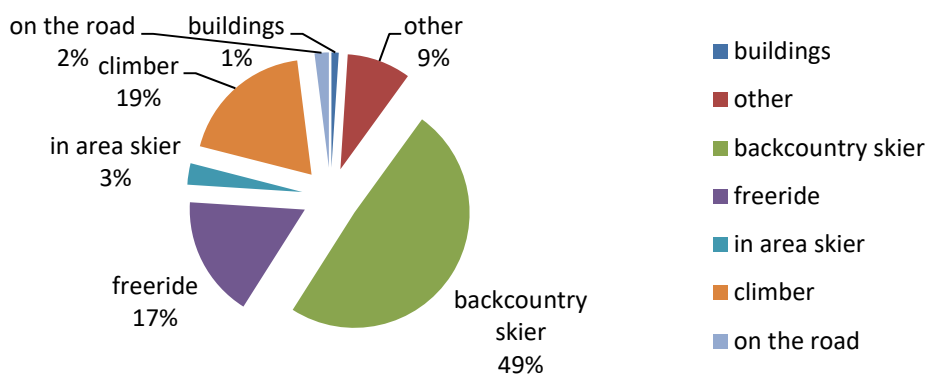


Fig 1.4-j: Avalanche victims distribution following activity categories [8]

In Italy the number of avalanche accidents during the last years is growing. However, excluding the accident of hotel Rigopiano in 2017, the trend of fatalities related to the number of accidents is decreasing. This is related to the development of avalanche transceivers. Nowadays, the accidents involving buildings and along roads are rare. This thanks to the development of avalanche monitoring systems and dedicated structures able to protect the houses.

Considering the total number of Italian avalanche accidents, in 47% of cases all people who were present in the site have been caught, whereas in 53% of cases one or more people have not been trapped by the avalanche. The majority of people caught are not buried (38%) or only partially buried (28%), and the remaining 34% of people trapped by an avalanche are buried. In Italy, the mortality of complete burials is 59%. As figure 1.4-k shows, in 53% of accidents people who are present in the site of the avalanche can rescue their companions. In Italy, the 23% of completely buried people are rescued using an avalanche transceiver. This factor is important to improve the survival rate.

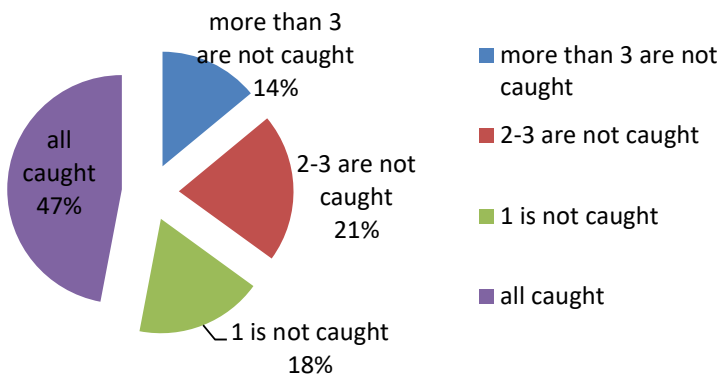


Fig 1.4-k: People who are present at the avalanche time [8]

Avalanche accidents happen in Italy during all months, with an high

concentration between December and April (89%). November and May show a similar number of events. Data on avalanche accidents provide an interesting reflection on how recreation activity has changed the avalanche trend during two decades (1985-1994 and 2000-2009). Along 1985-1994 period, 59% of avalanche events happened between February and April and only 30% between November and January. During 2000-2009 decade, the period between November and January registered the 45% of all avalanche accidents. The histogram below (fig 1.4-l) shows these results.

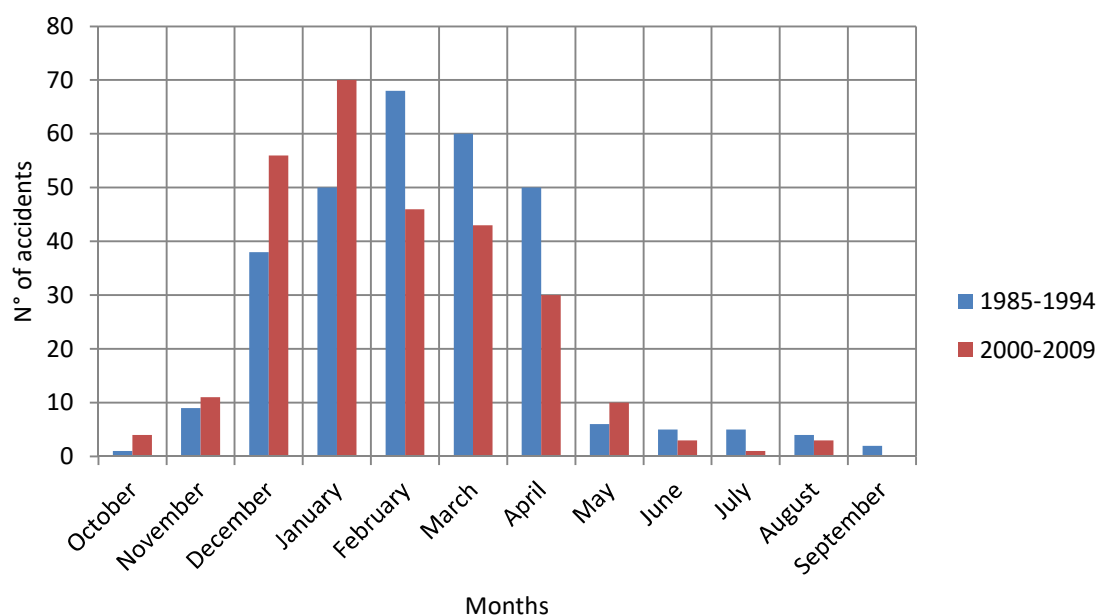


Fig 1.4-l: Avalanche accidents during 1985-1994 and 2000-2009 periods [8]

The major part of recreational avalanche accidents in Italian mountains are located on north west, north east and south east slopes. The mean value of the fracture line is comprised between 2200 and 2500 meters. Mean slope inclination of the fracture line is 37°.

All the avalanche characteristics analyzed in this section (from Himalayan region and from Italian mountains) are similar to those found in the other mountainous regions of the world.

Chapter 2: State of the art of avalanche research technologies

The technology is a device, a thing, a method or knowledge used to accomplish a task [10]. The avalanche rescue needs an approach that combines people, processes and technologies in order to be able to face any kind of situation that an avalanche can cause. The first devices capable of facilitating rescue operations appeared in the late 1960s in the United States. Before that time, the rescue was entirely done by manually probing the area of the avalanche. The avalanche research technologies are the methods and the knowledge that help rescuers to become more efficient and effective. During the last decades, a lot of technologies have been developed. Surviving an avalanche is luck, but technology is an instrument that allows to be in a better place to be lucky. Today avalanche rescue is defined as a structure of different classes and subsystems working together. The opportunity to save a life begins with the intervention of the companions and then continues with the arrival of the professional rescuers. Table 1 illustrates how 282 buried avalanche victims were found during the decade 2003-2013 in the United States [10].

Method	Found alive	Found dead	Total
Attached object or body part	31	29	60
Spot probe	4	9	13
Coarse or fine probe	3	32	35
Rescue transceiver	43	82	125
Avalanche dog	1	18	19
Voice	8	0	8
Other (digging, RECCO)	1	7	8
Found after a long time	-	10	10
Not found, not recovered	-	4	4
Inside vehicle	1	-	1
Inside structure	-	-	0
Totals	91	191	282

Table 1: Rescue method for buried avalanche victims, 2003/04-2012/13

In order to accomplish a good SAR (search and rescue) operation in the favor of buried or injured victims, the rescuers and the companions have to know the five phases of rescue (fig 2-a). In each of these phases the technology plays a key role. Each step must be solved sequentially. The technologies applied to each phase help rescuers to save time increasing the probability of saving lives. The sequential phases are the following [10]:

- NOTIFY rescuers. Using cell phones or satellite emergency notification devices rescuers can be immediately notified. So, when an avalanche accidents happens the companions must immediately call for help.
- LOCATE the victim. Special technologies and methodologies improve the efficiency and the speed of rescuers. The electronics technologies (transceivers) reduce the search time.
- ACCESS the victim. Knowing specialized shoveling techniques can be very important, in order to access the victim as quickly as possible.
- STABILIZE the victim. People involved in avalanche accidents suffer critical injuries. First aid can improve physical comfort, treat injuries and save a life. It is important to clear the airways immediately.
- TRANSPORT the victim. This operation is simple when the accidents happen in the ski area, but can become complicated when the avalanches occur far into the backcountry. This phase often requires the use of the helicopter.

The aim of all rescuers is to identify and use technologies that allow them to optimize the time and the effort spent within each phase of a SAR problem.



Fig 2-a: Avalanche rescue phases [10]

Let's assume that the size of each block indicates the length of time devoted to a phase. It's considered the case of search and rescue of a buried skier who is not equipped with a transceiver (or RECCO). In this kind of scenario, the companions and rescuers who responded by helicopter have to use a probe line to find the victim, increasing significantly the searching time. Furthermore, let's imagine that it is not possible to notify immediately rescuers due to bad phone coverage. In this case, the companions have to search help losing a lot of time precious to find the person alive. In the next figure are shown these two scenarios (fig 2-b).



Fig 2-b: Avalanche rescue phases without transceiver search and in absence of phone coverage [10]

Another source of delay during the rescue operation can be the lack of a shovel between the companions, also if the buried victim is wearing a transceiver. The absence of a shovel increases the access time (fig 2-c).

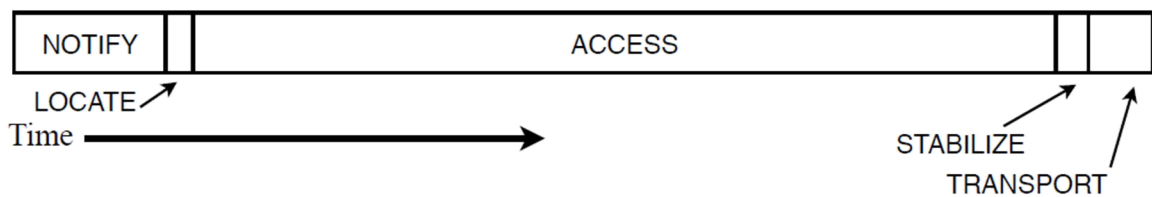


Fig 2-c: Avalanche rescue phases without shovel [10]

In any accidents, if notification phase is performed out of sequence, are generated significant time delays. To notify the rescuers only after finding the victim, causes an important delay in the rescuers arrival, which can have a serious impact on the survival probability of the victim. In order to take the maximum advantage from avalanche research technologies, the recreationalists and the mountain professionals must be familiar with the use of these tools. There are two categories of rescue scenarios and then of detection methods:

- Active targets: all the objects that produce a constant flow of information, detectable through use of suitable sensors. The nature of the information can be different: electromagnetic, sound and so on. These types of targets are detected using active devices (ARTVA, RECCO and more in general transceivers).
- Passive targets: all the objects that don't transmit any kind of data useful for the detection. In this case the research becomes more complex and are used the so called passive devices (GPR, microwave, etc.)

In this chapter is analyzed the state of the art of both technologies. For simplicity, the chapter is divided in two macro areas:

- Technologies currently in use;
- Technologies in phase of development and testing.

Technologies currently in use

In this section is discussed the working principle of the following technologies:

- ARTVA;
- RECCO;
- Smartphone apps technology.

2.1 ARTVA

The ARTVA (or avalanche beacon) is an active device that helps companions and rescuers during avalanche researches (fig 2.1-a). This tool works as transceiver which operates at $457 \text{ kHz} \pm 80 \text{ Hz}$ that is the international standard frequency according to ETSI standard EN 300 718. The wave transmitted by the avalanche beacon is about but not perfectly omnidirectional and consists of a train of low-power pulses. The pulse width is the interval 70-900 ms, with a duty-cycle in the range $10\% \div 69\%$ [12].



Fig 2.1-a: ARTVA devices

The transmitting frequency is able to penetrate through some meters of snow, this is enough to localize the major part of people trapped by avalanches. There are two kind of avalanche beacons:

- Digital: that show an higher performance;
- Analog: that nowadays are not so used.

In order to detect multi targets, the modern digital devices use three antennas and thanks to digital signal processing (DSP) it can recognize direction and distance of the buried transmitter. These digital instruments are often equipped with a radio transmitting at higher frequency (called W-link frequency), which varies between the different countries. European countries utilize a frequency fixed to 869.8 MHz (ETSI standard), instead United states and Canada use frequencies in the range $916 \div 926 \text{ MHz}$ (ETSI standard) [11]. This second transmitter helps rescuers to better differentiate individual transceivers during complex burial situations, when there are multiple victims.

The advantage of this technology is that assists the staff engaged in the research by avoiding that more operators focus simultaneously on the identification of a single subject and they forget the remaining buried victims. Nevertheless, Russia, China and other countries in Asia and Eastern Europe do not allow the use of this higher frequency. Using this frequency it is also possible to detect and transmit vital signs and heartbeat.

When an avalanche accident happens, the ARTVAs of people buried under snow continue to transmit. The remaining other hikers, who are not affected by the avalanche, can switch the avalanche beacon device in the receive mode, and then they can start to locate each buried person, following the indication of the device. The detectable signal is a function of the used ARTVA. Analog and digital devices have a different limit on maximum distance detectable among the two transmitting and receiving antennas, for a good detection. Normally, for a digital avalanche beacon the maximum distance is about 20-30 m. Wireless data of the W-link channel help to find location of buried victims in a faster and more accurately way. When an entire group of skiers wear the ARTVA device, each of them can possibly assume the role of rescuer, with the big advantage to start immediately the research. In order to perform the search along the entire area, where the avalanche has invested people, there is a specific procedure that rescuers have to follow. This procedure take into account the NLOS (no line of sight) of the sensors, that is the distance within which there is the certainty of the detection between transmitter and receiver, considering the worst case [12]. Based on the number of researchers at work, there are two different approaches that must be followed to do a good search:

- If there is only one researcher (fig 2.1-b), he have to move horizontally along all the width of the avalanche, and then he have to move vertically by a distance equal to the double of d (d is the maximum distance within which is possible to detect another ARTVA device).
- If there are two or more rescuers (fig 2.1-c) they must move from the bottom of the avalanche to the top. They have to move parallel and spaced the double of d .



Fig 2.1-b: ARTVA research with one rescuer



Fig 2.1-c: ARTVA research with more rescuers

A minor distance between the rescuers increases the total time of the research. Contrary, a greater distance between the researchers increases the risk to not detect some people. Though the major part of people who wear ARTVA are able to use it, a disadvantage of this technology is the difficulty to utilize it for people that are not experts. If the hikers don't know the research procedure, can become very difficult the rescue of a buried person. However, this technology is currently the most used between the amateur skiers and the mountain professionals.

2.2 RECCO

Since 1973, a less expensive avalanche beacon system has been introduced. The name of this device is RECCO (fig 2.2-a). Its functioning principle is based on a passive reflector [11]. When an electromagnetic radiation affects this instrument, it operates as tuned resonant circuit. Normally, the reflector is placed in the clothes or in the ski boots of the skiers. More precisely, each skier wears two reflectors, one inside the jacket's sleeve and the other inside the ski boots. In comparison to ARTVA, the principal advantage of this application is the absence of battery. However, the limit of this technology is the uncertainty that the skier buried under snow is fully equipped with necessary transceiver. Rescuers use a small hand-held transceiver to capture the signal coming from the resonant circuit. The frequency of the transmitted signal is equal to 917 MHz. The passive reflector retransmits the electromagnetic wave doubling its frequency. Consequently, the receiver used by the rescuer operates at a frequency of 1834 MHz [12]. Knowing the TOF of the transmitted wave and measuring the time between the transmission and the reception it is possible to calculate the distance of the victim. This instrument can capture a buried person in the 20-30 m range, but compared to ARTVA has a lower efficiency. If the victim is not buried under snow the system is able to detect until 200 m. At present, modern transceivers are able to receive both signals ARTVA and RECCO.



Fig 2.2-a: Example of RECCO technology research

RLC resonant circuit

The functioning principle of the RECCO application is based on a resonant circuit that duplicates the transmitted frequency. In this paragraph is analyzed an RLC series resonance circuit [13]. The structure of the circuit is reported in the figure below (fig 2.2-b).

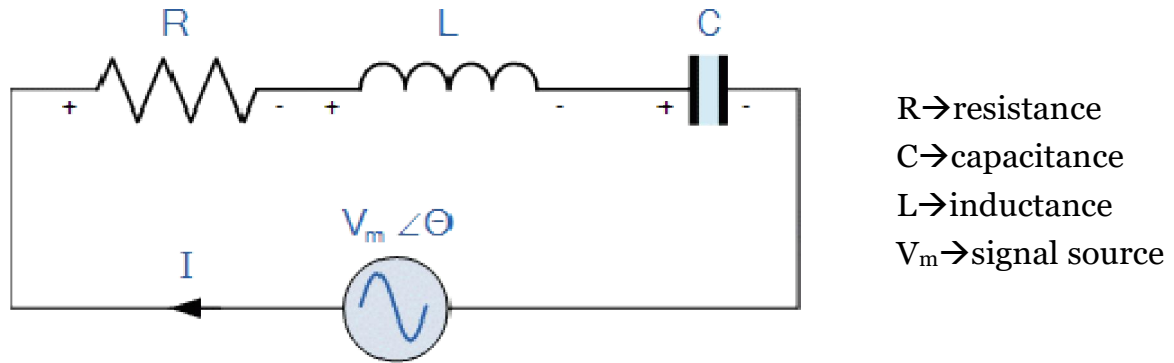


Fig 2.2-b: RLC series resonance circuit

Let's analyze each element of the circuit:

- Inductive reactance: $X_L = 2\pi fL = \omega L$;
- Capacitive reactance: $X_C = \frac{1}{2\pi fC} = \frac{1}{\omega C}$;
- When $X_L > X_C$ the circuit is inductive;
- When $X_C > X_L$ the circuit is capacitive;
- Total circuit reactance: $X_T = X_L - X_C$ or $X_C - X_L$;
- Total circuit impedance: $Z = \sqrt{R^2 + X_T^2} = R + jX$.

From the above equation of the inductive reactance, if either the frequency or the inductance is increased the total reactance value of the inductor would also increase. In DC condition the inductive reactance is equal to zero (short circuit condition), and increasing the value of the pulsation ω ($\omega = 2\pi f$, with $f \rightarrow$ frequency) also increase the value of the inductive reactance. The frequency f and X_L are directly proportional following a linear curve. Contrary, in presence of DC condition the capacitive reactance tends to infinity (open circuit condition), and increasing the frequency X_C tends to zero. In this case the reactance and the frequency are inversely proportional following an hyperbolic curve. The capacitive reactance is negative and the inductive reactance is positive. The values of both reactances depend on the frequency of the supply signal.

In a series RLC circuit there is a particular frequency point where the capacitive reactance becomes equal in value to the inductive reactance ($X_L = X_C$). This point is the so called resonant frequency (f_r) point of the circuit

(fig 2.2-c). This resonance frequency produces a series resonance.

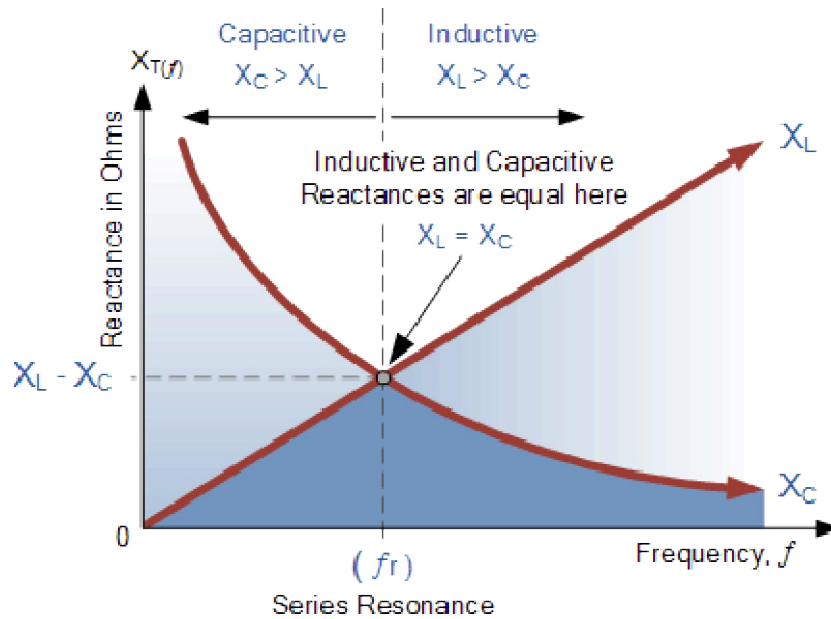


Fig 2.2-c: Resonant frequency point

Electrical resonance occurs in an AC circuit when the two reactances that are opposite and equal cancel each other. The point on the graph above where this condition is verified is where the two reactance curves cross each other. The resonant frequency f_r can be calculated as follows:

$$X_L = X_C \quad \Rightarrow \quad 2\pi fL = \frac{1}{2\pi fC} \quad \Rightarrow \quad f^2 = \frac{1}{2\pi L \times 2\pi C} = \frac{1}{4\pi^2 LC}$$

$$f = \sqrt{\frac{1}{4\pi^2 LC}} \quad \Rightarrow \quad f_r = \frac{1}{2\pi\sqrt{LC}} \text{ [Hz]} \quad \text{or} \quad \omega_r = \frac{1}{\sqrt{LC}} \text{ [rad/s]}$$

Sizing the values of L and C it is possible to calculate the resonant frequency. When the two reactances are equal the only opposition to current flow is represented by the resistance R. So the total impedance of the series circuit becomes just the value of the resistance and $Z=R$.

2.3 Smartphone apps technology

Nowadays, all the people bring a smartphone with them. This can be an important tool that can be exploited during an avalanche accident. A study conducted in Canada during 2013 analyzes three different smartphone apps, which can be used during an avalanche scenario [14]. The applications in analysis are the following:

- Isis Intelligent Rescue System;
- Snog Avalanche Buddy;
- Snowhere.

Snog Avalanche Buddy is only an Android app, while the other two apps are available only for Iphone. The smartphone research system makes use of different kinds of technologies including: cell network, Wi-Fi and Bluetooth. Two apps use also the GPS technology to communicate the position (Snowhere and Isis Intelligent Rescue System). In general, each app uses different types of technologies to communicate the location of the buried person to another smartphone. A disadvantage of this kind of search is that only the identical apps can communicate between them. It is not possible to establish a connection between two different apps. When the apps search another smartphone using Wi-Fi and Bluetooth signals, an increase of the signal strength is directly proportional with the proximity to the victim. Since smartphone has only one antenna, there is a problem with the orientation. The following table (table 2) resumes the basic working principles of these three applications.

App	Primary search	Fine search	Notification
Isis (ios)	GPS location sent by Wi-Fi or cell internet connection (1000 m claimed) or direct via Bluetooth (45 m claimed)	Micro-grid search using Bluetooth	Automatic (using trajectory analysis) alert from victim or manual alert from rescuer
Snog (Android)	Wi-Fi signal strength analysis (50 m claimed)	Same as primary	None
Snowhere (ios)	GPS location sent by Bluetooth (40 m claimed)	Map-assisted Bluetooth signal strength analysis	Rescuer can share location using email or SMS

Table 2: Summary of search technologies used by avalanche search apps [14]

Wi-Fi and Bluetooth signals are strongly affected by transmission through water-based mediums like snow. This means that the signal strength is significantly reduced when the smartphone is buried under an avalanche. The developers report a range of 40/50 m for Wi-Fi/Bluetooth searches. However, this is an ideal range. The effective performance in presence of forested terrain

is reduced to around 12 m. A similar range reduction can be expected in an avalanche environment, when the phone is buried under snow. Like discussed in the previous section, the GPS technology is not sufficiently accurate to guarantee a precise victim location. There is an horizontal position error of about 10 m. The GPS performance also degrades rapidly with burial depth.

The international standards avalanche transceivers transmit and receive at a frequency of 457 kHz. In contrast, smartphones do not adhere to international transceivers standards. The incompatibility with the existing avalanche transceivers and the absence of inter-compatibility between different apps is an high limitation for the development of this technology. Another problem is represented by the battery life of the smartphone. The cold effect substantially reduces the duration of battery. Other factors that limit the battery life are the use of GPS location, Bluetooth and Wi-Fi communications. Recent studies have analyzed the effects of interference on avalanche transceiver performance for a range of devices including smartphones. Based on these studies, the recommendation is that the separation distances between an avalanche transceiver and other electronic devices must be the following:

- Transmit mode (send): 20 cm;
- Search mode (receive): 50 cm.

Since the Wi-Fi and Bluetooth frequencies (about 2.4 GHz) are quite different from the 457 kHz frequency, the risk of interference between these two communication channels is very low. However, interference between Bluetooth and Wi-Fi can occur because the operating frequencies are very similar. In conclusion, it is possible to say that the smartphone app technology has a series of limitations, which have been described in the previous paragraph, that slows its development.

Technologies in development

During the second part of this chapter are analyzed the avalanche research technologies in phase of development, that are the following:

- 4G technology;
- GPS detection technology;
- Breath and skin detection sensors;
- Radar detection technology;
- Ground penetrating radar (GPR).

2.4 4G technology

During 2014, the University of Colorado conducted a study to explore the feasibility of using Fourth Generation Long Term Evolution devices (4G devices) for avalanche research operations [15]. In this test, a 4G LTE device has been mounted on an Unmanned Aerial Vehicle (UAV). Then, it has been installed an app on the smartphone of the victim, that allows to communicate the position of the trapped person to the rescuers. The application also provides information about the strength of the 4G signal. During the experience are assumed the following factors:

- An avalanche has occurred and someone has been buried;
- The avalanche victim has a smartphone with a loaded application;
- First responders have been notified of the avalanche and initiated search and rescue operations;
- First responders have a 4G LTE locator device;
- There is 4G LTE cellular service in the search area.

In order to determine the feasibility of this kind of technology, the 4G signal strength has been analyzed for different snow depths. The mainly reason for which 4G LTE provide good position location capabilities is the fact that it uses a separate technology standard in the radio uplink than from the radio downlink. For this reason is easier to distinguish between signals coming from the smartphone than from those coming from the cell tower station. During the research, the 4G technology has been tested with a smartphone buried under snow and with the device on the surface of the snowpack, so it is possible to compare the measurements. Two devices are needed to send and receive the test signals. Since the buried person is not able to use smartphone to communicate with rescuers, an Android app in Eclipse has been created to

automate the transmission process. Rescuers can receive the position of the buried smartphone by means the application. Furthermore, the app allows to extract measurements for 4G LTE metrics such as signal strength in dBm, signal level, Received Signal Strength Indicator (RSSI) and Reference Signal Receive Power (RSRP). The Signal to Noise Ratio (SNR) was also investigated. The app has been designed to capture position and metrics of the buried device and send them, as an attachment in an email, to the mail account of the device used by rescuers. The buried smartphone sent one email with these metrics every 30 seconds for ten minutes. Thanks to the app, the receiving device automatically checks the received email and shows the results on the screen. During the test they have been used a Samsung Galaxy model EK-GC120 LTE camera with an Android operating system as the sending device and a seven inch Samsung Galaxy Tab 2.0 model SCH-1705 tablet to receive and display the results. The measurements recorded from the device buried under the snow and from the spectrum analyzer have been compared with those previously recorded when the device was on the surface of the avalanche site. The experiment was conducted at Copper Mountain Ski Resort. In order to simulate avalanche debris conditions, a large ten foot high mound of dense snow has been created. Then, the device has been buried at different depths from one foot deep to seven feet deep. The measurements are reported in the following table (table 3).

Depth in feet	Peak transmit power (dBm)	Average transmit power (dBm)
7	-40	-45
6	-35	-40
4	-40	-50
3	-30	-45
1	-20	-35

Table 3: Propagation through snow of 4G signal, Copper Mountain test [15]

The results prove that 4G LTE signal propagates well through the snow, which is very important for a future utilization of this technology in avalanche research rescue. Even if the attenuation in the snow is greater than the attenuation in air, the signal propagates with very little 4G signal loss through densely packed snow.

In conclusion, in the future this app can be modified to transmit latitude,

longitude and altitude data which can help rescuers to detect the location of the victim. The big limitation of this technology is the low 4G signal coverage in mountain environments.

2.5 GPS detection technology

Nowadays, all the smartphones include a GPS sensor. This kind of technology can be useful for detecting avalanche victims. The performance of High Sensitivity Global Positioning System (HSGPS) receivers has been investigated during an experience conducted by Schleppe and Lachapelle [16]. Two different tests have been conducted under avalanche deposited snow at two sites in the Canadian mountains during April 2006. The first test has been performed at Mosquito Creek in Banff National Park (in Alberta). The second one has been conducted at the Fernie Ski Resort in British Columbia. The HSGPS is capable to acquire and track weak signals both indoors and outdoors under a wide range of conditions. When a GPS signal propagates through snow is subjected to attenuation, reflection, scattering, refraction, fading and multipath. The amount of the attenuation depends on the water content of the snow. Wet snow introduces an high attenuation. The GPS signal reflection from the surface of the avalanche debris also contributes to increase the attenuation. Scattering occurs when there is a density variation between the avalanche debris. During the two tests 8 Global Navigation Asset Tracker (GNAT) have been used (fig 2.5-a). Four of them have been equipped with Falcom JP7T GPS modules (GNAT2) and the other four with JP13 modules (GNAT3). During the practical tests, the GNAT systems have been placed in a 5 cm diameter by 12 cm long cylindrical enclosure. Subsequently, the GNAT receivers have been placed in 6 cm diameter boreholes inside the snowpack. In the following sections are reported the results obtained during both experiences.

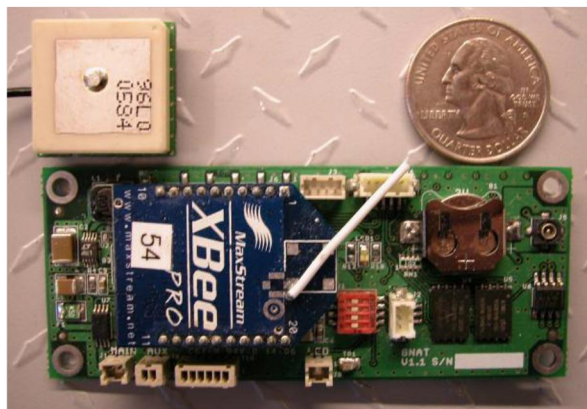


Fig 2.5-a: GNAT circuit board [16]

Banff test

The first HSGPS performance test has been executed on 6th April 2006. The avalanche field was approximately 100 m across and 200 m long. The slope angle was 22°. The major part of the snow surface has been covered by snow and ice blocks. Two 6 cm holes have been drilled in the middle of the avalanche debris. The lower hole contained two GNAT2 receivers placed at depths of 1.53 m and 1 m. A third receiver of this type has been placed on the top of the hole, on the surface of the avalanche. Inside the second hole have been fixed two GNAT3 receivers at depths of 1.45 m and 1.05 m. The other GNAT3 receiver has been placed on the surface of the hole. The following figures show the environment of the test site (fig 2.5-b and fig 2.5-c).



Fig 2.5-b: Banff test site [16]

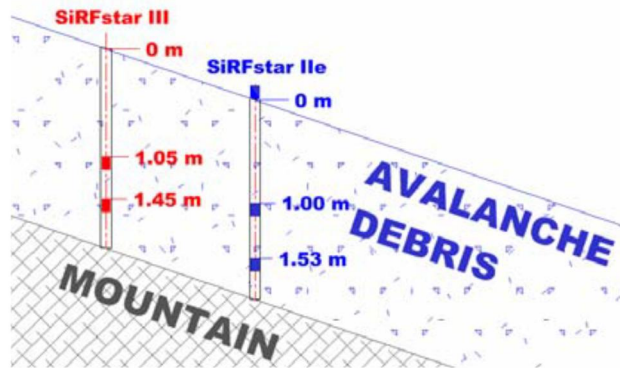


Fig 2.5-c: GPS receivers placement at Banff [16]

Starting from this configuration some GPS parameters have been measured. In the next parts are reported these results.

Satellite availability

During the test it has been measured the number of GPS satellites tracked and used by the receivers. These data are summarized in table 4. It is possible to see that the number of satellites tracked by the GNAT2 system decreases when the depth increases. In contrast, the GNAT3 receiver shows difficulty tracking satellites at a depth of 1.05 m, but increasing the depth the performance improves.

Depth (m)	Satellites tracked		Satellites used	
	mean	stdev	mean	stdev
GNAT2				
0.0	9.0	1.2	8.9	1.3
1.00	7.9	1.3	7.4	1.5
1.53	7.8	1.4	7.0	1.7

GNAT3				
1.05	3.4	4.3	3.3	4.3
1.45	9.4	1.0	8.6	1.5

Table 4: GPS satellite tracking, Banff [16]

Signal attenuation

Comparing the data collected with the buried receivers with those measured by the receivers placed on the surface of the snowpack, it is possible to measure the signal attenuation introduced by the snow. Table 5 illustrates these results. When there are wet snow conditions, the attenuation of the signal increases.

Depth (m)	Mean (dB)	Std dev (dB)
GNAT2		
1.00	8.9	4.6
1.53	9.6	4.6

Table 5: GPS signal attenuation, Banff [16]

The results obtained with GNAT2 receivers are comparable with those measured with GNAT3 receivers.

Position accuracy

The position data have been collected at 1 Hz on each of the active GPS receivers. In order to analyze the accuracy of the GPS systems, the position data have been compared with the precise position measured in absence of snow. The mean horizontal position error is within 2 m except for the GNAT3 receiver buried at 1 m. Height RMS values are larger than the horizontal values by a factor of 1.5. Table 6 shows the mean error and RMS for each receiver.

Depth (m)	Mean (m)			RMS(m)		
	north	east	height	north	east	eight
GNAT2						
0.0	-0.7	-0.4	0.6	1.9	1.5	3.4
1.00	-0.2	-1.9	3.8	7.6	6.0	17.0
1.53	-0.8	-1.4	2.1	9.9	7.4	22.2
GNAT3						
1.05	1.2	12.2	-16.2	6.7	45.0	51.7

1.45	0.4	-0.4	-0.5	3.3	2.3	5.4
------	-----	------	------	-----	-----	-----

Table 6: GPS position error, Banff [16]

The GNAT3 receiver gradually lost track of all satellites over a 30 minute period and in the table above it is possible to observe the bad accuracy of this system. The horizontal position errors of the three GNAT2 receivers are plotted on the following figure (fig 2.5-d). The horizontal axis show the north and the east error, while the vertical axis represents the snow depth of the receiver. In the graph are represented the RMS position errors. It is possible to see that increasing the snow depth of the receiver, the accuracy gets worse.

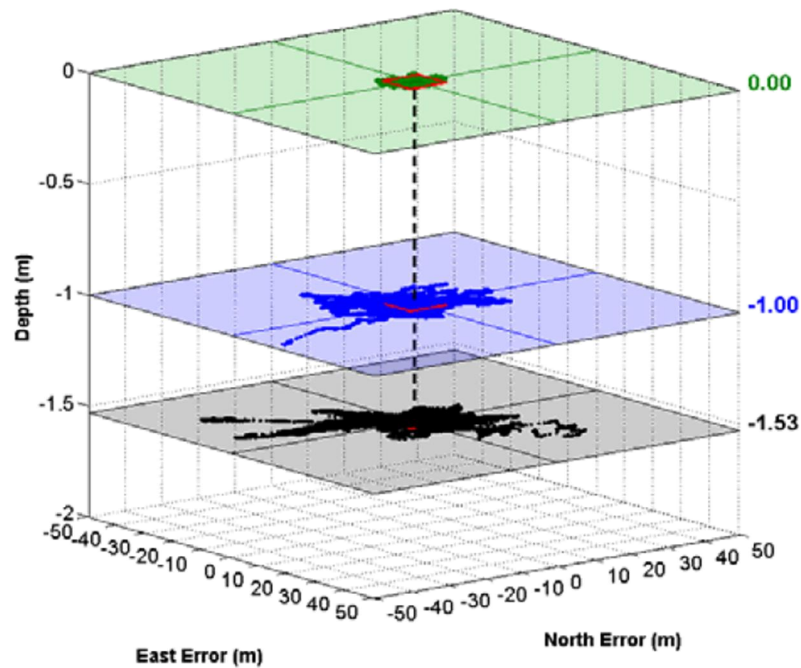


Fig 2.5-d: GNAT2 horizontal position error at various snow depths, Banff [16]

From the figure above it is possible to observe that the horizontal position accuracy is not adequate to quickly locate an avalanche victim. However, the position accuracy can be improved taking advantage of the fact that the victim is not moving. In order to improve the accuracy, the instantaneous least-squares position is computed. Then it is filtered using a simple moving average with a window of 180, 300 and 600 seconds. The results of this computation are reported in the table below (table 7).

Depth (m)	Mean (m)			RMS (m)		
	north	east	height	north	east	height
GNAT2 – instantaneous least-squares						
0.0	0.2	-0.5	4.5	4.4	4.5	11.6

1.00	3.0	-3.6	10.7	11.6	11.6	26.4
1.53	2.3	-4.0	12.4	14.1	10.1	31.6
GNAT2 – 180 seconds moving average						
0.0	0.2	-0.5	4.6	1.4	1.6	5.4
1.00	3.0	-3.7	11.1	7.5	9.1	19.0
1.53	2.3	-4.0	12.4	10.1	7.1	25.1
GNAT2 – 300 seconds moving average						
0.0	0.3	-0.5	4.6	1.2	1.4	5.2
1.00	3.0	-3.7	11.1	7.0	8.4	17.9
1.53	2.4	-4.0	12.4	9.2	6.5	23.1
GNAT2 – 600 seconds moving average						
0.0	0.3	-0.4	4.7	1.0	1.3	5.0
1.00	3.0	-3.8	11.0	6.5	7.5	16.5
1.53	2.6	-4.0	12.4	8.1	6.2	21.1

Table 7: Position accuracy of least-squares solutions, Banff [16]

Increasing the moving average window from 180 to 600 seconds, it is possible to see that the horizontal and vertical positions (RMS values) are more precise. The good results of the 600 seconds moving average is shown in figure 2.5-e. The grey lines represent the instantaneous least-squares position error, while the colored lines indicate the filtered errors (with 600 seconds moving average).

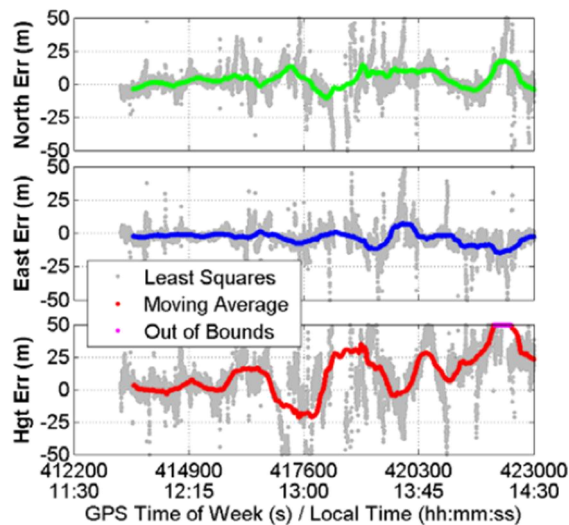


Fig 2.5-e: GNAT2 position error under 1.5 m of snow, Banff [16]

It is easy remarkable that the moving average reduces horizontal positioning errors from over 50 m to less than 20 m.

Fernie test

The second test has been performed on 11th April 2006 at the Fernie ski resort in British Columbia. The avalanche location was composed by debris from at least four avalanches (fig 2.5-f). The slope angle was 19°. The snow depth was over 3 m. The surface of the avalanche site has been covered with 6 cm of new wet snow. The mountain behind the site masked GPS signals. All the GPS sensors have been placed inside a 6 cm diameter hole with a depth of 3.1 m (fig 2.5-g). Three GNAT2 receivers were placed at depths of 1.6, 2.2 and 2.9 m. In addition, three GNAT3 devices were placed at depths of 1.33, 2.0 and 2.68 m. Reference receivers have been placed on the surface of the snowpack.



Fig 2.5-f: Fernie test site [16]

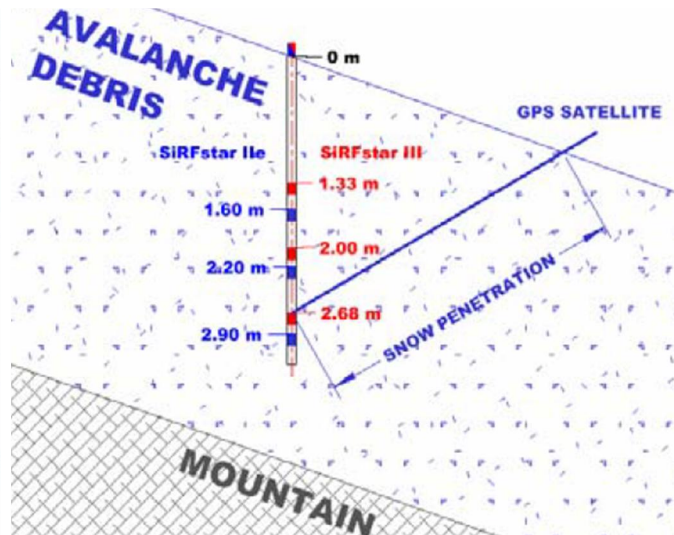


Fig 2.5-g: GPS receivers placement at Fernie [16]

Satellite availability

Also during the second test, it has been measured the number of satellites tracked by the GPS receivers. All the data are reported in table 8. Generally, the number of satellites tracked and used decreases the deeper a receiver is buried. Only the GNAT3 receiver increases the number of tracked satellites at a 2.68 m depth. The GNAT3 sensor shows better performance than GNAT2.

Depth (m)	Satellites tracked		Satellites used	
	mean	stdev	mean	stdev
GNAT2				
0.0	8.5	1.0	8.3	1.0
1.6	6.6	1.1	6.0	0.9

2.2	6.3	1.4	5.3	1.4
2.9	4.7	1.1	3.4	1.9
GNAT3				
0.0	8.9	0.7	8.4	0.9
1.33	8.1	1.0	6.7	1.0
2.0	7.1	1.5	6.1	1.4
2.68	8.0	0.8	7.4	0.7

Table 8: GPS satellite tracking, Fernie [16]

Signal attenuation

Comparing the data collected with the buried receivers against those measured with the surface receiver is possible to evaluate the signal attenuation resulting from the avalanche debris. Table 9 shows the mean GPS signal attenuation of GNAT2 and GNAT3 receivers at different depths.

Depth (m)	Mean (dB)	Std dev (dB)
GNAT2		
1.6	8.9	4.8
2.2	10.7	4.1
2.9	11.8	3.6
GNAT3		
1.33	12.2	6.8
2.0	15.6	5.0
2.68	10.6	5.9

Table 9: GPS signal attenuation, Fernie [16]

Position accuracy

The position has been collected at 1 Hz on each of the GPS sensors. The accuracy of GNAT2 receivers has been compared with those of GNAT3 systems. The mean horizontal position error is better for the GNAT3 receivers, with values below 4 m. Horizontal RMS values for the buried GNAT3 receivers are half those seen with the GNAT2. Generally, the GNAT3 systems show a better accuracy than GNAT2 receivers when they are buried under snow. Since the accuracy is a very important parameter for the avalanche research, this kind of technology (GNAT3 system) is more suitable to accomplish a faster and

more precise search. Table 10 gives the mean error and RMS for each receiver.

Depth (m)	Mean (m)			RMS(m)		
	north	east	height	north	east	eight
GNAT2						
0.0	1.9	-0.2	7.6	3.8	3.8	8.9
1.6	9.0	5.5	12.6	22.1	8.2	29.6
2.2	1.5	10.3	9.1	23.6	23.5	23.8
2.9	-6.2	5.1	15.5	33.3	41.0	53.4
GNAT3						
0.0	-1.8	3.3	0.7	2.2	3.6	3.3
1.33	0.5	1.7	-0.4	11.3	3.7	15.0
2.0	-2.1	3.9	3.2	8.7	9.2	14.8
2.68	-0.5	1.4	1.4	5.2	3.9	9.4

Table 10: GPS position error, Fernie [16]

The horizontal position error for each of the four GNAT3 receivers is plotted in figure 2.5-h. The horizontal axis represent the north and east error and the vertical axis indicates the snow depth.

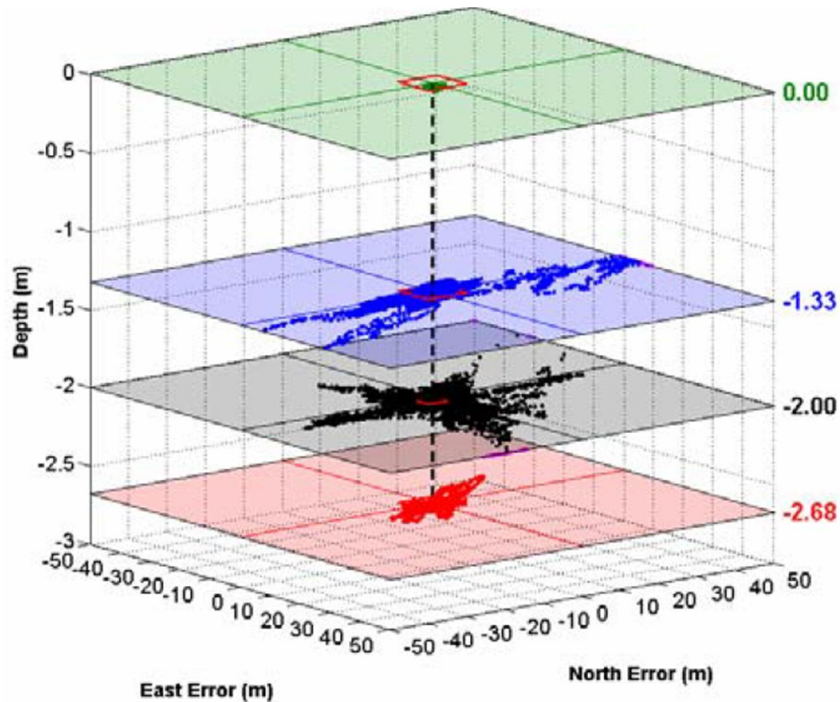


Fig 2.4-h: GNAT3 horizontal position error at various snow depths, Fernie [16]

The receivers buried at 1.33 m and 2.0 m show position errors over 50 m. Increasing the depth of the receivers the accuracy improves. The error related to the surface receiver is less than 5 m. These results are not sufficiently adequate to quickly locate an avalanche victim. In order to improve the accuracy and the search time is possible to compute the instantaneous least-squares positions, and then filter them using a simple moving average with a window of 180, 300 and 600 seconds. This is the same procedure used in the Banff test. The mean and RMS position errors for the instantaneous least-squares and filtered positions are given in table 11.

Depth (m)	Mean (m)			RMS (m)		
	north	east	height	north	east	height
GNAT3 – instantaneous least-squares						
0.0	0.6	3.5	3.7	13.9	11.4	28.7
1.33	1.3	1.1	1.5	17.6	8.1	33.3
2.0	0.9	1.5	2.8	16.3	14.5	21.1
2.68	0.1	0.7	2.5	8.8	5.5	16.5
GNAT3 – 180 seconds moving average						
0.0	0.6	3.6	3.7	3.1	3.8	5.3
1.33	1.2	1.1	1.4	5.4	2.6	9.8
2.0	0.9	1.6	2.9	8.4	7.0	7.6
2.68	0.1	0.7	2.6	5.1	3.0	9.2
GNAT3 – 300 seconds moving average						
0.0	0.6	3.6	3.7	3.0	3.8	5.0
1.33	1.2	1.1	1.4	4.5	2.2	8.4
2.0	1.0	1.6	2.9	7.5	6.0	6.2
2.68	0.2	0.7	2.8	4.1	2.6	6.9
GNAT3 – 600 seconds moving average						
0.0	0.7	3.7	3.8	3.0	3.8	4.8
1.33	1.3	1.0	1.7	3.1	1.6	6.0
2.0	1.1	1.5	3.2	5.9	4.4	5.6
2.68	0.2	0.7	3.1	2.6	1.1	5.2

Table 11: Position accuracy of least-squares solutions, Fernie [16]

As was observed with the Banff test, increasing the moving average window from 180 to 600 seconds improve the vertical and horizontal RMS position errors. The 600 seconds moving average filter reduces the horizontal RMS for the GNAT3 receiver from an instantaneous value of 21.8 m to a filtered value of 7.4 m (at a depth of 2 m of snow). The improvements introduced by the moving average filter are shown in the following figure (fig 2.5-i). The grey lines represent the instantaneous least-squares position error, while the colored lines are the filtered errors. The filter reduces the errors from over 25 m to less than 10 m.

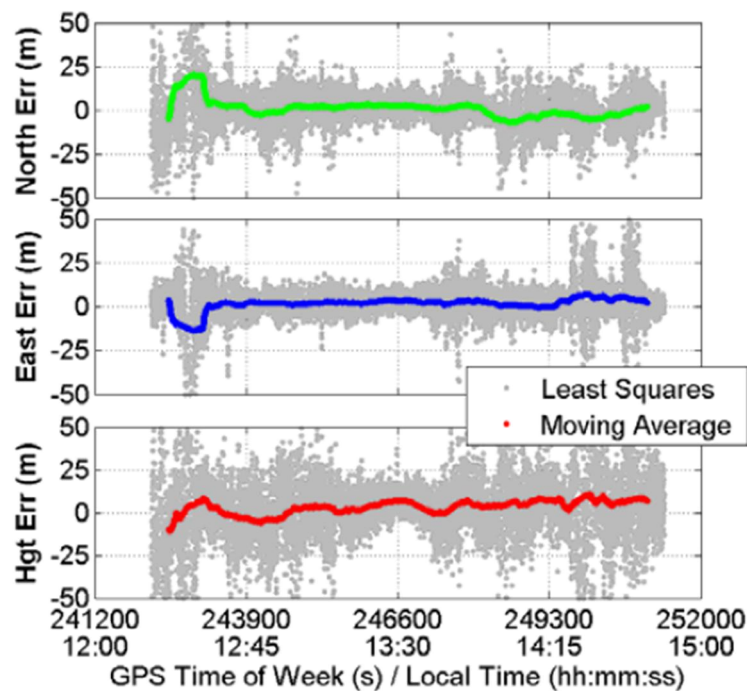


Fig 2.5-i: GNAT3 position error under 2 m of snow, Fernie [16]

Discussion of the results

These two experiences have verified that HSGPS receivers are able to identify weaker GPS signals through 15 m of deposited snow. Signal attenuation of approximately 1.8 dB per meter of snow depth has been measured. The GNAT3 receiver offers the best performance considering the accuracy of the research. However, this kind of technology is not so precise to guarantee a perfect localization. The position error is still too high. A possible solution can be the combination of this technology with a more accurate technique. The big advantage of the GPS is the large research field, and the research time is quite short.

2.6 Breath and skin detection sensors

During a study at Zurich university [17], a compact and orthogonal sensor array has been designed to detect the substances emitted by breath and skin. This kind of sensor is able to detect the concentration of acetone, ammonia, isoprene, CO₂ and humidity. All these factors indicate the presence of vital signs and they can be useful during an avalanche research. The array is composed by three nanostructured metal-oxide sensors (Si-doped WO₃, Si-doped MoO₃ and Ti-doped ZnO), and commercial CO₂ and humidity sensors. Following an earthquake or an avalanche event, many victims can be entrapped under collapsed buildings or snow. Dogs are very important for this kind of research, with their high ability to sniff entrapped humans from their scent. The purpose of the sensor array described before is to improve the efficiency during the researches, and its working principle can be compared to a dog used during avalanche accidents.

The Si-doped WO₃, Si-doped MoO₃ and Ti-doped ZnO sensors have a high sensitivity to detect concentrations of acetone, isoprene and ammonia respectively. These three substances are mainly emitted by skin of a human body. However, the CO₂ and RH (humidity detection) sensors are used to identify signs emitted by human breath. In order to study the performance of the sensor array described before, an experiment has been conducted. During the experience, nine volunteers have been enclosed individually inside plethysmographic chambers, to simulate entrapment conditions. The test has been separated in two phases:

- Skin emission: during the first 60 minutes only skin-emitted volatile compounds have been targeted. In order to avoid breath emission during this part of the test, the subjects freely inhaled and exhaled room air by means of a two-way non-rebreathing valve of a silicone head mask connected with two tubes which communicate with the outside of the room;
- Skin and breath emission: during the second 60 minutes the volunteers breathed directly in the chamber, in order to also measure the breath emissions.

For each of the volunteers have been conducted the two tests described before and the results have been collected. The sensors were heated up to 350 °C (Si-doped WO₃), 400 °C (Si-doped MoO₃) and 325 °C (Ti-doped ZnO) for optimal sensitivity and selectivity to acetone, isoprene and ammonia. All the volunteers were sitting on a chair during the measurements. The figure below (fig 2.6-a)

illustrates the test configuration and the array design of the sensors.

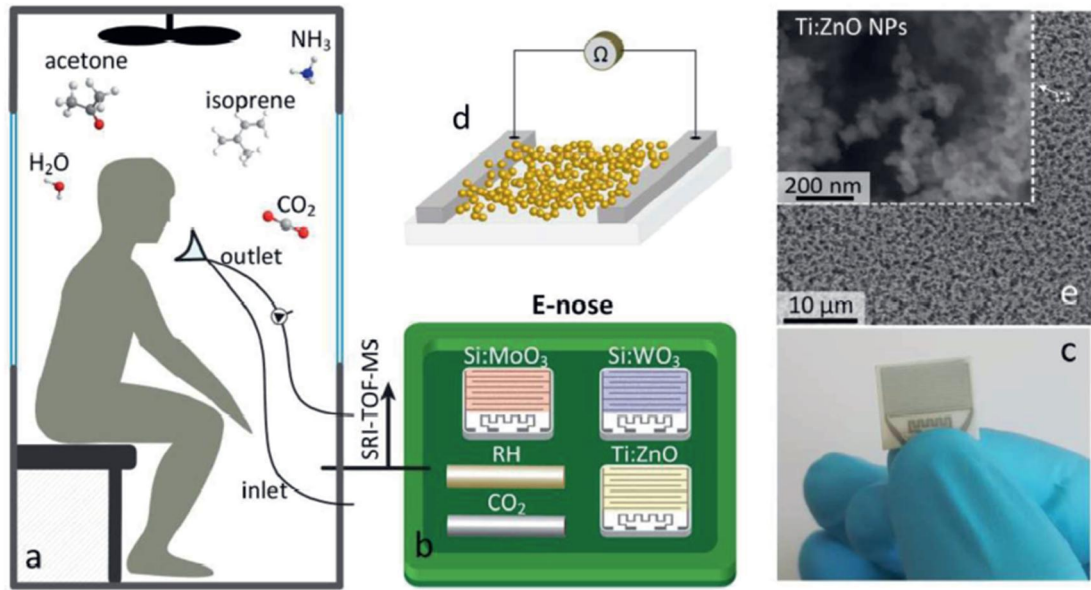


Fig 2.6-a: a) Volunteer entrapped in the chamber. b) Sensor array. c) Image of a single sensor. d) Nanoparticles form a porous sensing network as shown by (e) scanning electron microscopy. [18]

Figure 2.6-b shows the sensor array estimated acetone, isoprene, ammonia, RH and CO₂ concentration profiles of five volunteers when measured every 20 minutes.

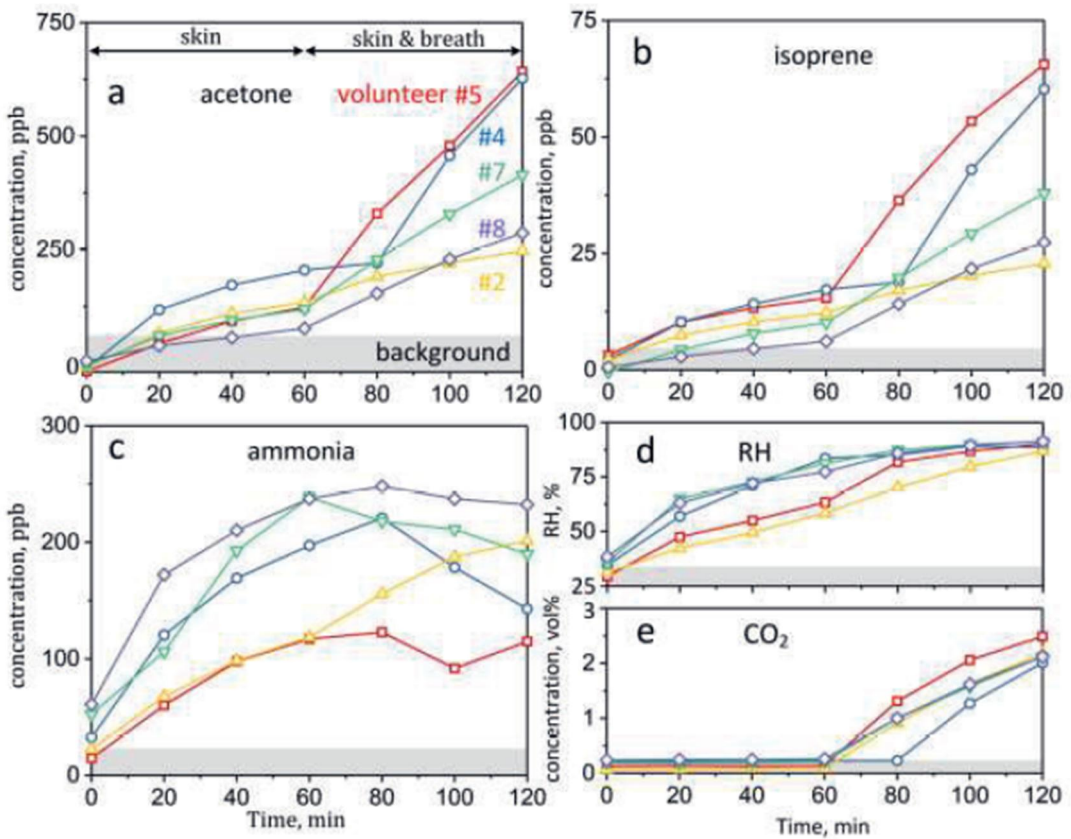


Fig 2.6-b: Sensor array measurements [18]

From the graphical representation is possible to see that acetone, isoprene and CO₂ concentrations, measured in ppb (part per billion), change only little during skin emission while they increase significantly during breath emission. On the other hand, ammonia and RH concentrations increase during skin emission and are almost constant during breath emission. In conclusion, it is possible to say that the sensor array is able to recognize human presence, also after very short entrapment time. So this kind of technology could be incorporated into portable detectors to support first rescuers to find trapped victims after avalanches. In order to satisfy the avalanche research requirements is important to improve the search time speed.

2.7 Radar detection technology

Classical detection technology makes use of borescopes and geophones for search and rescue people trapped under debris and avalanches. An improved approach to this issue can be the use of the following radar systems [19]:

- UWB (ultra wide band): this system is used to detect vital signs, and consists in the transmission of a very short wide band pulse.
- CW (continuous wave): this detection system is applied for measuring movements like respiration.
- FMCW (frequency modulation continuous wave): this is an improvement of CW including a frequency modulation. The big advantage of FMCW radar systems is that allow the detection of the distance from the target (i.e. buried people).
- Pulse radar systems: they are used to search people carrying electronic RF-devices. Frequency filters of these devices can be exposed to a radar pulse near the resonance frequency of the filters. At this point it is possible to detect an echo, enabling the localization of a device and probably its owner.

Generally, pulsed radar systems use UWB signals. Nowadays, both UWB and CW radar systems are used for the detection of buried people. In this section are described these different technologies.

Radio frequency device detection

Actually, all people carry at least one technical RF device with themselves. Typical electronics elements that are found near avalanche victims are radio controlled watches, mobile phones, headsets and GPS devices. Modern electronics applications are equipped with a multiplicity of radio interfaces like

W-LAN, Bluetooth and GPS which increase the probability to detect at least one of these interfaces. The table 12 illustrates the frequencies at which the radio interfaces operate.

Standard	Frequency ranges in MHz
Mobile communication	880 - 915
	925 - 960
	1710 - 1785
	1805 - 1910
	1930 - 1990
	2110 - 2170
Bluetooth	2402 - 2484
W-LAN	5150 - 5725
GPS	1227.60
	1575.42

Table 12: Frequency bands of RF front-ends found in modern RF devices [19]

When an avalanche accident occurs, there is a good probability that the electronics devices are located next to a buried person. Independently from the fact that they are still working or not, it is possible to detect them. Pulse radar systems are used to locate these electronics applications. The following figure (fig 2.7-a) represents a possible schematic structure of a communication between a buried device and a RF transceiver used by the rescuers.

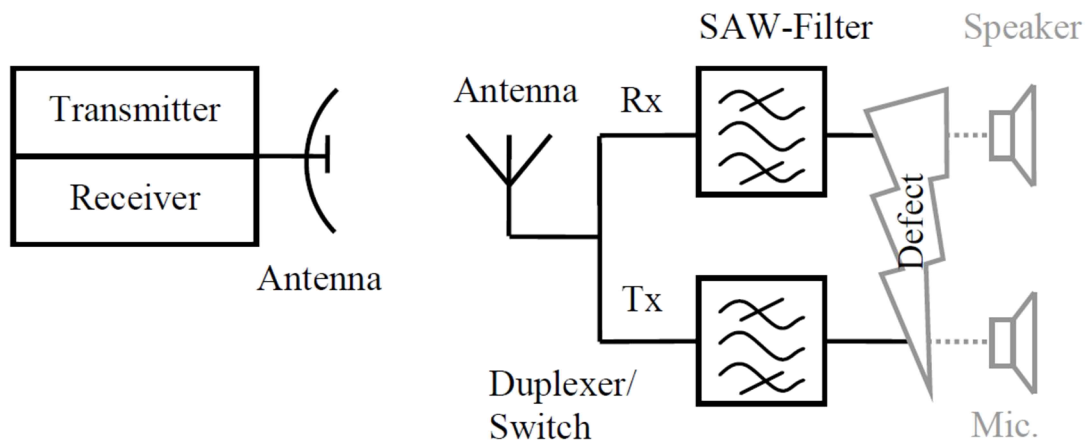


Fig 2.7-a: Schematic setup for the detection of defect mobile phones [19]

Using the radar system on the left side of the picture a radar pulse is sent to a buried and broken device. The antenna of the phone receives the impulse, and the signal is forwarded through the duplexer to the filter that selects between the frequencies contained in the signal. The quality factor Q of a mobile phone RF filter is typically between 3000 and 5000. If the spectrum of pulse lies in

the range of RF filter bandwidth, the energy is stored in the filter. When the transmission impulse is switched off, the stored energy generates a RF echo which propagates through the duplexer and the transmitting antenna of the smartphone. Finally, the radar of the rescuer can detect and evaluate the RF echo. The graph (fig 2.7-b) below shows the time characteristics of a transmitted pulse and its corresponding received echoes. Switching off the impulse, there is an evident difference between the resonant and the non-resonant case.

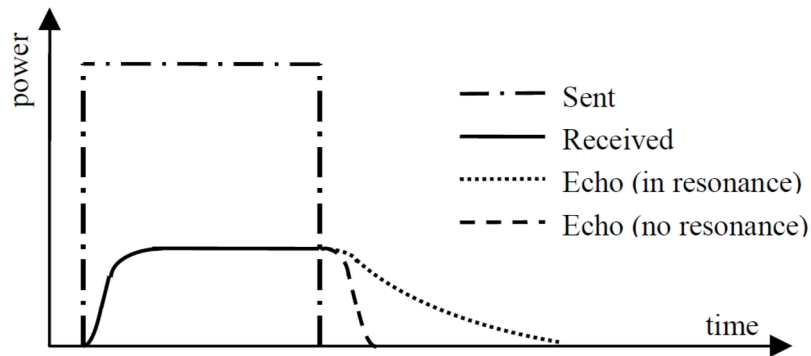


Fig 2.7-b: Time characteristics of a transmitted received signal of a RF filter [19]

In order to accomplish a good research of mobile RF devices, all the frequency ranges illustrated in table 12 must be scanned for such resonance echoes. The old device architectures have at least one direct connection between the antenna and the filter. If the modern RF devices are switched off or are defective, the FET switches (built up using field-effect transistors) are open and they act as attenuators. In this case is very difficult to detect the echo signal at the receiver of the radar system. However, increasing the transmitting power (without exceeding the danger limit for humans) it is possible to solve this problem. Figure 2.7-c shows two measured frequency responses of mobile RF devices in the range 875 MHz to 965 MHz.

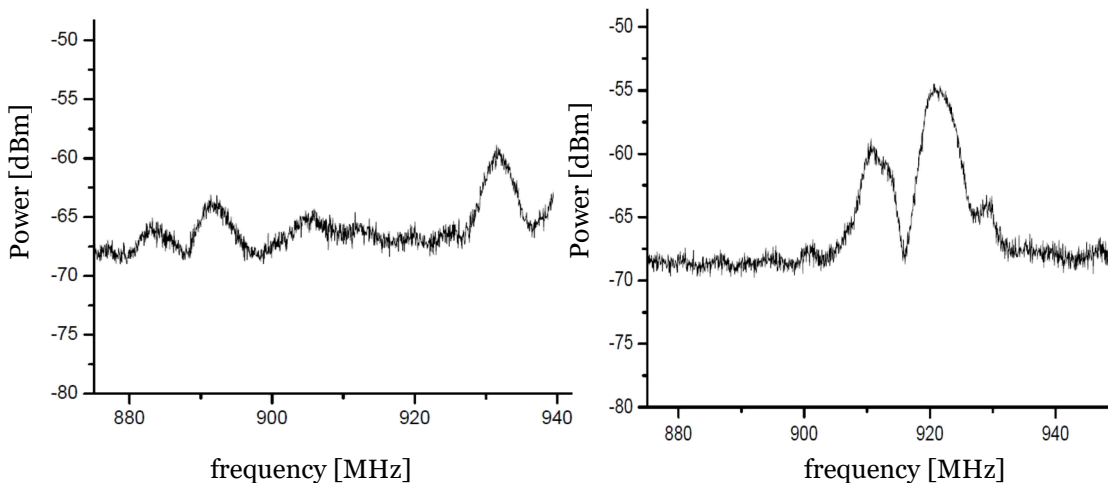


Fig 2.7-c: Frequency characteristics of received signals from two different defect devices [19]

Detection of heartbeat and breathing using microwave transceiver

The potential of a continuous wave transceiver to detect breathing and heartbeat has been tested in a scenario that replicated an avalanche accident [20]. Microwave propagation becomes difficult in inhomogeneous medium like rubble, because local discontinuities can act as backscatterers. Since snow is an homogeneous medium, it is possible to use microwave transceivers to detect vital signs. The device used during the experience is a microwave coherent transceiver that irradiates a monochromatic wave by two directional antennas (transmit and receive). The radiated microwave power is equal to 10 mW with 12 dB antenna gain. The receiver detects the in-phase (I) and quadrature (Q) components of the backscattered wave. This signal can be represented in the I-Q plane, where both amplitude and phase are sensitive to movement on the order of a fraction of wavelength. Figure 2.7-d illustrates the block scheme of the transceiver used during the experimental operations.

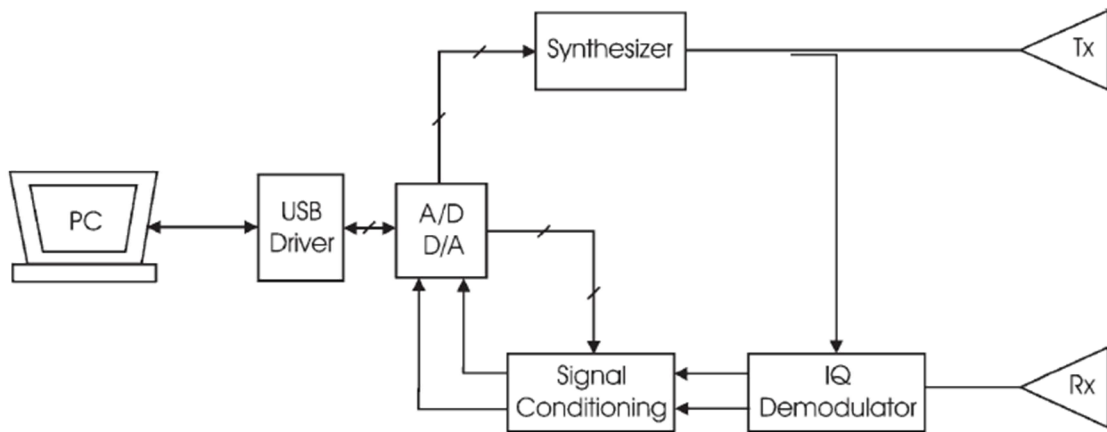


Fig 2.7-d: Block scheme of the microwave transceiver [20]

The phase-locked loop synthesizer works at 2.42 GHz frequency. This is a compromise between the increased penetration depth of lower frequencies and the increased phase shift due to breathing and heartbeat at higher frequencies. The functioning of the transceiver has been tested in two different experiment setups:

- Snow barrier with thickness of 180 cm;
- Igloo with thickness of about 120 cm.

The test field configuration of the second experiment is shown in figure 2.7-g. In order to better detect the heartbeat was asked to the volunteer to hold his breath for few seconds (apnea). The breathing movement detected by the transceiver shows a frequency rate of 0.24 Hz. Instead, the heartbeat frequency is 1.08 Hz. The results are reported in the following graphs (fig 2.7-e and fig 2.7-f).

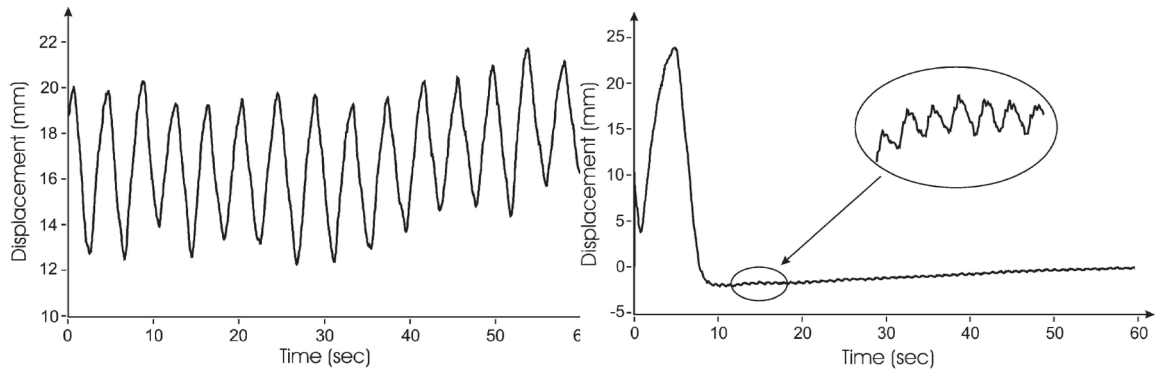


Fig 2.7-e: Breathing detection [20]

Fig 2.7-f: Heartbeat detection [20]

The measures of both experiments are very similar. These two experiences demonstrate that a continuous wave transceiver is able to detect breathing and heartbeat through a snow barrier of more than one meter. The limitation of this technology can be the detection in case of very wet snow. In the analyzed scenarios the snow was relatively dry. The good functionality in presence of wet snow and snow thickness of several meters must be proven.

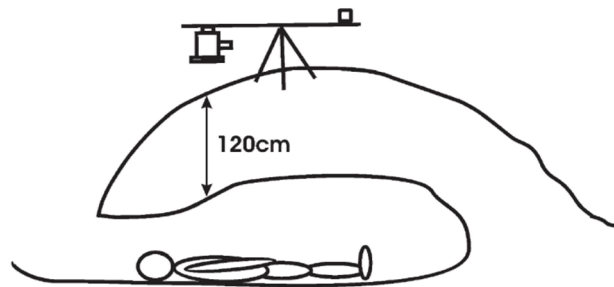


Fig 2.7-g: Experimental setup of igloo [20]

Life signal detection using an on-chip solid state microwave sensor

During 2014, another technique for measuring amplitude and frequency of vital signs has been developed and tested. The experience has been conducted by Chinese researchers [21]. The technology consists in an on-chip solid state sensor integrating a semiconductor microwave sensor and a split ring operating at a resonance frequency of 4.2 GHz. The lock-in amplifier performs the real-time measurements. The advantage of this application is that it is more portable than the one described above and it has a user friendly DC output. In conventional microwave life detection systems, the in phase (I) and the quadrature (Q) of the reflected wave are measured using vector network analyzer or an equivalent electronic circuit. The frequency of breathing and heartbeat is then detected by performing clutter cancellation and amplitude/phase reconstruction. In this case, a split ring integrated solid state sensor is used with a lock-in amplifier to detect the reflected microwaves

coming from the subject in analysis. This kind of amplifier is able to detect very low frequency signals inside an extremely noisy environment. The proposed approach can detect vital signs of subjects 40 m away from the microwave transceiver. The figure below (fig 2.7-h) shows the measurement scheme.

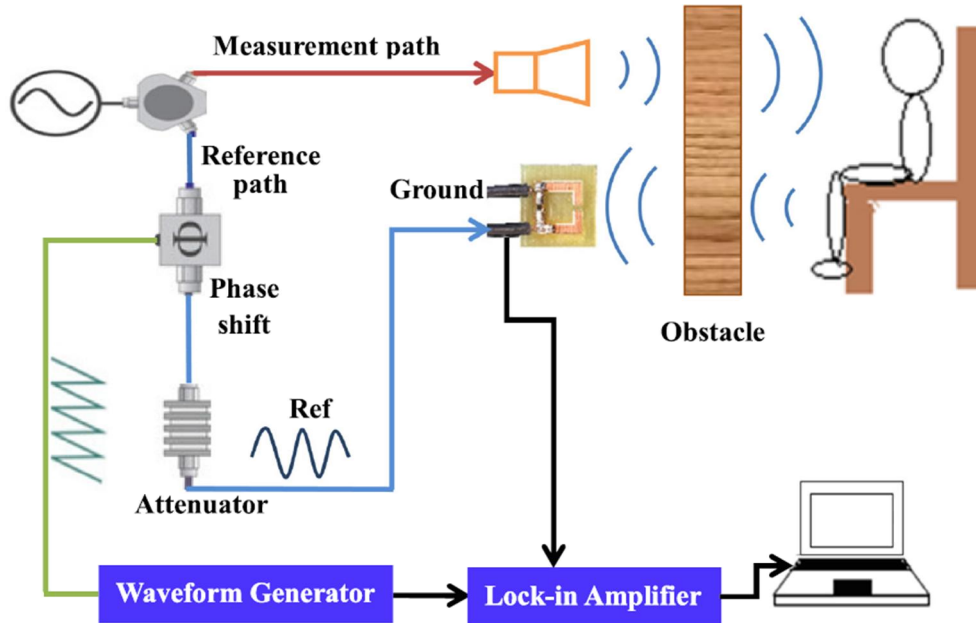


Fig 2.7-h: Measurement scheme using on-chip solid state microwave sensor [21]

In order to perform real time measurement of the microwave phase and amplitude is used the phase resolved technique, which is based on the interference principle. Two different experiences have been done. The first one sitting down the volunteer on a chair without barriers, and the second one placing the person behind a piece of plywood.

Referring to the scheme above, the microwave signal exits from the generator and it is split into two parts using a microwave power divider. The first part of the electromagnetic output goes along the measurement path to the horn antenna from which it is transmitted and subsequently reflected by the target situated behind the obstacle. The second part of the electromagnetic field from the power divider travels along the reference path that includes a voltage controlled phase shifter (which is controlled by a waveform generator) and an attenuator of 40 dB. The waveform generator produces a sawtooth wave at frequency $\omega_v = 10 \text{ kHz}$. Then, the microwaves coming from both the paths, with frequencies equal to ω and $\omega + \omega_v$, undergo interference at the split ring integrated sensor. At this point, a down-converted signal with frequency ω_v is produced. The output voltage generated by the microwave sensor is given by:

$$V(t) \propto |E_{reference}| |E_{reflected}| \cos(\Delta\phi - \phi_1 - \omega_v t) \quad \phi_1 \rightarrow \text{phase reflected wave}$$

This resultant low frequency signal is sent to the lock-in amplifier for the measurement of amplitude and phase. The two quantities measured by the lock-in amplifier correspond to the phase difference between the reference and the reflected wave, and the product of the intensities of these two waves. Both the measured quantities depend from the distance of the subject.

The detection of breathing and heartbeat in absence of an obstacle is clearly evident. However, these parameters are detectable also with obstacles between the microwave transceiver and the person. The figure 2.7-i shows the amplitude and phase measurements in the presence of an obstacle. It is possible to see that the breathing signal is stronger than the heartbeat signal. This is due to the fact that the amplitude of the oscillations related to breathing is larger than that due to heart beating and hence it introduces a larger phase difference. It is also remarkable that the phase method is more sensitive and has an higher resolution than the magnitude method.

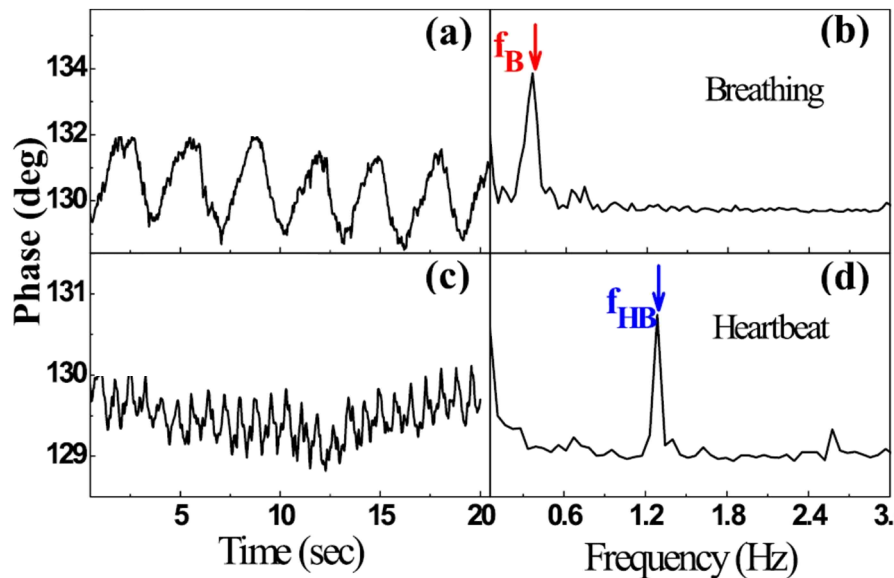


Fig 2.3-i: Breathing and heartbeat detection using solid state microwave sensor. a) phase measurements for breathing; b) FFT result for breathing; c) phase measurements for heartbeat; d) FFT result for heartbeat. [21]

The frequencies of breathing and heartbeat can be deduced by performing a Fast Fourier Transform (FFT) on either the complex phase or the magnitude of the resultant microwave. Performing a FFT analysis on the phase data measured in case of obstacle, it is possible to determine the frequency of breathing signal (0.3 Hz) and the frequency of heartbeat (1.3 Hz). This means that the measured breathing rate is 18 breaths/min and the resulting heart rate is 78 beats/min.

In order to determine the optimal power to detect the vital signs, an additional experiment has been performed. More in details, the microwave power has been gradually changed between 25 dBm and -10 dBm. The figure below (fig 2.7-j) illustrates the results of the experience described before. The figure clearly shows that even though the breathing signal can be seen from all the microwave powers in analysis, there is a noise increase when the microwave power decreases. It is possible to detect a breathing signal (at 30 dBm power) even if the target is 40 m away from the microwave sensor used in the experience. The dynamic range to detect the breathing signal is about 40 dB (from 30 dBm to -10 dBm microwave power). Since the change in phase due to heartbeat is smaller, it is possible to observe a clear signal when the microwave power is between 30 dBm and 0 dBm.

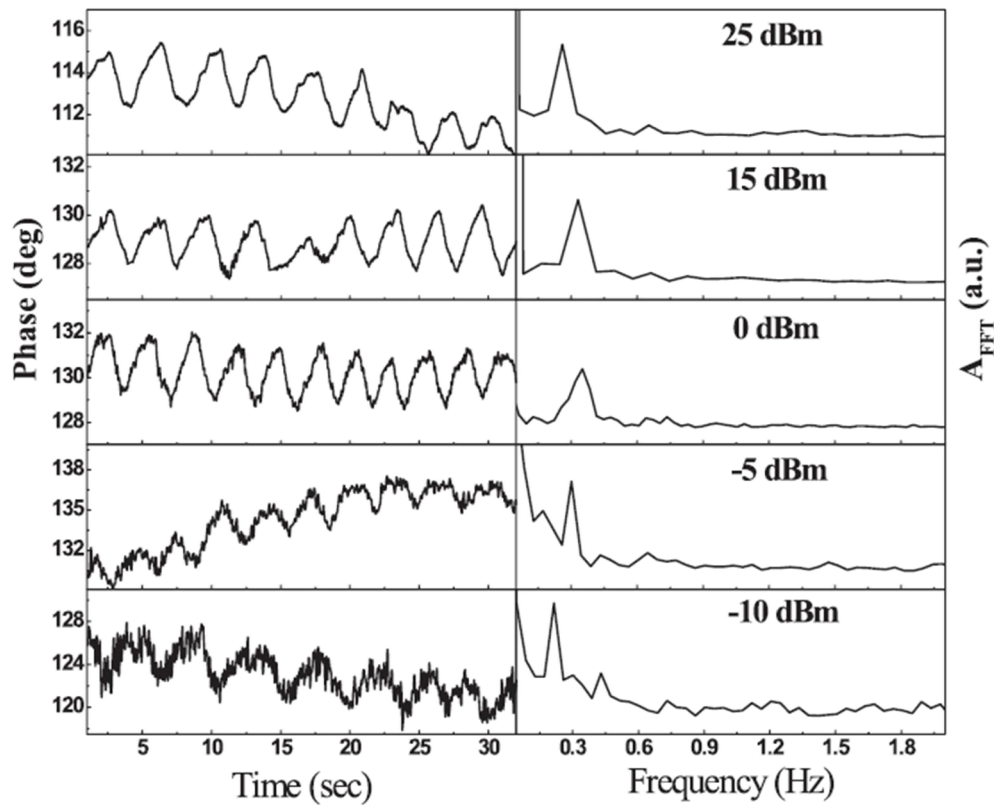


Fig 2.7-j: Breathing signals and corresponding FFT results for different powers [21]

Distance detection using microwave transceiver

The microwave transceivers described before only provide the information about vital signs of a victim, but don't provide any kind of information about its distance to the antenna. In order to solve this limitation it is possible to use a frequency modulation technique [19]. The FMCW is characterized by a time-dependent change of the transmitted frequency. The block diagram of this application is shown in figure 2.7-k.

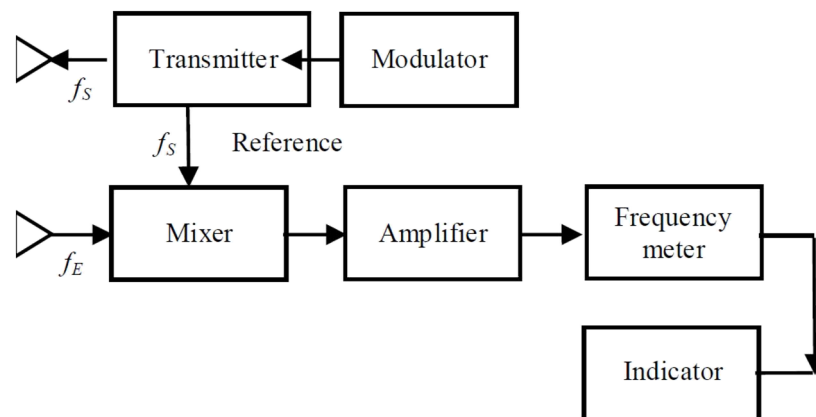


Fig 2.7-k: Block diagram of a FMCW radar [19]

From the scheme above, it is possible to observe that the received signal (f_E) is mixed down with the reference signal (f_s) coming from the transmitter. After an appropriate amplification and signal selection it is possible to perform a measurement of the difference frequency f_{dif} . This kind of measurement contains the information about the target distance. Solving a series of equations it is possible to calculate the distance of the victim. If there are multiple victims to detect with FMCW radar, at the mixer output there are multiple signals with corresponding difference frequencies. In order to separate these individual frequencies a filter bank consisting of narrow filters can be used.

2.8 Ground Penetrating Radar (GPR)

Starting from 1980, researchers investigated on the use of ground penetrating radar for detecting avalanche victims. GPR uses normally two separate antenna elements: the transmitter and the receiver. The working principle of GPR systems is the following:

- An electromagnetic wave is transmitted into the ground for a propagation in depth;
- The wave is reflected when meets a layer of the terrain with different dielectric properties compared to the layer in which the wave was propagating;
- Measuring the time between transmission and reception of the wave, and knowing the velocity of propagation of the electromagnetic wave, it is possible to calculate the distance of the obstacle;
- Analyzing the characteristics of the reflected wave, it is possible to distinguish the nature of the obstacle that caused the reflection. This point is very important to recognize a human victim.

The figure below (fig 2.8-a) shows an example of GPR system that transmits EM waves into the ground and receives signal scattered by discontinuity surface of two contiguous layers of different permittivity and conductivity. On the left side there is a scheme that illustrates the working principle of this technology (fig 2.8-b).

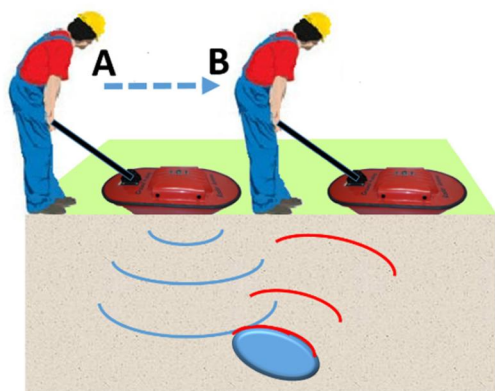


Fig. 2.8-a: Example of GPR utilization [11]

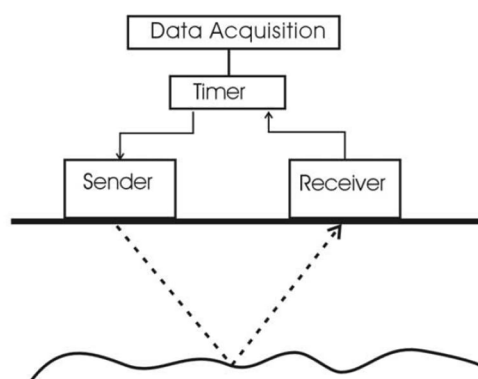


Fig. 2.8-b: Technical principle of ground penetrating radar [22]

The frequency band of standard GPR systems dedicated at the snowy environment of survey is in the range between 0.4 GHz and 2 GHz. The choice of the appropriate frequency is a compromise between resolution and penetration depth of radio wave. The resolution decreases when the frequency increases. A good compromise is a frequency of about 0.9 GHz, that allows to have a sufficient spatial resolution for detecting details of human body [11]. The electromagnetic waves propagate well through snow medium, which shows characteristic of almost homogeneous medium. So this technique can be used in avalanche environments. There is a limitation in presence of debris, for example during earthquake disasters. During this last situation, the big amount of debris it is not an homogeneous medium and the waves don't propagate well. Nevertheless, the strong scattering generated by the interface between a buried human body and the snow can be used to locate an avalanche victim. In the case of an object of finite geometrical dimension, and characterized by dielectric properties different from those of the snow medium where it is buried, if the GPR moves along a direction, the object is shown as diffraction hyperbola in the resulting radargram. The characteristics of the hyperbola are related to the velocity of the radar motion and to the dimension of the object. The presence of little debris inside the snowpack can complicate the detection of a person. In addition, avalanche victims roll and float in the snow, creating more layer interfaces such as:

- Snow/body;

- Snow/air/body;
- Ice/body.

In the following part of the section are analyzed two different cases of GPR utilization. In the first part is analyzed the use of a GPR system on the surface of the snowpack, while in the second case are analyzed the performances of a ground penetrating radar airborne. The adoption of aerial vehicles decreases the time to perform all the search operations. In fact, it simplifies acquisition of data in whole area.

GPR system sliding on the ground surface

A commercial GPR system has been developed to work in the rough environment of snow and ice [22]. The applied device is a 900 MHz system that easily reaches snow depths up to 10 meters. The depth resolution depends on the snow type, but is around 0.1 meter. The GPR system is triggered by an odometer wheel at regular adjustable steps. All the equipment is mounted in a sledge and is pulled by a snowmobile over the snow surface. The instrument can be used for the study of snow distributions, for the detection of glacier crevasses under the snow cover and for the search of avalanche victims in avalanche debris. The ground penetrating radar offers an alternative to traditional snow surveys. The following figure shows a scheme of the GPR device used during the test (fig 2.8-c).

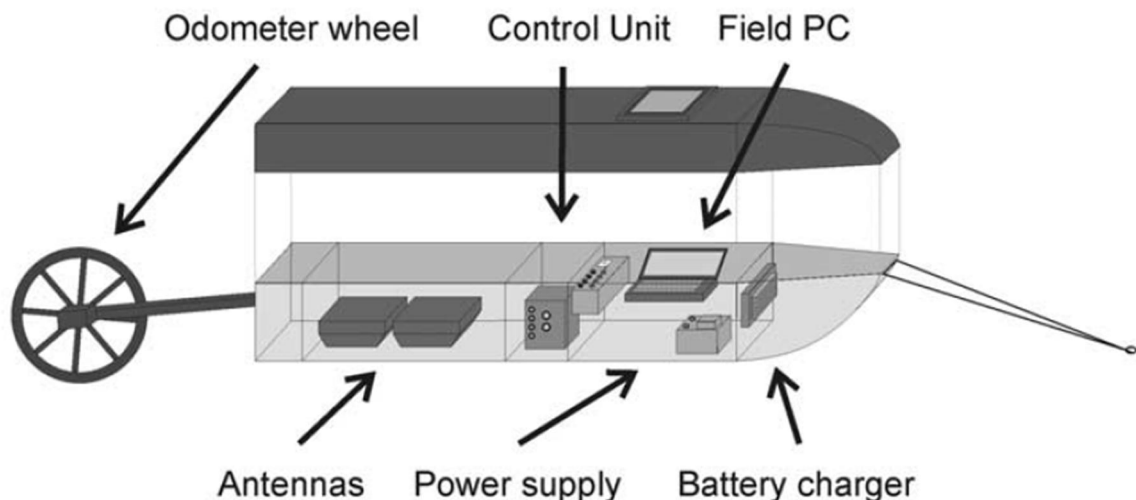


Fig 2.8-c: Setup of the radar system in the designed sledge [22]

The system can work with fixed frequencies from 225 MHz to 900 MHz. For snow measurements a good solution is to choose the 900 MHz antennas. The radar consists of the transmitter and receiver antennas, a control unit, power supply and a PC to analyze the radar measurements. The radar can move at 15-

30 km/h which allows an efficient coverage of large areas. The radar system previously described has been applied in two rescue operations after avalanche accidents on Spitsbergen and in the French Alps. In the next paragraph are analyzed the results of the GPR system during a test.

Since manual rescue methods are limited to a snow depth of 3-4 meters, deeply buried avalanche victims are often difficult to locate. GPR can reach a snow depth of ten or more meters, improving the range and the efficiency of the search operation. In February 2001, this method of research has been used to recover the bodies of deeply buried avalanche victims. Subsequently, the performances of the system have been verified during a test. For this purpose, it has been practiced a snow pit of two meters of depth in the accumulation area of a glacier. Different objects have been buried under the hard snowpack (density almost equal to 380 kg/m³). A backpack and a person have been placed in the tunnel inside the snow. Finally, scanning the section with different radar step sizes (0.5 m, 0.25 m and 0.1 m), the measurements were collected and analyzed.

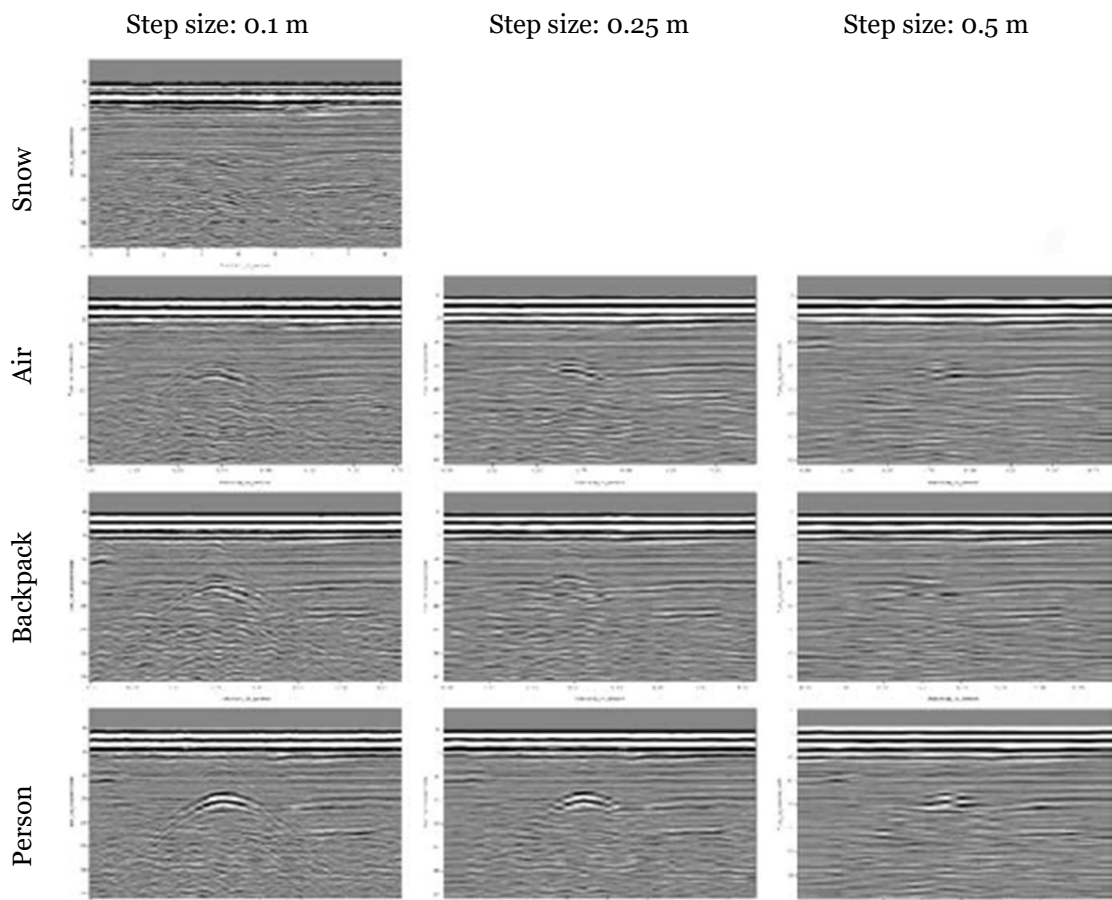


Fig 2.8-d: Results from radar detection objects in the snowpack at 900 MHz [22]

The resulting radar profiles are represented in the figure above (fig 2.8-d). The

test has been conducted in four different situations:

- Snow only;
- Air hole inside the snowpack;
- Backpack inside the snowpack;
- Person inside the snowpack.

In all the cases, the strongest signal is given at 0.1 m resolution. At a resolution of 0.25 m, the air hole is difficult to see while the person and the backpack can still be detected. At a step size of 0.5 m only the person gives a detectable signal. A profile of the snow without the horizontal tunnel is given as a reference. All these resulting profiles are generated after a data handling in the office. Considering that during an avalanche accident the conditions on the site can affect the judgment of the operator, the signal from a person at 0.5 m resolution is too weak to ensure detection. On the contrary, with a step size of 0.1 m the system works too slowly. Therefore, a good compromise between searching time and signal strength is a resolution of 0.25 m. Larger objects like cars can also be detected at 0.5 m resolution. In conclusion, the results show that the GPR system can detect cavities, a backpack, or a person covered under a snowpack of two meters. The experience has been carried out on dry and cold snow of medium density. Other tests are necessary on real avalanche debris and wet snow conditions. The wet snow slows down the radar signals and decrease the density difference between a human body and the surrounding snow. This factor causes a weaker signal in wet snow conditions. The system used during the test must be improved to guarantee a small and easy to operate radar system.

GPR system mounted on a helicopter

During a research at University of Innsbruck [23], the potential of a ground penetrating radar mounted on an aerial vehicle has been studied. The goal is to use this technology to detect avalanche victims. The GPR technology mounted on a flying helicopter is applied with the assumption that the background media consists of three different regions (air, snow and subsurface). Consequently, in the radargram there appear reflections caused by jumps in the value of the background velocity of propagation and reflections on buried objects. When a small buried object is detected, manifests itself as a diffraction hyperbola. The big limitation of this technique is that there is a need of an expert to analyze the diffraction hyperbolas in the radargrams. However, during this study it has been developed a real-time software for semi-automatic location of avalanche victims with radar technology from

helicopters. The algorithm consists of two steps. During the first part is adopted a parametric active contour method for automatic extraction of snow layer. Then, in order to highlight diffraction hyperbolas in radargrams is used a matched filter algorithm. The working principle of the GPR system and the interpretation of the radargrams are described below [23].

Let's assume that the helicopter with the emitting and receiving radar dipole-antenna travels in the horizontal direction, and parallel to the snow surface. The dipole-antenna points in the vertical direction like is shown in the figure below (fig 2.8-e).

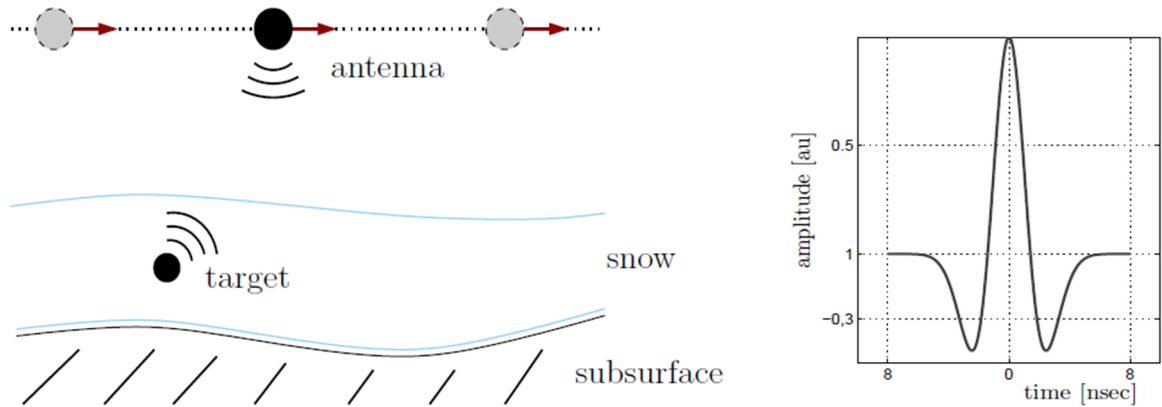


Fig 2.8-e: Left image: radar antenna emission with target reflection. Right image: temporal shape of the emitted electromagnetic pulse. [23]

At each position the radar antenna emits a short radar pulse. The induced electromagnetic wave is reflected, and the scattered signals are recorded and collected in radargrams. The reflected electric field is the sum of the field $eE_1(x, \tau)$ scattered on the interface between air and snow, reflection $eE_{ob}(x, \tau)$ resulting from the objects inside the snowpack, and the field $eE_2(x, \tau)$ scattered on the interface between snow and subsurface:

$$E_{reflected}(x, \tau) = e(E_1(x, \tau) + E_{ob}(x, \tau) + E_2(x, \tau))$$

where x is the position, τ is the time and e indicates the vertical direction. The receiving antenna at position x_{ant} is modeled as projecting the reflected field $E_{reflected}(x_{ant}, \cdot)$ onto the axis e followed by the convolution $*$ in time with w_{ant} (that represents the spectral characteristics of the used dipole-antenna). The resulting one dimensional signal is the following:

$$u_0(x_{ant}, \cdot) = (E_{reflected}(x_{ant}, \cdot) \cdot e) * w_{ant}$$

This signal is recorded within the time window $\tau \in [0, \tau_{end}]$ and is called a-scan. By varying $x_{ant} \in [0, x_{end}]$ and after using the re-scaling $x = x_{ant}/x_{end}$, $\tau = \tau/\tau_{range}$ the radar data set forms a two dimensional gray-scale image:

$$u_0: [0,1] \times [0,1] \rightarrow \mathbb{R} : (x, \tau) \mapsto u(x, \tau)$$

which is called radargram. A small buried object manifests itself in the radargram as a diffraction hyperbola. The following figure (fig 2.8-f) shows an example of an a-scan and a radargram measured during a field test in St. Anton in Tyrol.

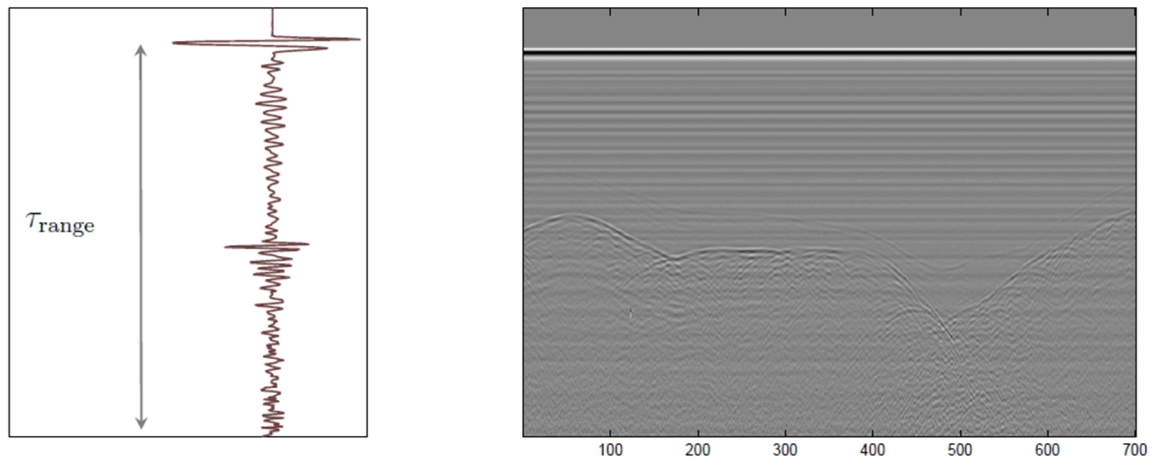


Fig 2.8-f: Left image: a-scan signal recorded within the time window. Right image: image of a radargram. [23]

During the experiment illustrates in the figure, the central wavelength of the dipole-antenna was 0.3 meters. Like is possible to see, the radargram contains a small diffraction hyperbola, that is caused by the reflections of a buried object. Two examples of diffraction patterns of objects inside the snowpack are illustrated in figure 2.8-g.

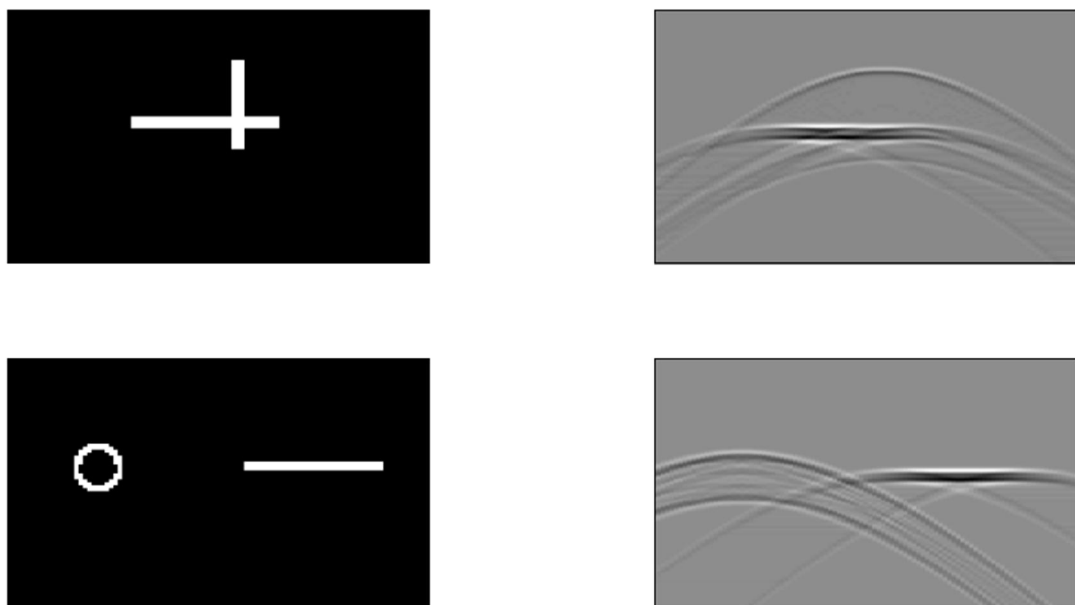


Fig 2.8-g: First column: velocity profiles (depth versus x). Second column: corresponding radargrams (τ versus x). [23]

It is possible to conclude that a diffraction hyperbola in the snow layer is a

clear indicator for the presence of a buried object. Therefore, following this procedure is very important to find a way to recognize diffraction hyperbolas. In order to do this, firstly clutter and noise are removed to better see the reflections coming from the objects inside the snowpack, and then a matched filter algorithm is applied to detect diffraction hyperbolas.

The radargram is decomposed into the following sum:

$$u(x, \tau) = u_0(x, \tau) + u_c(x, \tau) + u_n(x, \tau)$$

where $u_0(x, \tau)$ is the wanted signal, $u_c(x, \tau)$ is the clutter component and $u_n(x, \tau)$ is the noise component. In the GPR systems the clutter is a signal component that contains the spectral characteristics of the dipole antenna but is not correlated with scattering from buried objects. Clutter occurs from multiple reflections on fixed structures and reflections resulting from the inhomogeneous background. The separation of noise and clutter from the signal coming from the target is an important factor in the successful interpretation of the GPR data. In the GPR aerial vehicle used during the test, the main part of disturbing signals consist of horizontal lines, resulting from multiple reflections on the helicopter. In this case, a good technique which allows to reduce the clutter is the mean a-scan subtraction:

$$\bar{u}(x, \tau) = u(x, \tau) - \int_0^1 u(x, \tau) dx$$

Another advantage of this clutter reduction method is the possibility to have a real-time application. Figure 2.8-h shows the filtered radargram $\bar{u}(x, \tau)$ after removing clutter and noise. Comparing the results with the radargram in figure 2.8-f is possible to see an improvement in the diffraction hyperbolas detection.

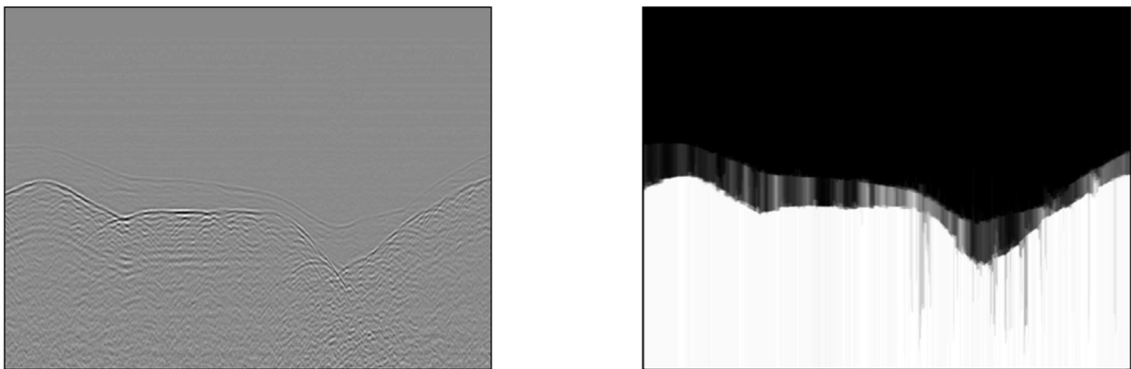


Fig 2.8-h: Left image: radargram after removing clutter and noise. Right image: result of minimizing the BV (bounded variation) functional for each column of the radargram. [23]

After removing clutter and noise, it is applied a matched filter to automatically detect diffraction hyperbolas. The working principle of this kind of filter is a

comparison between an original image with a template, and then it indicates where two features are most likely to correspond. In the application used during the analysis, the matched filter is only used to extract radargram u_S coming from reflections inside the snowpack. The template is a radargram m of a single diffraction hyperbola. The key point of the implementation of a matched algorithm is the definition of measure of similarity of two images. A typical measure is the squared Euclidean distance:

$$\int_0^1 \int_0^1 (u_S(x, \tau) - m(x - x_0, \tau - \tau_0))^2 dx d\tau$$

between the image u_S and the template m positioned at (x_0, τ_0) . If U is the support of the template and $\int_U u(x + x_0, \tau + \tau_0) dx d\tau$ is approximately constant, then the magnitude of the distance measured with the squared Euclidean method is determined by the following convolution:

$$(u_S * m)(x_0, \tau_0) := \int_0^1 \int_0^1 u_S(x, \tau) m(x - x_0, \tau - \tau_0) dx d\tau$$

According to the Fourier convolution theorem, the previous convolution can be evaluated with the FFT algorithm. Figure 2.8-i shows the results after applying the match filter and its envelope, which is calculated using the FFT algorithm.

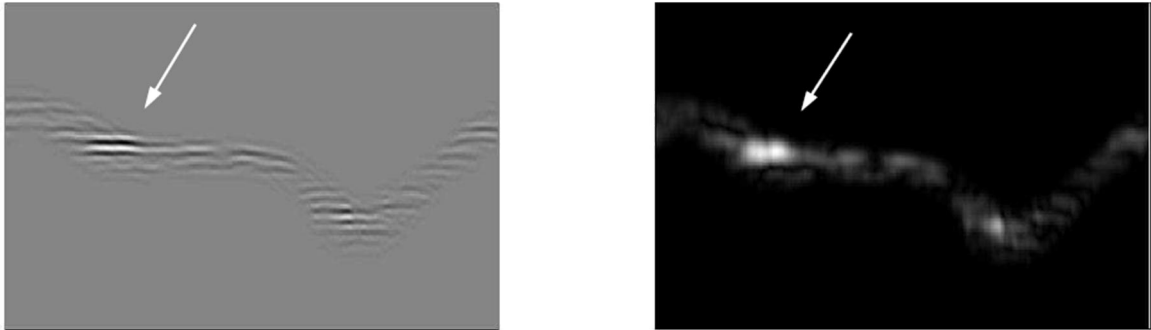


Fig 2.8-i: Results of the matched filter [23]

The left figure illustrates the result of the matched filter applied to the radargram previously shown in figure 2.8-h. The right image shows its envelope. The arrow highlights the presence of a diffraction hyperbola, that indicates the presence of an avalanche victim. As is possible to see, the diffraction hyperbola is easier to detect with respect to the radargrams illustrated before. This means that the matched filter improves the quality of the image, and is a good support during the analysis of GPR measurements. The following figure (fig 2.8-j) shows an example where the algorithm described along the paragraph has been applied to a real life data set. This is a possible application of the data elaboration process described in this part,

removing clutter and noise and applying the matched filter.

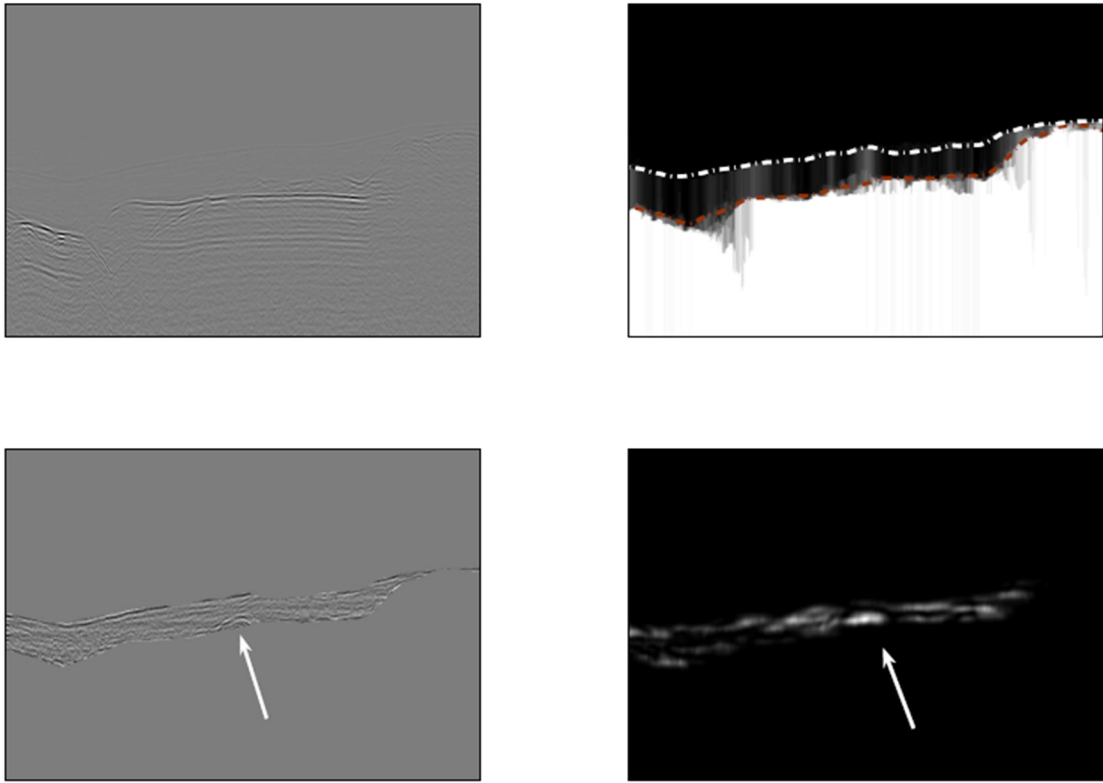


Fig 2.8-j: Results of algorithm applied to real life data [23]

In the top left is shown the radargram after removing clutter and noise. The top right image represents the boundaries of the snow layer. The bottom left figure illustrates the radargram that only contains the reflections coming from within the snowpack. Finally, the bottom right image shows the envelope after applying the matched filter. The arrows indicate the presence of diffraction hyperbolas. In conclusion, it is possible to say that the combination between the GPR transported by the helicopter and the algorithm described before is a technology that can be an important support for avalanche rescues. The use of aerial vehicles adds a new source of reflection, that is caused by the air-snow layer. However, this reflection can be excluded during the radargram analysis, in order to better recognize diffraction hyperbolas caused by avalanche victims. Another test of GPR helicopter mounted system has been conducted in the Swiss Alps [24]. During this second attempt, the researchers analyzed the conformation of a rock glacier area. The results of this second experience are very similar to those analyzed during the previous part. The most important feature to improve in this kind of technology is the searching time. As exposed in the first chapter, the survival time of an avalanche victim is approximately 15 minutes, after this interval time the probabilities to find a person alive rapidly decrease. In order to reduce the rescue interval time, another study on

airborne ground penetrating radar has been conducted. The next paragraph shows the analysis of this new experience.

Airborne ground penetrating radar

The detection of snow avalanche victims who are not equipped with traditional avalanche beacon systems is a demanding problem for rescue operations. The development of alternative methods is a challenge which is urgently at issue. An airborne ground penetrating radar can be a possible solution to this problem. This kind of radar search is technologically challenging because a very large amount of data have to be processed and visualized in real time, and the interaction of electromagnetic waves with snow, subsurface and different kinds of objects must be understood. Also in this case a two steps algorithm is used to locate avalanche victims in real time. The working principle of this algorithm is illustrated in the next section. In this part are analyzed the following features:

- Distance dependence of the reflection energy increasing the flight height;
- Coherence between the use of more antennas;
- Detectable range;
- Reflection images of different avalanche victims.

Previous studies show that the airborne search is feasible in real scenarios when the aerial vehicle flies at a maximum of 12 meters above the snow surface. During an experience conducted by some researchers [25], two different scenarios have been analyzed:

- Aerial tramway system 6 m above the snow surface;
- Chairlift about 12 m above the snow surface.

The flight on a chairlift is a more realistic comparison to a helicopter-flown. The radar scans were triggered by an odometer wheel with the resolution of one vertical scan per horizontal centimeter on tests on the tramway, where the radar antenna was moved along a steel cable in one direction. The scans of the chairlift had to be triggered by constant time intervals. The sampling rate was set to at least 512 samples per scan. Avalanche debris was simulated by a snow accumulation (4 m wide and around 2 m high). Human volunteers and a phantom body (made of three 10 liters bags filled with water to simulate human victims) have been buried inside the snowpack. The three bags was about 1 m in length, 0.4 m in width and 0.1 m in height. The test was performed using two different antennas on the aerial tramway system. The antennas were mounted parallel to each other at a distance of 1.5 m, with an

orientation orthogonal to the radar line. The two antenna configurations are the following:

- Monostatic antenna mode: both antennas transmit and receive radar signals separately.
- Bistatic antenna mode: One antenna transmits, and the other receives the radar signal.

The next figure (fig 2.8-k) shows the environment configuration of the test. The snow accumulation has been created with the help of a snow grooming machine.



Fig 2.8-k: Artificial avalanche accumulation [25]

A RIS One GPR instrument was used during the experience. Measurements were conducted with 400 MHz antennas.

Aerial tramway test

The results obtained with the aerial tramway system are reported below. With the monostatic antenna mode, the GPR has an object perceptibility of 1.5 m horizontal distance to both sides of the antenna. Using the bistatic mode the detection range is the same, but the resolution of the radargram is deteriorated compared to the monostatic mode. Six different tests have been performed during the aerial tramway experiment:

- a) Radar line measurement with the water bags (phantom body) without an avalanche mound above;
- b) Radar line measurements with a phantom body under the avalanche mound;
- c) Radar line measurements with a human body under the avalanche

- mound;
- d) Radar line measurements with only a snow mound;
- e) Radar line measurements with a phantom body and an air hole under the avalanche mound;
- f) Radar line measurements with only an air hole under the avalanche mound.

All the results of the analysis are reported below (fig 2.8-l).

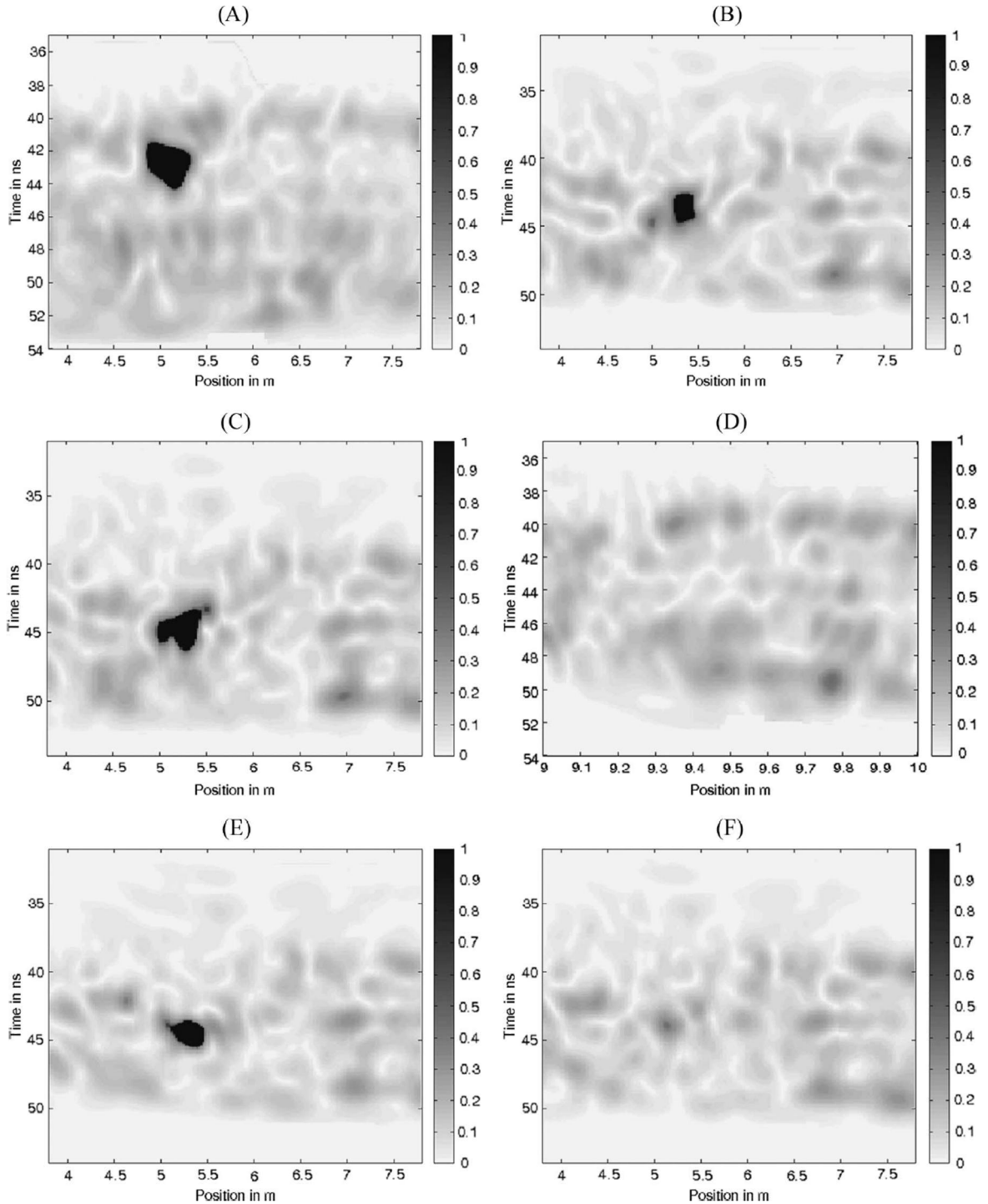


Fig. 2.8-l: Results of the aerial tramway experiment [25]

The measurements with and without an artificial avalanche mound above the phantom body confirm that the snow properties are almost negligible compared to the reflection values of water bags. A permittivity contrast between air and snow exists. However, this contrast is very small with respect to the contrast of phantom body or human. The results of the localization algorithm illustrated in figure 2.8-l show dark areas at position where a diffraction hyperbola is detected. The snowpack is represented with grey areas. As it possible to observe, the presence of the avalanche mound is not an obstacle for the victim detection. The GPR system works very well during dry snow conditions. In all the test configurations the phantom and the human bodies have been detected.

Chairlift test

During this second test, different radar scans with different scan rates per second were performed. The lift speed was constant at about $v_{cl} = 4.2 \text{ m/s}$. The reflection energy decreases with increasing distance of the radar source to the target. The mean of the raw reflection magnitude of snow in a vertical distance of 6 m to the radar source is 2.08 times higher than the snow reflection values at a distance of 12 m. Reflection energy decreases about linearly with height. The snow properties during this test were very similar with respect to the previous experiment. The system in analysis was composed by two antennas on a crossbeam. This configuration increases the detectability borders when both antennas are used as individual transmitters and receivers. During the experience, the phantom body has been buried at different horizontal distances from the chairlift. Also in this case are performed six different tests:

- a) Phantom body at zero meter horizontal distance from the chairlift;
- b) Only snow;
- c) Phantom body at one meter horizontal distance from the chairlift;
- d) Phantom body at two meters horizontal distance from the chairlift;
- e) Phantom body at three meters horizontal distance from the chairlift (downhill flight);
- f) Phantom body at three meters horizontal distance from the chairlift (uphill flight).

The following figures (fig 2.8-m) show the results of this analysis. Also in this case the dark areas represent the detected victim (diffraction hyperbola), while the grey areas indicate the snowpack. The 3 m horizontal distance has been analyzed by two different measurements. The first measurement was

performed by a downhill flight of the chairlift, and the second by an uphill flight of the chairlift.

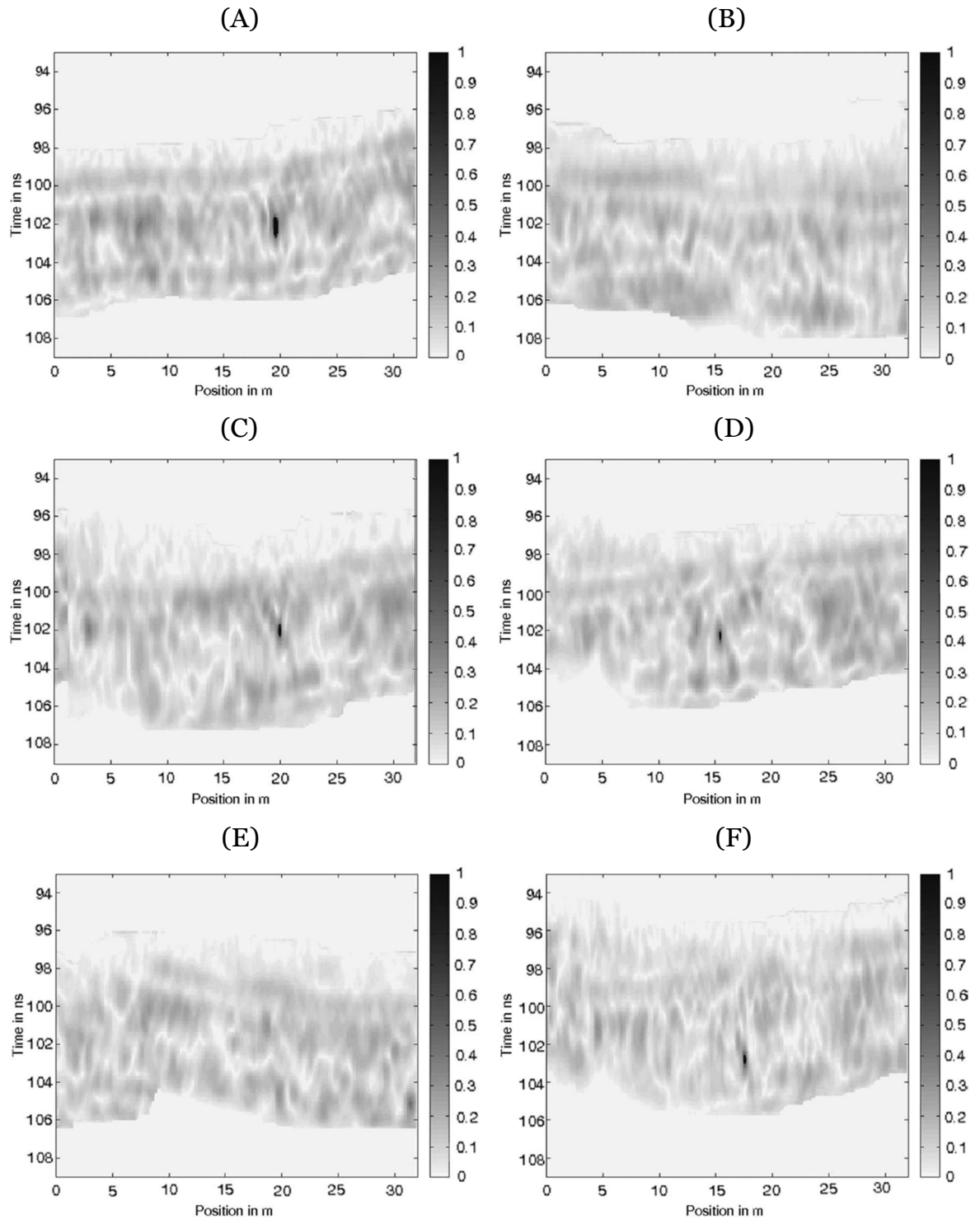


Fig 2.8-m: Results of the chairlift experiment [25]

From the previous images is possible to observe that the detectability range is between 2 m and 3 m for a radar altitude of 12 m above the ground. At an horizontal distance of 3 m, the phantom body is only detected while chairlift flying uphill. The reflection energy quotients are not affected by snow

properties in dry snow. An air gap above the body does not influence the avalanche victim detection, in fact there is a very small difference between the permittivity of snow and air. Air gaps in avalanche debris and above an avalanche victim create only negligible reflections. All these results prove that this technology can be a valid alternative to traditional avalanche beacon systems. Both tests confirm the feasibility of the real-time processing with direct data transfer. The next section describes the localization algorithm used to analyze and evaluate the GPR data during the two experiments.

Localization algorithm

In this part is described in details the localization algorithm used to detect avalanche victims through GPR airborne systems [25]. A human body manifests itself as a diffraction hyperbola in the radargram. However, there are objects (different from a human body) that generate additional hyperbolas in the radargram. In order to accomplish a good detection, firstly the snowpack must be extracted, and secondly the hyperbolas in the snowpack (generated by a victim) have to be localized. The extraction and denoising of the snowpack is done in three steps:

- 1) The radargram is pre-processed;
- 2) The snowpack is segmented using an active contour algorithm;
- 3) The extracted snowpack is post-processed to improve the signal to noise ratio of the diffraction hyperbolas.

The localization of the diffraction hyperbolas inside the snowpack is done using a matched filter. In this final step a template of an hyperbola is used to match it with the stored result of the first three steps. During the test the GPR antenna moves across a straight line with a constant velocity v . The radargram is considered as a mapping:

$$u_0: \begin{cases} [0,1] \times [0,1] \rightarrow \mathbb{R} \\ (x, t) \mapsto u_0(x, t) \end{cases}$$

where $x = \xi/\Xi$ and $t = \theta/\Theta$. The notations used during the analysis are the following:

- ξ is the position of the antenna;
- Ξ is the position of the antenna after n scans;
- θ is the time;
- Θ is the range, that is the receiving time for each scan.

The method is described in a continuous setting , but it is discretized for the implementation. At this point, the different steps can be analyzed.

Pre-processing

First of all, the clutter from raw data u_0 is reduced. Then, it is included a linear gain function, and after that a median filter is applied. The result of this filtering operation is denoted like u_1 . In the following figure (fig 2.8-n) is possible to see the raw data u_0 (left side) and the resulting u_1 (right side) after the pre-processing operation.

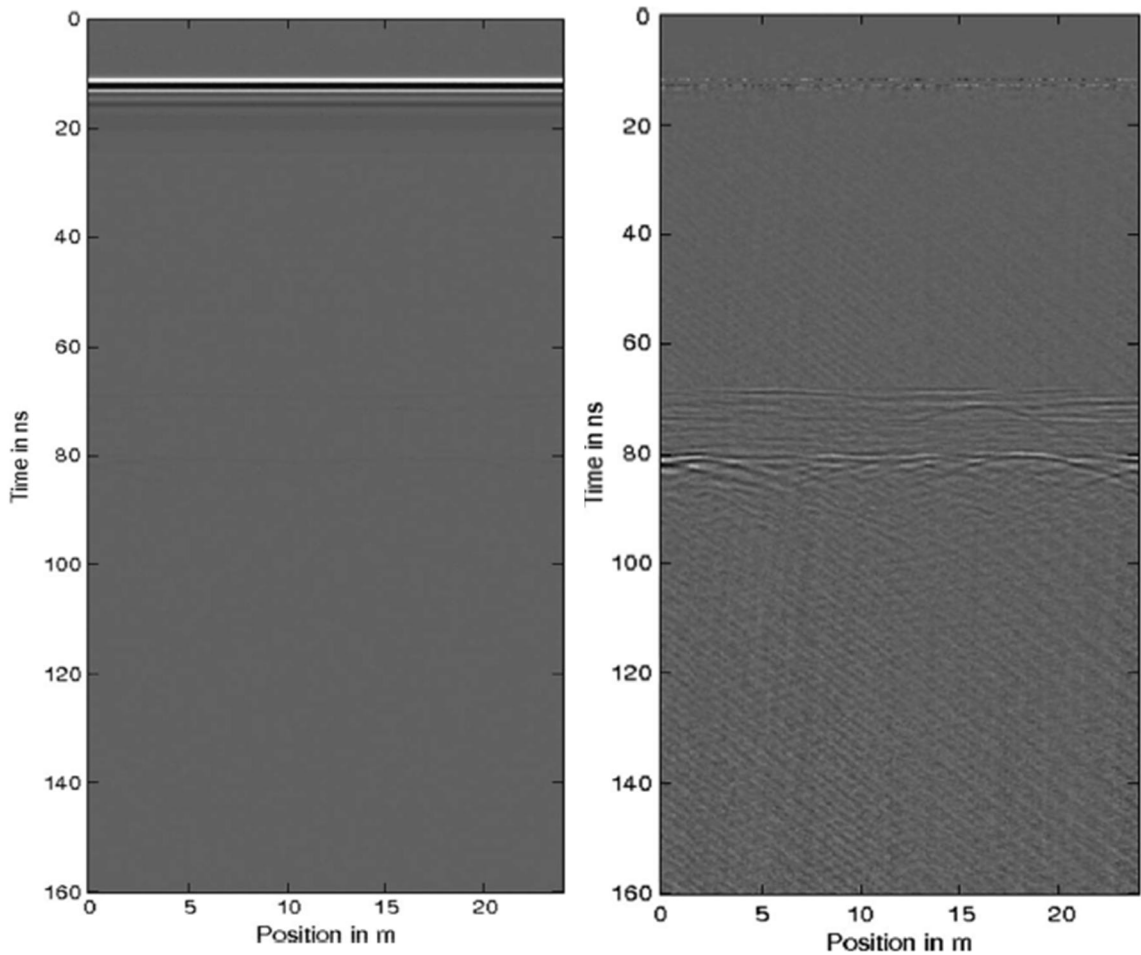


Fig 2.8-n: Left side: raw radar data u_0 . Right side: data u_1 after pre-processing step. [25]

Extraction of the snowpack

In order to automatically detect the boundaries of the snowpack is used an active contour model. To apply an active contour model to the GPR data is used an average amplitude Φ_λ , which depends on a scaling parameter λ . To find the air-snow boundary is introduced a threshold c_1 and the average amplitude is defined as:

$$\Phi_\lambda(x, t) := \begin{cases} f_\lambda(t), & \text{if } f_\lambda(t) \geq c_1 \\ 0, & \text{otherwise} \end{cases}$$

$f_\lambda(t)$ is a one dimension bounded variation functional. The air-snow boundary corresponds to the first edge within the image Φ_λ . At this point is important to

define the potential:

$$p_x: \tau \mapsto -\gamma\tau + \Phi_\lambda(x, t)$$

for a fixed x and $\gamma > 0$. In figure 2.8-o is shown a schematic plot of p_x . The idea of an active contour method is to find the first local minimum of p_x .

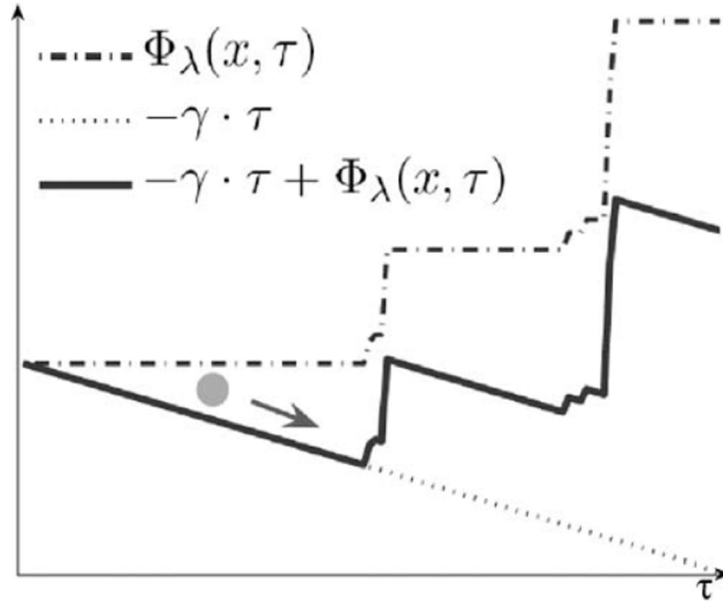


Fig 2.8-o: Potential p_x composition [25]

The arrow in the previous image indicates the local minimum. Since the boundary can be represented as a function $h(x)$, it is considered the following energy functional:

$$\int_0^1 p_x(h(x)) dx + \frac{\alpha}{2} \int_0^1 h'(x)^2 dx$$

The air-snow boundary has been chosen as a local minimizer h_1 of the previous equation. h_1 is calculated numerically by a steepest descent method. The first term in the equation above forces $h_1(x)$ to be in the first local minimum, and the second term makes h_1 smooth. The parameter α controls the influence of the two terms. The knowledge of h_1 is used to determine the snow-subsurface boundary h_2 . The following function is set:

$$u_i(x, t) := \begin{cases} \int_{h_1(x)}^t |u_1(x, \tau)| d\tau, & \text{if } t > h_1(x) \\ 0, & \text{otherwise} \end{cases}$$

Then the function:

$$\bar{u}(x, t) := \min \left\{ 1, k \cdot \frac{u_i(x, t)}{\max(u_i(x, \cdot))} \right\}$$

has an edge at the snow-subsurface boundary. This boundary is observable by an high reflection in the radargram. At this point, it is important to define

another function, introducing a new threshold c_2 :

$$\Psi(x, t) := \begin{cases} \bar{u}(x, t), & \text{if } \bar{u}(x, t) \geq c_2 \\ 0, & \text{otherwise} \end{cases}$$

The parameter $k > 0$ affects the location of h_2 . In order to obtain the snow-subsurface boundary is necessary to apply the active contour method. In this case Φ_λ is substituted by Ψ . To find the second boundary is necessary to search for a local minimizer h_2 of:

$$\int_0^1 (-\gamma h(x) + \Psi(x, h(x)) + \frac{\alpha}{2} h'(x)^2) dx$$

The snow boundaries h_1 (air-snow boundary) and h_2 (snow-subsurface boundary) are shown in the following radargram (fig 2.8-p).

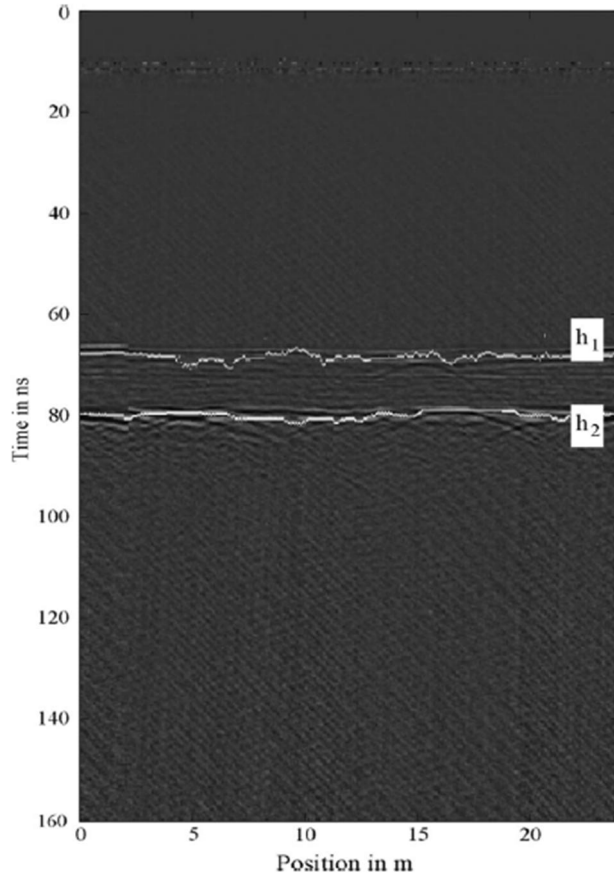


Fig 2.8-p: Snowpack boundaries in the radargram [25]

The figure 2.8-q illustrates the extracted snowpack $u_S = u_1 \cdot \chi_S$ where:

$$\chi_S(x) := \begin{cases} 1, & \text{if } x \in S \\ 0, & \text{otherwise} \end{cases}$$

is the characteristic function of:

$$S := \{(x, t): h_1(x) \leq t \leq h_2(x)\}$$

The following image shows the snowpack extraction, where the displayed range indicates the values of the boundaries of the snowpack.

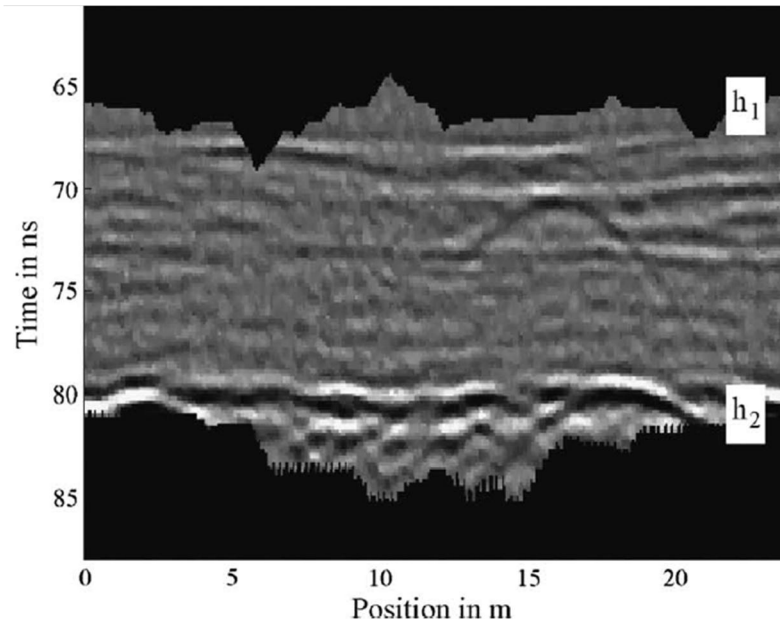


Fig 2.8-q: Extracted snowpack representation [25]

Preparation of the snowpack

Applying the matched filter (to amplify the intensity of the diffraction hyperbola) to u_s , there are some perturbations at the boundaries of the snowpack. This factor makes detection of the hyperbolas more difficult. The next figure (fig 2.8-r) shows this phenomena.

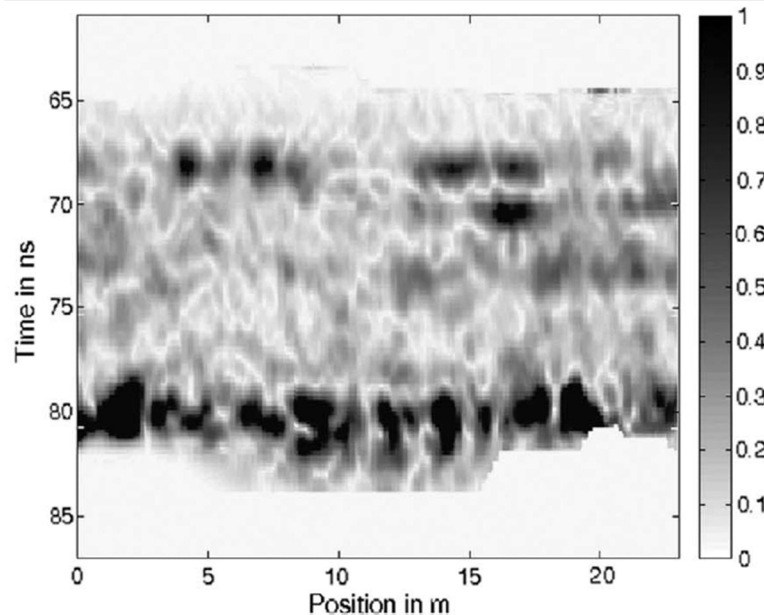


Fig 2.8-r: Result of the matched filter applied to u_s without preparation of the snowpack [25]

In order to prevent these perturbations, it is important to introduce a post-processing step after the extraction of the snowpack. The perturbations are caused by the high amplitudes of the signal, which happen only near the snowpack boundaries. The high amplitudes are absorbed using a scaling

function (fig 2.8-s). The scaling function is divided in three different regions:

- The first region contains the small values of $|u_s|$ (white area in figure 2.8-s), $|u_s| \leq 1000$. In this region the values of u_s are kept;
- The second region contains the high values of $|u_s|$ (dark grey area in figure 2.8-s), $|u_s| \geq 6500$. In this region the values of u_s are set to zero;
- The third region contains the remaining values of $|u_s|$ (light grey area in figure 2.8-s). In this region the values of u_s are damped by two polynomials of degree five.

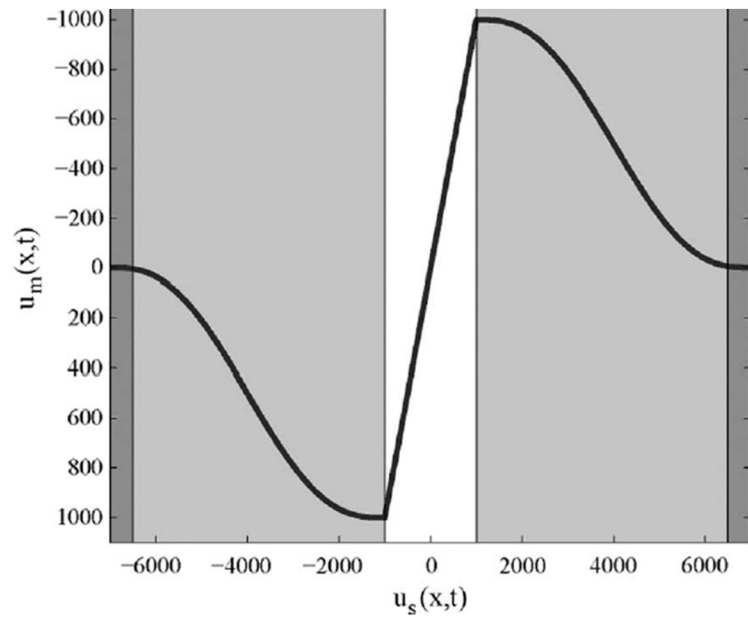


Fig 2.8-s: Scaling function [25]

The scaled snowpack is denoted by u_M . The following image (fig 2.8-t) shows the results of the post-processing operation.

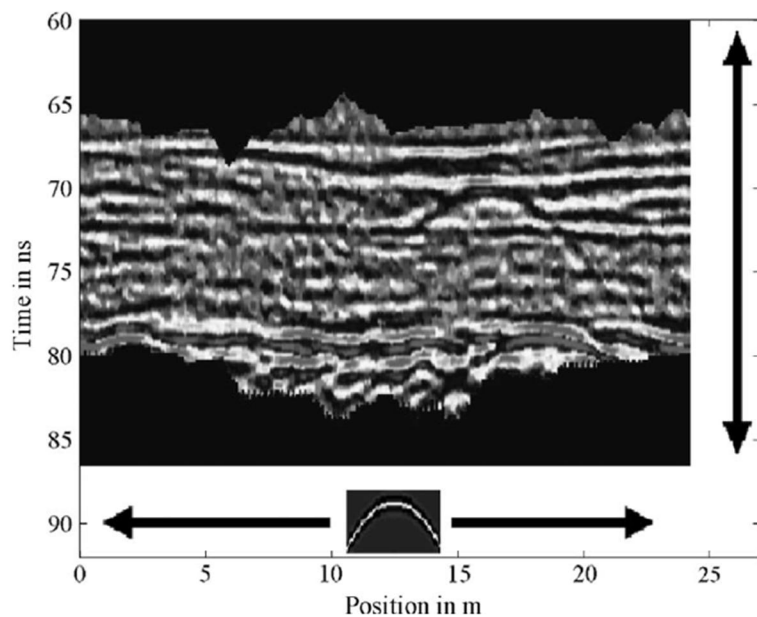


Fig 2.8-t: Prepared snowpack representation [25]

After the scaling operation the high values at the boundaries of the snowpack disappear, and in this situation the diffraction hyperbolas are clearly detectable through the use of a matched filter.

Matched filter

There are different methods to highlight the diffraction hyperbolas, and to locate the position of a possible avalanche victim. Using a matched filter algorithm, the prepared snowpack u_M is compared with a template m of a diffraction hyperbola. The template m depends on the settings of the radar equipment, the flight altitude and the velocity of the aerial vehicle. The definition of the measure of similarity of two images is very important for a matched filter implementation. In this case is used a squared Euclidean distance:

$$\int_0^1 \int_0^1 (u_M(x, t) - m(x - x_0, t - t_0))^2 dx dt$$

between u_M and the template m at position (x_0, t_0) . The magnitude of the Euclidean distance is determined by a convolution:

$$(u_M * m)(x_0, t_0) := \int_0^1 \int_0^1 u_M(x, t) m(x - x_0, t - t_0) dx dt$$

This convolution method allows a fast calculation with the fast Fourier transform algorithm. In the last step, it is taken the Hilbert envelope of the result of the convolution, denoted by u_r , and it is introduced a threshold L . The displayed image is the following:

$$u_0(x, t) = \begin{cases} \frac{u_r}{L}, & \text{if } u_r \leq L \\ 0, & \text{otherwise} \end{cases}$$

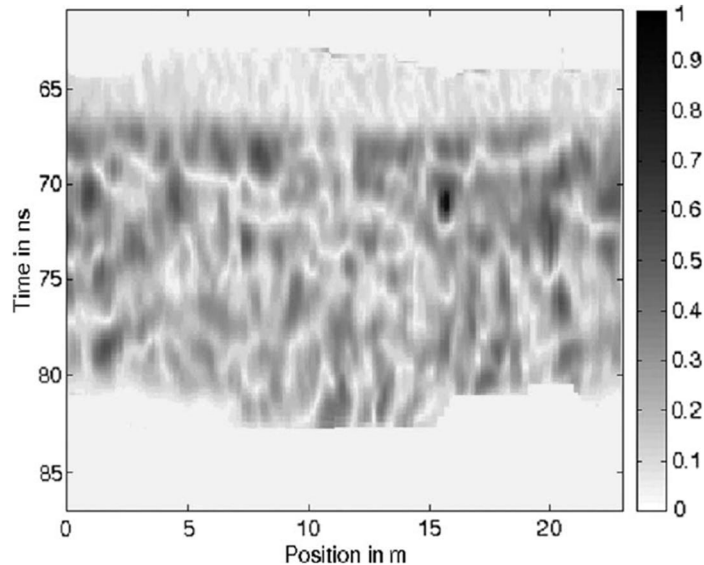


Fig 2.8-u: Result of the data processing algorithm [25]

The previous figure (fig 2.8-u) shows the result of the location algorithm after applying the matched filter. The snowpack is displayed by light grey values, while the dark area (around 15.75 m and 70.5 ns) indicates the position of the diffraction hyperbola.

Comparison of technologies

In this section are compared the different aspects that characterize each of the technologies described during chapter 2. Table 13 shows the advantages and disadvantages of the various technologies.

Technology	Advantages	Disadvantages
ARTVA	<ul style="list-style-type: none"> • Good search time • Good precision • Easily portable • Good search range 	<ul style="list-style-type: none"> • Difficult to use in the search mode for the inexperienced • Can only detect people wearing ARTVA devices
RECCO	<ul style="list-style-type: none"> • Easily portable • Good search range • Good precision 	<ul style="list-style-type: none"> • It is a passive device • Cannot be used in search mode
Smartphone apps	<ul style="list-style-type: none"> • Easily portable • Very intuitive to use also for inexperienced 	<ul style="list-style-type: none"> • Smartphones are not compatible with ARTVA devices • The battery of the smartphone has a short life in a cold environment • Bluetooth and Wi-Fi technologies don't have a large communication range inside snow
4G	<ul style="list-style-type: none"> • Easily portable • 4G signal propagates well through the snowpack 	<ul style="list-style-type: none"> • Low 4G signal coverage in mountain environment

4G		<ul style="list-style-type: none"> • The 4G technology is used as a communication channel between two smartphones
GPS	<ul style="list-style-type: none"> • Wide search range • Can detect a GPS signal even under 15 meters of snow • Easily portable 	<ul style="list-style-type: none"> • It is not very accurate in identifying the victim's position (accuracy of approximately 10 m from the victim)
Breath and skin detection sensors	<ul style="list-style-type: none"> • Can detect the substances emitted by human breath and skin 	<ul style="list-style-type: none"> • They have not yet been tested in an avalanche environment
Radar detection	<ul style="list-style-type: none"> • Can detect breathing and heartbeat perturbations • Can detect radio frequency devices • Good search range 	<ul style="list-style-type: none"> • The correct operation in very wet snow has yet to be tested • The good precision (in calculating the distance to the victim) has yet to be tested
GPR	<ul style="list-style-type: none"> • Can detect an avalanche victim with a good accuracy • Wide search range • Good signal transmission in the snowpack 	<ul style="list-style-type: none"> • Search time needs to be improved • To detect a victim the GPR data must be collected and processed by a specific algorithm • Not so easy to carry

Table 13: Advantages and disadvantages of avalanche research technologies

Between all these technologies, the most interesting seems to be the ground penetrating radar (GPR). This device is in phase of development. It can be integrated in ground or aerial vehicles and is able to perform an extensive research on the avalanche area. The signal propagates very well inside the

snowpack, and can reach a large depth. As most of the avalanche victims are buried at a maximum depth of 3 meters, this system can detect all of them. Another advantage of this technology is that can locate also people who are not wearing avalanche beacon transceivers. Then, combining this technology with a specific localization algorithm, it was seen that is possible to find a buried person after the analysis of the radar images. In order to test the potential of this technology it was decided to perform a practical experience. The results of this test are reported in the next chapter.

Chapter 3: Practical test with GPR technology transported by a drone

To study the potential of the ground penetrating radar, the performances of a GPR system transported by a drone have been tested during a practical experience conducted in Sant'Anna (Gressoney La Trinité – 2170 m), a place inside the Monterosa ski resort in Aosta Valley. The experiment has been conducted on 16th February 2021 in a test field set up by Monterosa ski society. In this section, firstly is represented the test configuration, then the instruments applied during the experiment are described, and finally the collected GPR data are analyzed.

Test configuration

The test site has been equipped with four different sectors. The different test configurations are reported below.

First snow mound

During this first test, a single person was buried at a depth of approximately 1.5 meters inside a hole created within the first snow mound (fig 3-a), and then he was covered with blocks of snow. The snowdrift was created using a snow grooming machine.



Fig 3-a: First snow mound configuration

Buried ARTVA devices

In the second test, three ARTVA devices have been buried at a depth of about 60 cm from the snow surface. The green poles indicate the position of the ARTVAs inside the snowpack (fig 3-b).



Fig 3-b: ARTVA buried under snow

Second snow mound

A second snow mound with inside two separated hole was created (fig 3-c). In this case two volunteers have been buried under the snow (at a depth of approximately 1.5 meters), and then the cavities were covered with blocks of snow.



Fig 3-c: Second snow mound configuration

Buried skis

During the last test, a pair of skis and a pair of ski poles have been buried under 30 cm of snow. The figure below (fig 3-d) shows the configuration of this experience.



Fig 3-d: Buried skis

The following map (fig 3-e) shows a scheme of the complete test field. The yellow points indicate the boundaries of the first snow mound. The red points represent the perimeter of the second snow mound, and the blue points are the positions of the ARTVA devices. The remaining orange and grey points indicate respectively the weather station of the forest ranger and the position where skis and poles have been buried.

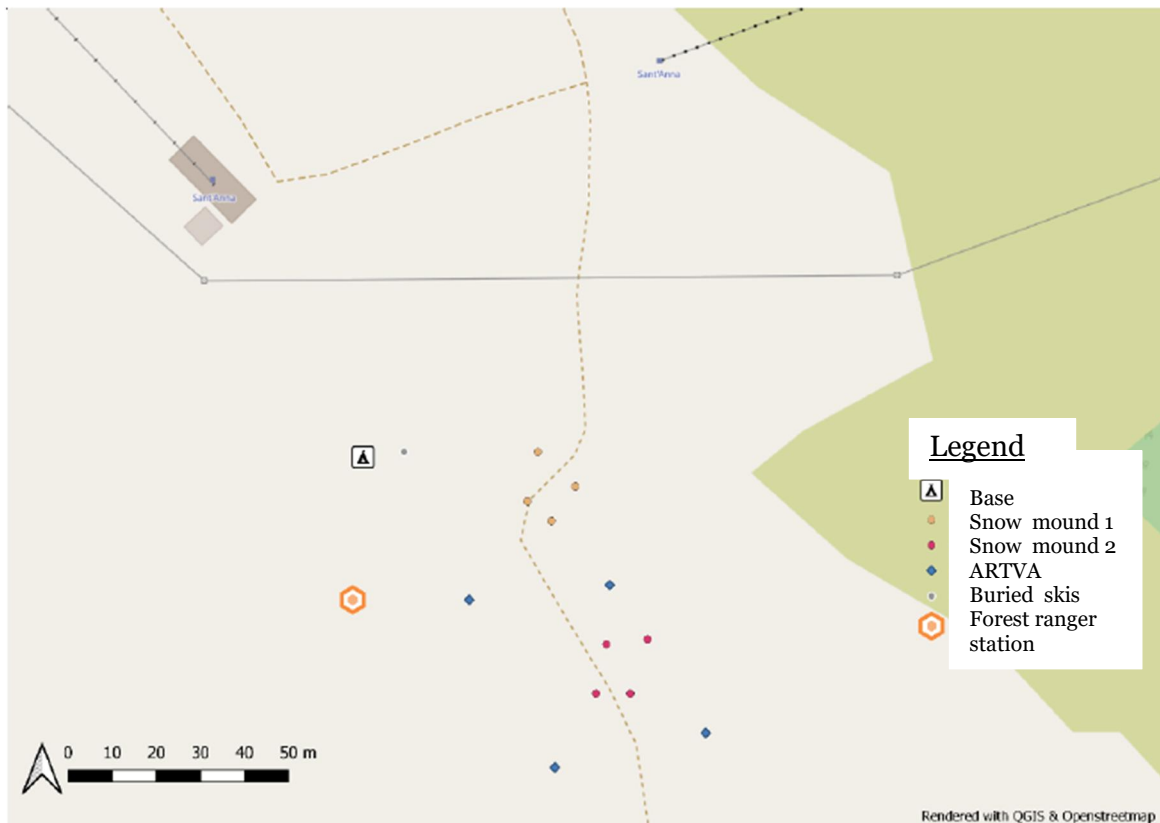


Fig 3-e: Scheme of the test field

During the experience the weather was sunny and the following table (table 14) describes the weather conditions during the time interval of the practical test.

Interval Time [h]	Thermometer [°C]	Snow thickness [cm]	Total solar radiation [W/m ²]	Reflected solar radiation [W/ m ²]
09-10	1.3	111.0	496.0	352.5
10-11	2.9	110.0	580.8	423.9
11-12	2.8	109.5	581.2	447.0
12-13	3.3	112.0	384.0	366.0

Table 14: Weather conditions in Sant’Anna test

All the data in the table have been collected from the weather station situated in Gabiet (Gressoney la Trinité – 2379 m). The snow density varied from 150 kg/m³ on the surface of the snowpack to 210 kg/m³ inside the snowpack. Increasing the depth inside the snowpack, the snow density regularly increased. The thickness of the snow layer was about 1 m. The following picture (figure 3-f) shows the complete test field environment.



Fig 3-f: Field test environment in Sant’Anna

Instrumentation

The drone used during the test was the VENTURE VFF_HO1 model (developed by PROS 3 srl), that it has been equipped with a GPR IDS two channels device with 900 MHz antennas (conic propagation of radar signal). The PC on board the drone was an Intel NUC (Mini-PC). For the remote control they have been used a Panasonic Toughbook CF-19 PC and a radio controller. The total weight of the drone was 14 kg, including all the on board devices. The aerial vehicle used during the experiment is represented in the following image (fig 3-g).



Fig 3-g: VENTURE VFF_Ho1 drone

In order to guarantee the flight control, the following devices were used:

- Autopilot Pixhawk;
- Barometric sensor;
- GPS;
- Laser distancemeter.

There is also a router for Wi-Fi communication between the drone and the remote control PC. The scheme of the total instrumentation setup is shown in the following figure (fig 3-h).

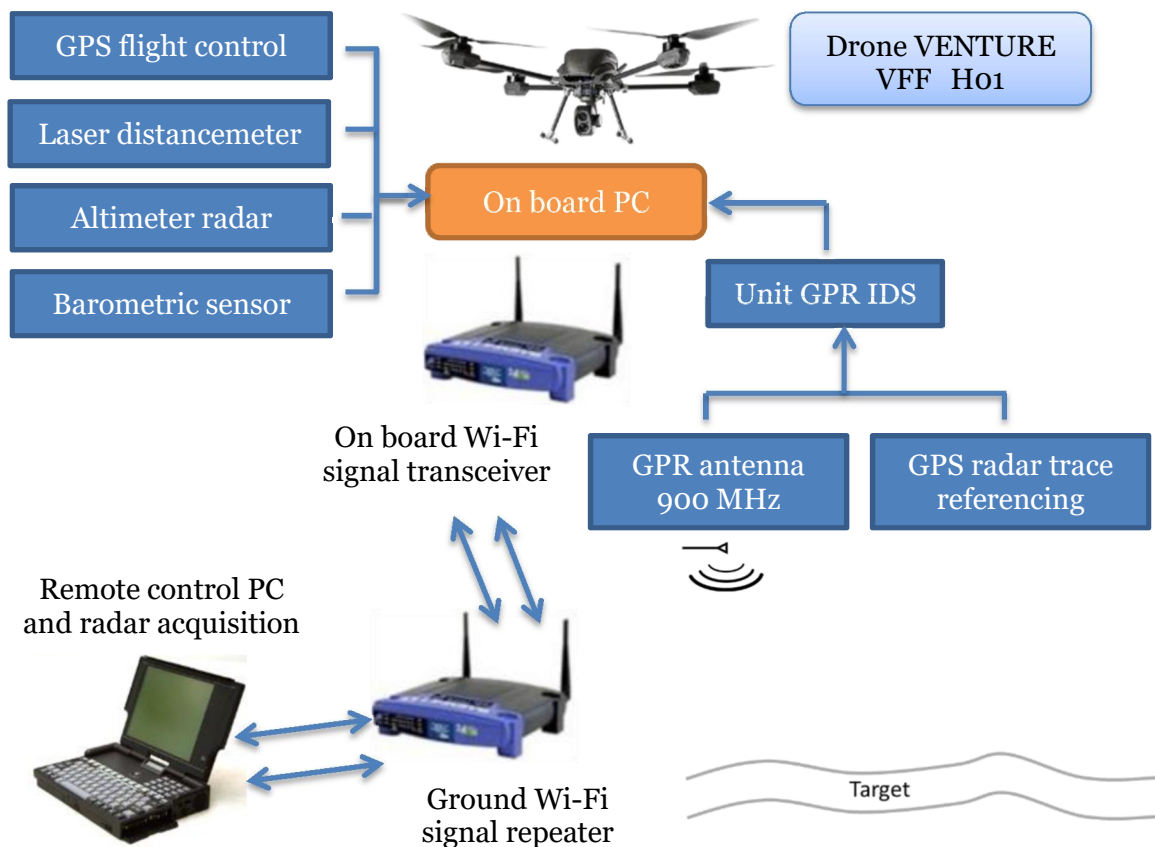


Fig 3-h: Instrumentation setup scheme

Collection and analysis of GPR data

During the experience, four different flights were carried out using the drone:

- 1) Drone flight in manual mode (piloted by radio controller), with data acquisition in the north sector of the avalanche test field. During this part the drone flew over the first snow mound, with only one person buried;
- 2) Drone flight in manual mode (piloted by radio controller), with data acquisition in the south sector of the avalanche test field. During this second part of the experiment, the drone flew over the second snow mound with inside two different people buried;
- 3) Drone flight (in manual mode) in the central area of the avalanche test field (north-south direction), with a pair of skis buried approximately 30-40 cm under the snow surface and a pair of ski poles buried 10 cm inside the snowpack;
- 4) Drone flight in automatic control mode (software: Mission Planner), with data acquisition in the west sector of the avalanche test field (near the forest ranger station). In this zone the snow was not beaten.

During the flight, the drone recorded its flight path using the GPS referencing technique. Knowing the snow density (approximately 200 kg/m³) it is possible to calculate the electrical permittivity of the snow. Finally, knowing these two data it is possible to obtain the speed of propagation of the electromagnetic wave in the snow, that is equal to 0.22 m/ns. Table 15 shows the data collected during the test. For some flights described above there is more than one line.

ID line	Time window [ns]	Number of samples	Number of tracks	Acquisition distance [m]	Acquisition duration [s]
L1	100	1024	3633	77.5	155
L2	100	1024	4156	80.7	126
L3	100	1024	26034	-	553
L4	100	1024	43263	-	920
L5	100	1024	27332	-	581
L6	100	1024	11630	-	247

Table 15: Acquisition parameters, Sant'Anna test

The drone is able to collect 47 tracks per second. By calculating the referencing of the GPS radar tracks, a malfunction in the acquisition of L3, L4, L5 and L6 was verified. Figure 3-i shows the flight paths of the L1, L2 and L3 ID lines. L1

is represented with magenta color, L2 with green color and L3 with blue color. The points are related to the GPS positions of the drone with data acquisition every second. The L1 and L3 lines start at the base point (in north-west position), while the L2 line starts in a south position (near the second snow mound). The two ellipses indicate the positions of the two piles of snow, where three different volunteers have been buried during the execution of the test. The yellow points indicate the positions of the buried ARTVA devices. The map represents in the horizontal axis the longitude and in the vertical axis the latitude. It is also possible to see the GPS coordinates. All the positions of the buried objects have been acquired using the Google maps application installed on a smartphone. L4, L5 and L6 lines are not represented in the following map, because the GPS referencing trace has been calculated only for the first three lines.

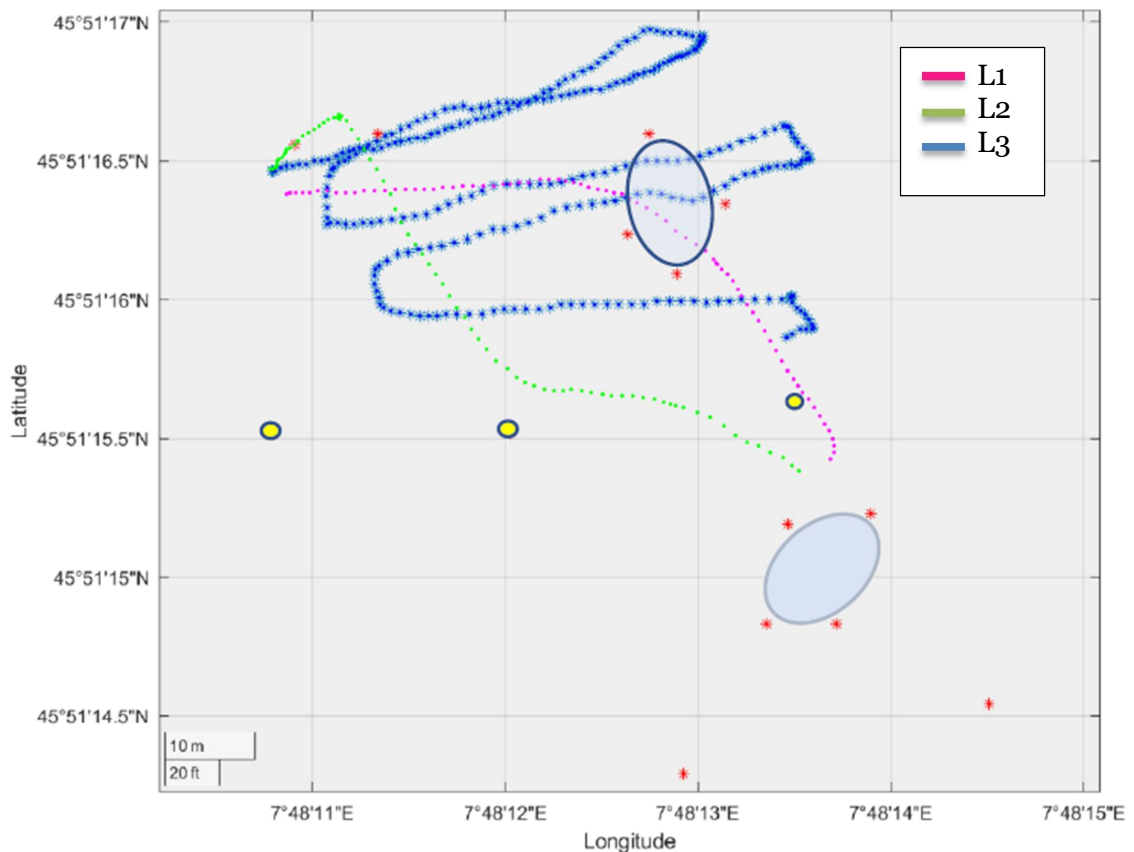


Fig 3-i: Flight paths of the drone

In the next section are analyzed the first, the third and the fourth flight of the drone (as described at the begin of this section). The data have been elaborated by the DIATI department (Politecnico di Torino). The next radargrams are represented with the travel time of the radar signal (measured in ns) in the vertical axis, and the progressive position of the drone along the flight line

(measured in m) in the horizontal axis. The vertical axis on the right side of the graphs shows the distance between the radar antenna and the target based on the speed of the radar wave in the air (0.3 m/ns), only in figure 3-j this distance is calculated using the wave speed in the snow (0.22 m/ns). The value 0 m indicates the flight altitude of the drone. The following figure (fig 3-j) illustrates the radargram relating to L1 line (first flight of the drone). The intensity of the reflected signal is shown on the scale on the right of the radargram.

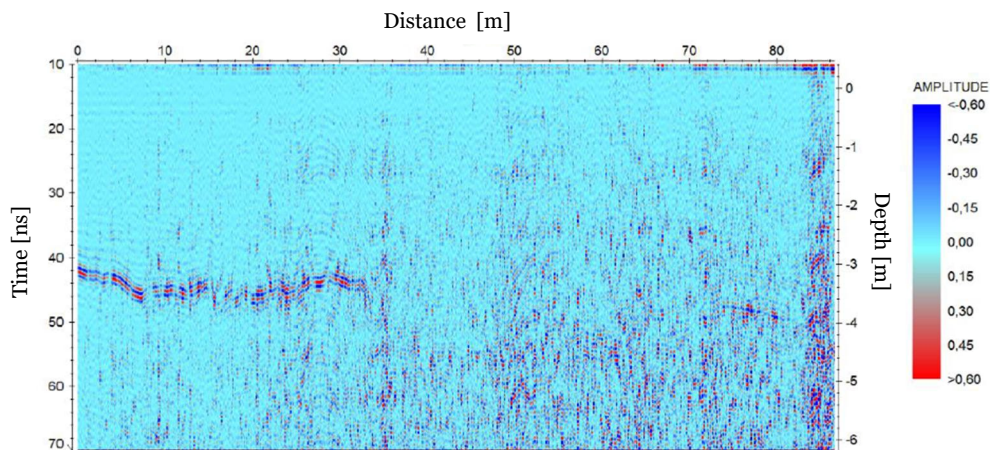


Fig 3-j: Radargram of line L1

In the first part of the graph (from 0 m to approximately 30 m), it is clearly detectable the reflection due to the snow-terrain layer (dark blue area). There is an high scattering of the signal from 35 m to 70 m, this is probably caused by the surface roughness of the snowpack. When the drone passes over the first snow mound, the person is not detectable.

The following images (fig 3-k) report the radargram of the line L2 and its signal envelope processing (figure below) collected during the third flight of the drone.

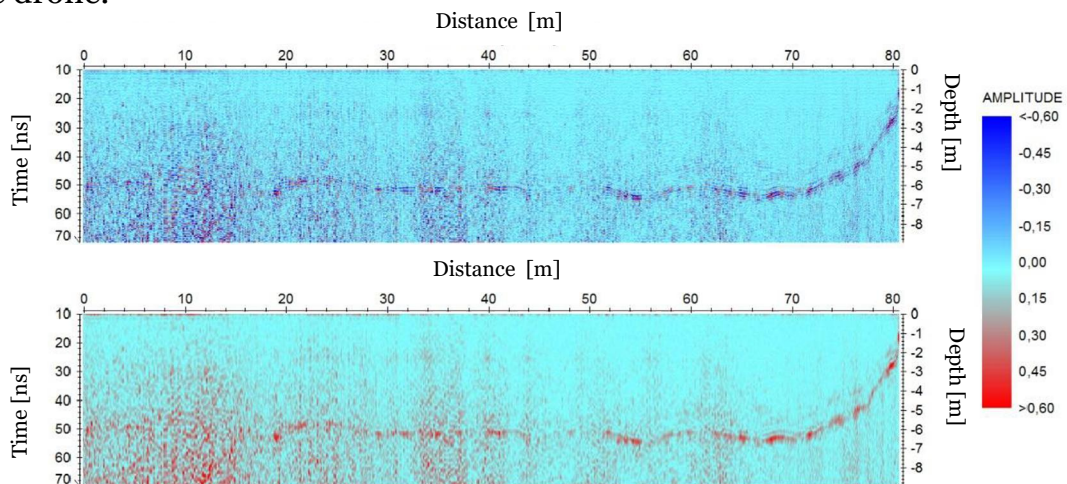


Fig 3-k: Radargram and signal envelope processing of line L2

At the abscissa values of 10-15 m, it is possible to observe a big disturbance of the signal, that is due to the flight over the ARTVA devices. Then, also in this case the reflection generated by the terrain is detectable. The other zones with high scattering (35 m and 65 m) are caused by the roughness of the snow surface. The buried skis and ski poles are not detectable.

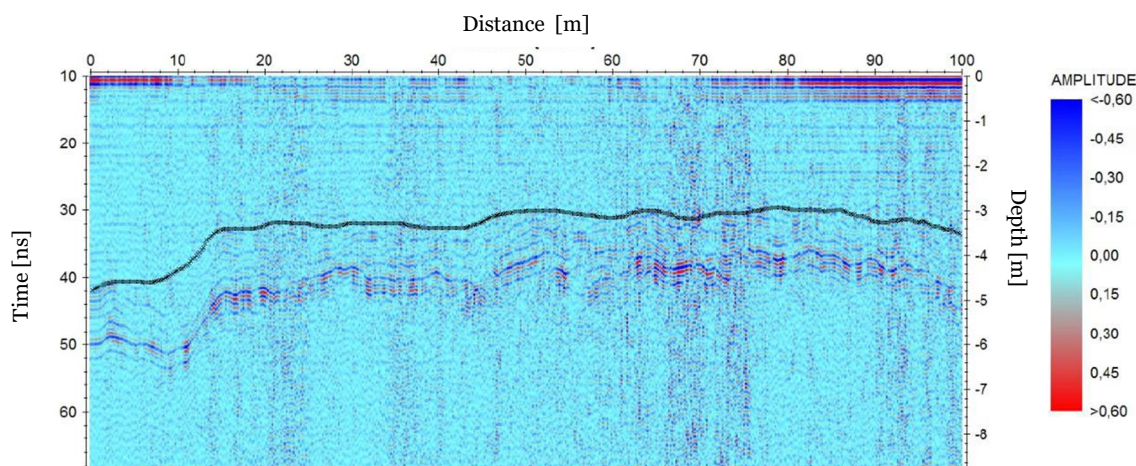


Fig 3-l: Radargram of line L3

The previous radargram (figure 3-l) shows the result of the first 100 m of flight during the line L3 path (first flight of the drone). The dark line indicates the surface of the snowpack. This line has been drawn knowing the flight altitude of the drone (measured with the laser distancemeter). The other dark blue zones under the line represent the reflections between snowpack and terrain. With these results it is possible to estimate the thickness of the snowpack, that is approximately 1 meter. During this test the drone was flying about 3.5 meters above the snow surface (fig 3-m).



Fig 3-m: Drone flight during the test

During the fourth flight of the drone (flight altitude of about 3 m), the aerial vehicle flew over the west sector of the avalanche test field (near the forest ranger station), where the snow was not beaten by grooming machine. The results of this analysis are reported in the following radargram (fig 3-n).

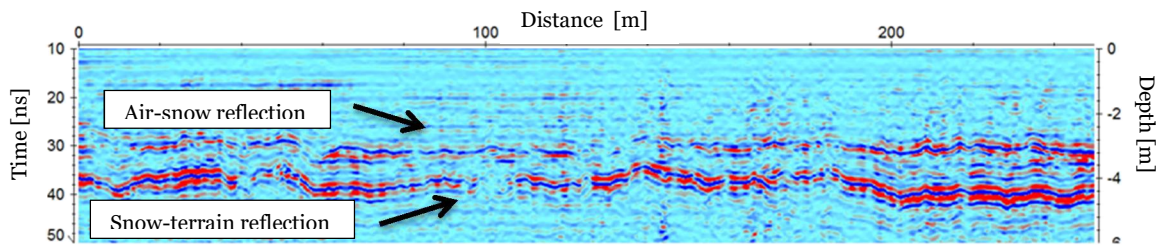


Fig 3-n: Radargram of the fourth flight of the drone

The arrows indicate the reflections related to the air-snow layer and to the snow-terrain layer. In contrast to the previous cases, now also the air-snow reflections are clearly detectable. This means that the GPR works better in the absence of surface roughness. With this results, it is possible to calculate the thickness of the snowpack (about 1 meter) without the use of the laser distancemeter.

Analysis of the results

The results reported in the previous part show that is not possible to detect the person buried within the snow mound. Also the buried skis are not detectable, while the ARTVA devices cause an electromagnetic disturbance when the drone passes over them. The only reflection that is clearly detectable is that generated by the terrain. The snow surface reflection is visible only when the drone flew over the not beaten snow. The main causes of these negative results are the following:

- Low signal quality in the passages above the area prepared with mechanical vehicles compared to the radar tracks of the not beaten area. This phenomena is caused by the increased scattering due to the roughness of the snow surface;
- The passage in the snow accumulation area highlights a further degradation of the quality of the radar signal. Also in this case the cause is the surface roughness.

In general, increasing the frequency of the antenna improves the resolution but the signal penetration depth decreases, and decreasing the frequency there is an improvement in the signal penetration depth but the resolution gets worse. Therefore, the use of a higher frequency antenna (1500 MHz) could improve the resolution of the system, but it would cause an increase in

scattering and clutter effects due to the roughness of the snow surface (composed by snow blocks). The scattering of rough surfaces depends on the size of the roughness with respect to the wavelength. For roughness dimensions equal to or slightly less than the wavelength, the scattering is amplified. From the following graph (fig 3-o) it is possible to see that using frequencies between 200 MHz and 400 MHz, the negative interference generated by the irregularities of the snow surface (large a few decimeters) is minimized. This could be a possible solution to avoid the scattering problem.

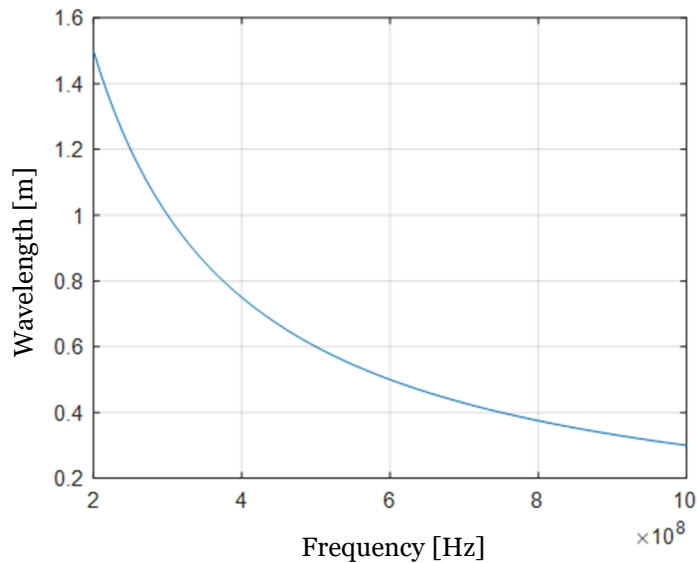


Fig 3-o: Relationship between wavelength and frequency

The absence of new snowfalls and the difficult moment of health emergency did not allow the development of a new test with antennas at different frequencies. In the future, a test with different antennas must be performed to verify the solution proposed before. Another limitation of this technology is that the radar signals are not processed in real time. A possible idea could be the combination of the tested system with the localization algorithm described in the previous chapter, that allows to extract the snowpack and to detect diffraction hyperbolas caused by the presence of a victim (the algorithm has a short elaboration time). The use of an aerial vehicle is a big advantage because it allows to decrease searching time during the rescue operations. During the drone flight in manual mode no particular problems were found, only a few gusts of wind destabilized the system, but the set-up was quickly recovered. Instead, the drone flight in automatic control mode it is not suitable for avalanche research operations, battery consumption is very high and limits this mode. For the moment manual flight seems to be the best alternative, with the speed and flexibility necessary for emergency situations.

Chapter 4: Conclusions

Inside this thesis, various technologies for finding avalanche victims have been discussed. In the first chapter they were also described the different factors that can cause an avalanche event. From this study it is possible to conclude that the human-triggered accidents have been growing over the last few years, and currently they are the leading cause of avalanche accidents. This is due to a strong increase in off-piste activities. A survival curve was analyzed, and it has been seen that is important to extract the buried person in the first 15 minutes after the accident. If a person remains buried for more than 15 minutes the probability of survival rapidly decreases. For this reason it is important to develop technologies that are precise and quick during the researches. Currently, the most used technology is the ARTVA device. This instrument is a good compromise between search speed and search accuracy. Furthermore, it can be easily portable and allows companions to directly help the victim, reducing the search time. Inside the second chapter it has also been analyzed the state of the art of the other avalanche research technologies, and between all of them the most interesting appeared to be the ground penetrating radar (GPR). For this purpose, in order to test the potential of this technology it was decided to perform a practical experience. During the third chapter of the thesis it has been described a practical test conducted using a GPR system transported by a drone. The abilities of this device to detect buried people has not been verified. The bad results are caused by the high roughness of the snow surface. A possible solution to this problem could be the use of an antenna at a lower frequency. Finally, returning to the idea described in the introduction section, the use of a GPR technology transported by an aerial vehicle could be a good idea to rapidly detect the victim. Currently, this technology has some limitations, but further studies can improve its efficiency. The big advantage of this system is that can be used in all the situations, also when the buried people don't wear the ARTVA. The combination of the GPR technology (transported by a drone) with a breath and skin sensor integrated on the ground robot, as described in the introduction, could be an idea to further improve the accuracy of the search, and to rapidly detect the airways of the victim. However, this second technology must be tested in avalanche environments to verify the feasibility of this solution.

Bibliography

- [1] *Unofficial network web page*. "The 10 deadliest avalanche events in history".
URL: <https://unofficialnetworks.com/>
- [2] *The local web page*. "Italy marks one year since deadly Rigopiano avalanche".
URL: <https://www.thelocal.it/>
- [3] *Piste hors web page*. "Avalanche survival curve".
URL: <http://pistehors.com/>
- [4] *Mountaineering Scotland web page*. "Where do avalanches happen and why?" – Avalanche causes.
URL: <https://www.mountaineering.scot/>
- [5] Jamieson, J. B., and C. D. Johnston. "Snowpack characteristics associated with avalanche accidents." *Canadian Geotechnical Journal* 29.5 (1992): 862-866.
- [6] Mt. Shasta. "Avalanche-poor position". *Wilderness Climbing Ranger Report 2015* (2016).
- [7] Ganju, Ashwagosha, Naresh K. Thakur, and Vijay Rana. "Characteristics of avalanche accidents in western Himalayan region, India." *Proceedings of the International Snow Science Workshop, Penticton, BC, Canada*. 2002.
- [8] Valt, M., I. Chiambretti, and R. Zasso. "1985–2009 twenty-five years of avalanche accidents in Italy." *Proceedings of the International Snow Science Workshop, Davos*. 2009.
- [9] *AINEVA web page*.
URL: <https://www.aineva.it/>
- [10] Atkins D. "Avalanche rescue technology." *Avon, Colorado 81620 USA*. 2017.
- [11] Ferrara, V. "Technical survey about available technologies for detecting buried people under rubble or avalanches." *WIT Transactions on The Built Environment* 150 (2015): 91-101.
- [12] Ferrara, Vincenzo. "Pervasive technologies for the reduction of disaster consequences: opportunities and questions." *Disaster Management* (2018): 193.
- [13] *Electronics tutorials web page*. "Series resonance circuit".
URL: <https://www.electronics-tutorials.ws/>

- [14] Floyer, James. "Smartphone Avalanche Search Apps—A Review." *Canadian Avalanche Centre* (2013).
- [15] Wolfe, Victor, et al. "Feasibility Study of Utilizing 4G LTE Signals in Combination With Unmanned Aerial Vehicles for the Purpose of Search and Rescue of Avalanche Victims (Increment 1)." *University of Colorado at Boulder, Research Report* (2014).
- [16] Schleppe, John B., and Gérard Lachapelle. "GPS tracking performance under avalanche deposited snow." *Proceedings of the 19th International Technical Meeting of the Satellite Division of The Institute of Navigation (ION GNSS 2006)*. 2006.
- [17] Güntner, Andreas T., et al. "Sniffing entrapped humans with sensor arrays." *Analytical chemistry* 90.8 (2018): 4940-4945.
- [18] Güntner, Andreas T., et al. "Detecting breath and skin emitted tracers of humans with flame-made sensor arrays."
- [19] Loschonsky, M., et al. "Detection technology for trapped and buried people." 2009 *IEEE MTT-S International Microwave Workshop on Wireless Sensing, Local Positioning, and RFID*. IEEE, 2009.
- [20] Pieraccini, Massimiliano, et al. "Detection of breathing and heartbeat through snow using a microwave transceiver." *IEEE Geoscience and Remote Sensing Letters* 5.1 (2008): 57-59.
- [21] Tang, H. J., et al. "Life signal detection using an on-chip split-ring based solid state microwave sensor." *Applied Physics Letters* 105.13 (2014): 133703.
- [22] Jaedicke, Christian. "Snow mass quantification and avalanche victim search by ground penetrating radar." *Surveys in geophysics* 24.5 (2003): 431-445.
- [23] Haltmeier, Markus, Richard Kowar, and Otmar Scherzer. "Computer aided location of avalanche victims with ground penetrating radar mounted on a helicopter". na, 2005.
- [24] Merz, Kaspar, et al. "Evaluation of ground based and helicopter ground penetrating radar data acquired across an Alpine rock glacier." *Permafrost and Periglacial Processes* 26.1 (2015): 13-27.
- [25] Fruehauf, Florian, et al. "Experiments and algorithms to detect snow avalanche victims using airborne ground-penetrating radar." *IEEE Transactions on Geoscience and Remote Sensing* 47.7 (2009): 2240-2251.